CHAPTER

SIX

NUMERICAL METHODS FOR INVISCID FLOW EQUATIONS

6.1 INTRODUCTION

The Navier-Stokes equations govern the flows commonly encountered in both internal and external applications. Computing a solution of the Navier-Stokes equations is often difficult or at least impractical and, in many of these applications, unnecessary. Results obtained from a solution of the Euler equations are particularly useful in preliminary design work, where information on pressure alone is desired. In problems where heat transfer and skin friction are required, a solution of the boundary-layer equations usually provides an adequate approximation. However, the outer-edge conditions, including the pressure, must be specified from the inviscid solution as the first step in such an analysis. The Euler equations are also of interest because many of the major elements of fluid dynamics are incorporated in them. For example, fluid flows frequently have internal discontinuities such as shock waves or contact surfaces. Solutions relating the end states across a shock are given by the Rankine-Hugoniot relations; these relations are contained in solutions of the Euler equations.

The Euler equations govern the motion of an inviscid nonheat-conducting gas and have a different character in different flow regimes. If the time-dependent terms are retained, the resulting unsteady equations are hyperbolic for all Mach numbers, and solutions can be obtained using time-marching procedures. The situation is very different when a steady flow is assumed. In this case, the Euler equations are elliptic when the flow is subsonic, and hyperbolic

when the flow is supersonic. This change in character of the governing equations is the reason that the development of methods for solving steady transonic flows has required many years. Many simplified versions of the Euler equations are used for inviscid fluid flows. When studying incompressible flows, it is often to our advantage to assume irrotationality. Under these conditions, a solution of Laplace's equation for the velocity potential or stream function provides the flow field information. Associated with the Euler equations is the companion set of small-perturbation equations. In subsonic and supersonic flow, we observe that the Prandtl-Glauert equation provides the first-order theory for the potential function. In transonic flow the equation obtained for small perturbations is still a nonlinear equation. The classification of the various forms of the inviscid equations of motion is given in Table 6.1.

Many different methods are used to obtain solutions to the Euler equations or any of their reduced forms. The main goal of this chapter is to present the most commonly used methods for solving inviscid flow problems. While many techniques may be used to solve the partial differential equations (PDEs) governing such flows, our attention will be restricted to finite-difference and finite-volume methods.

The methods presented in this chapter are selected to illustrate the basic ideas as well as give information on useful solution schemes. In a textbook, only fundamental methods that appear to have some measure of permanence should be included. Although some question always exists regarding the long-term survivability of "current techniques," it is hoped that those selected for discussion will stand the test of time.

6.2 METHOD OF CHARACTERISTICS

Closed-form solutions of nonlinear hyperbolic PDEs do not exist for general cases. In order to obtain solutions to such equations we are required to use numerical methods. The method of characteristics is the oldest and most nearly exact method that can be used to solve hyperbolic PDEs. Even though this technique has been replaced by newer, more easily implemented finite-difference/finite-volume methods, a background in characteristic theory and its application is essential.

In our discussion in Chapter 2, we observed that certain directions or surfaces that bound the zones of influence are associated with hyperbolic equations. Signals are propagated along these particular surfaces influencing the solution at other points within the zone of influence. The method of

Table 6.1 Classification of the Euler equations

	Subsonic, $M < 1$	Sonic, $M = 1$	Supersonic, $M > 1$
Steady	Elliptic	Parabolic	Hyperbolic
Unsteady	Hyperbolic	Hyperbolic	Hyperbolic

characteristics is a technique that utilizes the known physical behavior of the solution at each point in the flow. A clear understanding of the essential elements of the method of characteristics can be obtained by studying a second-order linear PDE.

6.2.1 Linear Systems of Equations

Consider the steady supersonic flow of an inviscid, nonheat-conducting perfect gas. Suppose the free stream flow is only slightly disturbed by a thin body, so the fluid motion satisfies the small perturbation assumptions given by (see Section 5.5.6)

$$\frac{u}{U_\infty} \ll 1 \qquad \frac{v}{U_\infty} \ll 1$$

where u and v are perturbation velocity components. If transonic and hypersonic flows are not considered, the governing PDEs reduce to the Prandtl-Glauert equation for supersonic flow. If the x axis is aligned with the free stream, this equation may be written

$$(1 - M_\infty^2)\phi_{xx} + \phi_{yy} = 0 \tag{6.1}$$

The free stream Mach number is denoted by M_∞, and the perturbation potential is denoted by ϕ. Initial data are specified along a smooth curve, C, which we choose to be $x = \text{const}$ in this case. Boundary conditions are prescribed at $y = 0$.

$$\begin{aligned} \frac{\partial \phi}{\partial y}(x, 0) &= U_\infty \left(\frac{dy}{dx}\right)_{\text{wall}} \\ \phi(0, y) &= 0 \end{aligned} \tag{6.2}$$

In order to present the formulation for a system of equations, it is advantageous to consider the similar formulation introduced in Chapter 2. Using the perturbation velocity components

$$u = \frac{\partial \phi}{\partial x} \qquad v = \frac{\partial \phi}{\partial y}$$

and denoting $M_\infty^2 - 1$ by β^2, Eq. (6.1) may be written as the system

$$\begin{aligned} \beta^2 \frac{\partial u}{\partial x} - \frac{\partial v}{\partial y} &= 0 \\ \frac{\partial v}{\partial x} - \frac{\partial u}{\partial y} &= 0 \end{aligned} \tag{6.3}$$

with associated initial data and boundary conditions

$$\begin{aligned} u(0, y) &= 0 \\ v(0, y) &= 0 \end{aligned} \Bigg\} \quad y > 0$$

$$v(x, 0) = v_{\text{wall}} \qquad y = 0 \tag{6.4}$$

In order to use the method of characteristics, the system given by Eq. (6.3) is written along the characteristics. The differential equations of the characteristics are developed as the first step in this procedure.

Suppose the initial data for this problem are prescribed along an arbitrary smooth curve, C, and we consider methods for constructing a solution of Eq. (6.3) in the neighborhood of this curve. If the solution is sufficiently smooth, the first method that might be considered is to write a Taylor series about a point on C. Assume that our interest is in a small neighborhood, and only terms through the first derivatives need to be retained. The solution for either u or v may then be written in the form

$$u(x + \Delta x, y + \Delta y) = u(x, y) + \Delta x \frac{\partial u}{\partial x}(x, y) + \Delta y \frac{\partial u}{\partial y}(x, y) + \cdots \quad (6.5)$$

In this expression, the coordinates (x, y) are on the initial data curve where u and v are known. However, we need to compute the first derivatives in the Taylor series. If s represents arc length along the curve C, we may write

$$\begin{aligned} \frac{du}{ds} &= \frac{\partial u}{\partial x}\frac{dx}{ds} + \frac{\partial u}{\partial y}\frac{dy}{ds} \\ \frac{dv}{ds} &= \frac{\partial v}{\partial x}\frac{dx}{ds} + \frac{\partial v}{\partial y}\frac{dy}{ds} \end{aligned} \quad (6.6)$$

The system of four equations in the unknown derivatives given by Eqs. (6.3) and (6.6) may be solved by any standard method, such as Cramer's rule. It is clear that the determinant of the coefficients of the system must not vanish. (If the determinant of the coefficients vanishes, the direction of curve C is along the characteristics of the system and, consistent with our discussion in Chapter 2, the derivatives may not be uniquely determined.) The differential equations of the characteristics are obtained by setting the determinant of this system equal to zero:

$$\begin{vmatrix} \beta^2 & 0 & 0 & -1 \\ 0 & -1 & 1 & 0 \\ \dfrac{dx}{ds} & \dfrac{dy}{ds} & 0 & 0 \\ 0 & 0 & \dfrac{dx}{ds} & \dfrac{dy}{ds} \end{vmatrix} = 0 \quad (6.7)$$

Expanding this determinant and solving the characteristic equation yields the expressions

$$\frac{dy}{dx} = \pm \frac{1}{\beta} \quad (6.8)$$

which are differential equations of the characteristics as illustrated in Fig. 6.1. Since β is constant, the characteristics can be obtained by integration and are

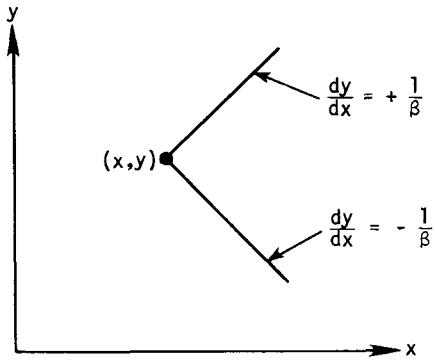

Figure 6.1 Characteristics of the Prandtl-Glauert equation.

given by

$$\begin{aligned} \xi &= x - \beta y \\ \eta &= x + \beta y \end{aligned} \tag{6.9}$$

The original differential equations written along the characteristics are called the compatibility equations. These compatibility equations may be derived by continuing to solve the original system of equations for the first derivatives. Along the characteristic directions, the determinant of the coefficients vanishes. If we solve for any of the first derivatives, for instance, $\partial u/\partial x$, and require that they are at least bounded, the determinant forming the numerator must also vanish. This may be written

$$\begin{vmatrix} 0 & 0 & 0 & -1 \\ 0 & -1 & 1 & 0 \\ \dfrac{du}{ds} & \dfrac{dy}{ds} & 0 & 0 \\ \dfrac{dv}{ds} & 0 & \dfrac{dx}{ds} & \dfrac{dy}{ds} \end{vmatrix} = 0 \tag{6.10}$$

If this determinant is expanded, the compatibility equations are given by

$$\frac{du}{ds} = \left(\frac{dy}{dx}\right)\frac{dv}{ds}$$

or

$$\frac{d}{ds}(\beta u + v) = 0 \tag{6.11}$$

along a right running characteristic, where

$$\frac{dy}{dx} = -\frac{1}{\beta}$$

and

$$\frac{d}{ds}(\beta u - v) = 0 \tag{6.12}$$

along the left running characteristic

$$\frac{dy}{dx} = \frac{1}{\beta}$$

A more general procedure for deriving the characteristics is given by Whitham (1974). We will repeat the details of the procedure here and omit the derivation of the technique. In order to find the characteristics of the system [Eq. (6.3)], we write these equations in the vector form:

$$\frac{\partial \mathbf{w}}{\partial x} + [A]\frac{\partial \mathbf{w}}{\partial y} = 0 \tag{6.13}$$

where

$$\mathbf{w} = \begin{bmatrix} u \\ v \end{bmatrix}$$

and

$$[A] = \begin{bmatrix} 0 & -\dfrac{1}{\beta^2} \\ -1 & 0 \end{bmatrix} \tag{6.14}$$

The eigenvalues of this system are the eigenvalues of $[A]$. These are obtained by extracting the roots of the characteristic equation of $[A]$. Thus we write

$$|[A] - \lambda[I]| = 0$$

or

$$\begin{vmatrix} -\lambda & -\dfrac{1}{\beta^2} \\ -1 & -\lambda \end{vmatrix} = 0$$

This produces the quadratic equation

$$\lambda^2 - \frac{1}{\beta^2} = 0$$

The roots of this equation are

$$\lambda_1 = \frac{1}{\beta}$$

$$\lambda_2 = -\frac{1}{\beta}$$

This pair of roots form the differential equations of the characteristics we have already derived in Eq. (6.8). Since our original Prandtl-Glauert equation for supersonic flow is just a wave equation in ϕ, we could have written the characteristic differential equations using the results from our discussion of the

second-order PDE [Eq. (2.15*a*)]. The next step is to determine the compatibility equations. Following Whitham, these equations are obtained by premultiplying the system given by Eq. (6.13) by the left eigenvector of $[A]$. This effectively provides a method of writing the equations along the characteristics.

Let $\mathbf{L}^1$ represent the left eigenvector of $[A]$ corresponding to λ_1 and $\mathbf{L}^2$ represent the left eigenvector corresponding to λ_2. We derive the eigenvectors of $[A]$, by writing

$$[L^i]^T[A - \lambda_i I] = 0 \tag{6.15}$$

If we let

$$\mathbf{L}^1 = \begin{bmatrix} l_1 \\ l_2 \end{bmatrix}$$

then

$$\left[l_1^1, l_2^1\right] \begin{bmatrix} -\dfrac{1}{\beta} & -\dfrac{1}{\beta^2} \\ -1 & -\dfrac{1}{\beta} \end{bmatrix} = 0$$

This provides the equations

$$\frac{l_1^1}{\beta} + l_2^1 = 0 \qquad \frac{l_1^1}{\beta^2} + \frac{l_2^1}{\beta} = 0$$

which are equivalent as expected. Since we are only able to obtain the normalized components of $\mathbf{L}^1$, assume $l_1^1 = -\beta$. Then the solution for l_2^1 is

$$l_2^1 = 1$$

and

$$\mathbf{L}^1 = \begin{bmatrix} -\beta \\ 1 \end{bmatrix}$$

In a similar manner, the solution for $\mathbf{L}^2$ is

$$\mathbf{L}^2 = \begin{bmatrix} \beta \\ 1 \end{bmatrix}$$

The compatibility equations are now obtained by writing our system [Eq. (6.13)] along the characteristics. To do this, we multiply Eq. (6.13) by the transpose of the left eigenvector:

$$[\mathbf{L}^i]^T\left[\mathbf{w}_x + [A]\mathbf{w}_y\right] = 0 \tag{6.16}$$

The term $[\mathbf{L}^i]^T[A]$ may be replaced by $[\mathbf{L}^i]^T\lambda_i[I]$ by substituting from Eq. (6.15). Thus, we may write Eq. (6.16) as

$$[\mathbf{L}^i]^T[\mathbf{w}_x + \lambda_i \mathbf{w}_y] = 0$$

The compatibility equation along λ_1 is obtained from

$$[-\beta, 1]\begin{bmatrix} u_x + \dfrac{1}{\beta}u_y \\ v_x + \dfrac{1}{\beta}v_y \end{bmatrix} = 0$$

Thus

$$\frac{\partial}{\partial x}(\beta u - v) + \frac{1}{\beta}\frac{\partial}{\partial y}(\beta u - v) = 0 \tag{6.17a}$$

In a similar manner, the compatibility equation along the right running characteristic in partial derivative form is

$$\frac{\partial}{\partial x}(\beta u + v) - \frac{1}{\beta}\frac{\partial}{\partial y}(\beta u + v) = 0 \tag{6.17b}$$

Equation (6.17*a*) is valid along the positive or left running characteristic. It expresses the fact that the quantity $(\beta u - v)$ is constant along λ_1. This can be demonstrated by letting s represent distance along the characteristic and writing

$$\frac{d}{ds}(\beta u - v) = \frac{\partial}{\partial x}(\beta u - v)\frac{dx}{ds} + \frac{\partial}{\partial y}(\beta u - v)\frac{dy}{ds}$$

However, if $(\beta u - v)$ is constant along the characteristic, we may write

$$\frac{d}{ds}(\beta u - v) = 0$$

or

$$\frac{\partial}{\partial x}(\beta u - v) + \left(\frac{dy}{dx}\right)\frac{\partial}{\partial y}(\beta u - v) = 0$$

which is the same as Eq. (6.17*a*). Therefore we conclude that $(\beta u - v)$ is constant along λ_1, and $(\beta u + v)$ is constant along λ_2. The quantities $(\beta u - v)$ and $(\beta u + v)$ are called *Riemann invariants* (Garabedian, 1964). Since these two quantities are constant along opposite pairs of characteristics, it is easy to determine u and v at a given point. If at a point (x, y) we know $(\beta u + v)$ and $(\beta u - v)$, we can immediately compute both u and v. An example illustrating this is in order.

Example 6.1 A uniform inviscid supersonic flow ($M_\infty = \sqrt{2}$) encounters a one-period sine wave wrinkle in the metal skin of a wind tunnel. The geometry of this configuration is shown in Fig. 6.2. The maximum amplitude of the sine wave is ϵ/L, where $\epsilon/L \ll 1$. Determine the solution for the perturbation velocities u and v using the method of characteristics.

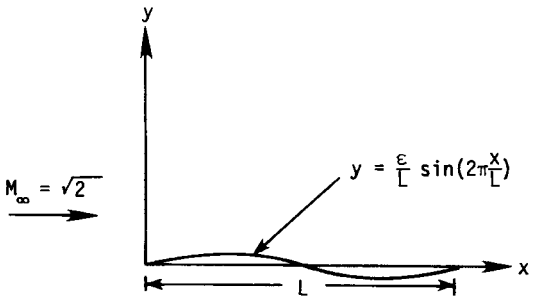

Figure 6.2 Wavy wall geometry.

Solution Since the flow is assumed to satisfy the small-perturbation assumption, the Prandtl-Glauert equation can be used. We choose to solve the system of equations [Eq. (6.3)] for the perturbation components u and v. In this case, $\beta^2 = 1$, and we solve the system of PDEs,

$$\frac{\partial u}{\partial x} - \frac{\partial v}{\partial y} = 0$$

$$\frac{\partial v}{\partial x} - \frac{\partial u}{\partial y} = 0$$

with initial data specified along $x = 0$, $y > 0$

$$u = 0$$
$$v = 0$$

subject to the surface boundary condition (see Section 6.7),

$$v = 2\pi U_\infty \frac{\epsilon}{L^2} \cos\left(2\pi \frac{x}{L}\right) \qquad 0 \leqslant x \leqslant L$$

Since the problem is two-dimensional and obeys the small-perturbation assumptions, we may apply the boundary conditions in the $y = 0$ plane. This makes the problem much easier.

We begin our characteristic solution by sketching the characteristics that originate at the initial data surface $x = 0$. Along the left running characteristics, we know that

$$\frac{dy}{dx} = 1 \qquad u - v = P = \text{const}$$

while along the other characteristic,

$$\frac{dy}{dx} = -1 \qquad u + v = Q = \text{const}$$

Therefore we determine u and v at any point as

$$u = \frac{P + Q}{2} \qquad v = \frac{Q - P}{2}$$

Since the right running characteristics that strike the surface originate in the free stream, the Q variable is initially zero. It is also true that $P = 0$ for those characteristics that originate in the free stream (see Fig. 6.3).

Consider the characteristic that strikes the wavy wall. An up or left running characteristic is introduced at that point in such a way that the surface boundary condition is satisfied. Thus at any station x_1, we have

$$Q = u + v = 0$$
$$v = \frac{2\pi\epsilon}{L^2} U_\infty \cos\left(2\pi \frac{x_1}{L}\right)$$

Therefore

$$u = -\frac{2\pi\epsilon}{L^2} U_\infty \cos\left(2\pi \frac{x_1}{L}\right)$$

and

$$P = u - v = -\frac{4\pi\epsilon}{L^2} U_\infty \cos\left(2\pi \frac{x_1}{L}\right)$$

The solution for u and v is constructed by marching outward from the initial data surface in the x direction. A grid with indices and the corresponding characteristics is shown in Fig. 6.4. The solution can now be obtained at the intersections of the characteristics. At point (1, 3),

$$P = 0$$
$$Q = 0$$
$$u = 0$$
$$v = 0$$

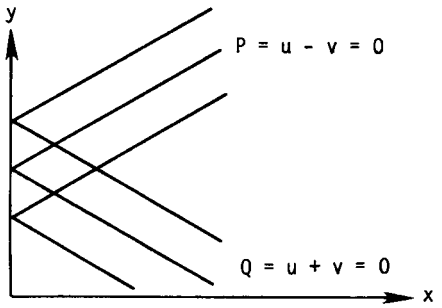

Figure 6.3 Initial data line.

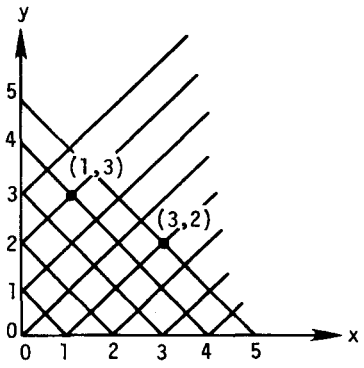

Figure 6.4 Characteristic net.

At (3, 2),

$$P = -\frac{4\pi\epsilon}{L^2} U_\infty \cos\left(2\pi \frac{x_1}{L}\right)$$

$$Q = 0$$

$$u = -\frac{2\pi\epsilon}{L^2} U_\infty \cos\left(2\pi \frac{x_1}{L}\right)$$

$$v = \frac{2\pi\epsilon}{L^2} \cos\left(2\pi \frac{x_1}{L}\right)$$

The solution is known everywhere in the domain of interest. The results of this example may be verified by solving the Prandtl-Glauert equation directly for the velocity potential and then computing the solution for u and v.

6.2.2 Nonlinear Systems of Equations

The development presented thus far is for a system of two linear equations and was chosen for its simplicity. In more complex nonlinear problems, the results are not as easily obtained. In the general case, the characteristic slopes are not constant but must vary as the fluid properties change. The governing PDEs may be nonhomogeneous. Clearly, the compatibility equations cannot be directly integrated in closed form along the characteristics in that case. For the general nonlinear problem, both the compatibility equations and the characteristic equations must be integrated numerically to obtain a complete flow field solution. Not only are the flow variables unknown, but the location in the field along the characteristics must be computed.

In order to illustrate the difference in applying the method of characteristics to a linear and a nonlinear problem, we consider the two-dimensional supersonic flow of a perfect gas over a flat surface. For simplicity, we choose a rectangular coordinate system and write the Euler equations (see Section 5.5) governing this

inviscid flow as the matrix system:

$$\frac{\partial \mathbf{w}}{\partial x} + [A]\frac{\partial \mathbf{w}}{\partial y} = 0 \tag{6.18}$$

where

$$\mathbf{w} = \begin{bmatrix} u \\ v \\ p \\ \rho \end{bmatrix}$$

and

$$[A] = \frac{1}{u^2 - a^2}\begin{bmatrix} uv & -a^2 & -\dfrac{v}{\rho} & 0 \\ 0 & \dfrac{v}{u}(u^2 - a^2) & \dfrac{u^2 - a^2}{\rho u} & 0 \\ -\rho v a^2 & \rho u a^2 & uv & 0 \\ -\rho v & \rho u & \dfrac{v}{u} & \dfrac{v}{u}(u^2 - a^2) \end{bmatrix}$$

The initial data, **I**, are prescribed and may be written as

$$\mathbf{w}(0, y) = \mathbf{I}(y) \qquad 0 \leqslant y \leqslant h$$

and the boundary conditions are

$$\begin{aligned} v(x,0) &= 0 \\ u(x,h) &= u_\infty \\ v(x,h) &= v_\infty \\ p(x,h) &= p_\infty \\ \rho(x,h) &= \rho_\infty \end{aligned}$$

The eigenvalues of $[A]$ determine the characteristic directions and must be found as the first step. These eigenvalues are

$$\lambda_1 = \frac{v}{u} \qquad \lambda_2 = \frac{v}{u}$$

$$\lambda_3 = \frac{uv + a\sqrt{u^2 + v^2 - a^2}}{u^2 - a^2} \qquad \lambda_4 = \frac{uv - a\sqrt{u^2 + v^2 - a^2}}{u^2 - a^2} \tag{6.19a}$$

The matrix of left eigenvectors associated with these values of λ may be written

$$[T]^{-1} = \begin{bmatrix} \dfrac{\rho u}{a^2} & \dfrac{\rho v}{a^2} & 0 & 1 \\ \rho u & \rho v & 1 & 0 \\ -\dfrac{1}{\sqrt{u^2+v^2-a^2}} & +\dfrac{u}{v}\dfrac{1}{\sqrt{u^2+v^2-a^2}} & \dfrac{1}{\rho v a} & 0 \\ \dfrac{1}{\sqrt{u^2+v^2-a^2}} & -\dfrac{u}{v}\dfrac{1}{\sqrt{u^2+v^2-a^2}} & \dfrac{1}{\rho v a} & 0 \end{bmatrix} \tag{6.19b}$$

We obtain the compatibility relations by premultiplying the original system by $[T]^{-1}$. These relations along the wave fronts are given by

$$-v\frac{du}{ds_3} + u\frac{dv}{ds_3} + \frac{\beta}{\rho}\frac{dp}{ds_3} = 0 \tag{6.20}$$

along

$$\frac{dy}{dx} = \lambda_3$$

and

$$v\frac{du}{ds_4} - u\frac{dv}{ds_4} + \frac{\beta}{\rho}\frac{dp}{ds_4} = 0 \tag{6.21}$$

along

$$\frac{dy}{dx} = \lambda_4$$

In these expressions,

$$\beta = \sqrt{M^2 - 1} \qquad M^2 = \frac{u^2 + v^2}{a^2}$$

Equation (6.20) is an ordinary differential equation, which holds along the characteristic with slope λ_3. Arc length along this characteristic is denoted by s_3. A similar result is expressed in Eq. (6.21). In contrast to our linear example using the Prandtl-Glauert equation, the analytic solution for the characteristics is not known for the general nonlinear problem. It is clear that we must numerically integrate to determine the shape of the characteristics in a step-by-step manner. Consider the characteristic defined by λ_3:

$$\frac{dy}{dx} = \frac{uv + a\sqrt{u^2+v^2-a^2}}{u^2 - a^2}$$

Starting at an initial data surface, this expression can be integrated to obtain the coordinates of the next point on the curve. At the same time, the differential equation defining the other wave front characteristic can be integrated. For a simple first-order integration, this provides us with two equations for the wave

front characteristics. From these expressions, we determine the coordinates of their intersection (point A in Fig. 6.5). Once the point A is known, the compatibility relations, Eqs. (6.20) and (6.21), are integrated along the characteristics to this point. This provides a system of equations for the unknowns at point A. Of course, auxiliary relationships are required to complete the problem, and these are provided by integrating the streamline compatibility equations or by using other valid equations relating the unknowns at A.

By using this procedure, a first-order estimate of both the location of point A and the associated flow variables can be obtained. These first-order estimates are usually used as a first step in a predictor-corrector scheme in calculating the solution to a system of hyperbolic PDEs using the method of characteristics. In the corrector step, a new intersection point B can be computed, which now includes the nonlinear nature of the characteristic curves. In a similar manner, the dependent variables at B are computed.

The calculation of the solution at point B presents an interesting problem. Because the problem is nonlinear, the final intersection point B does not necessarily appear at the same value of x for all solution points. Consequently, the solution is usually interpolated onto an x = const surface before the next integration step is started. This requires additional logic and adds considerably to the difficulty in structuring an accurate code.

The problem of integrating the compatibility equations and satisfying the boundary conditions at both permeable and impermeable boundaries is discussed in Section 6.7. It should be clear that the wall boundary condition is iterative in the sense that we attempt to satisfy a particular boundary condition at a point on a surface with an initially unknown x coordinate.

The two-dimensional (2-D) flow problem used in this section actually can be treated using characteristics in a much simpler setting (see Prob. 6.3). The main reason for this discussion is to present the ideas behind the numerical integration of the equations of motion using characteristic methods and to introduce some of the inherent difficulties in the general method. More complete descriptions are given by numerous authors, including Owczarek (1964), Shapiro (1953), and Courant and Friedrichs (1948).

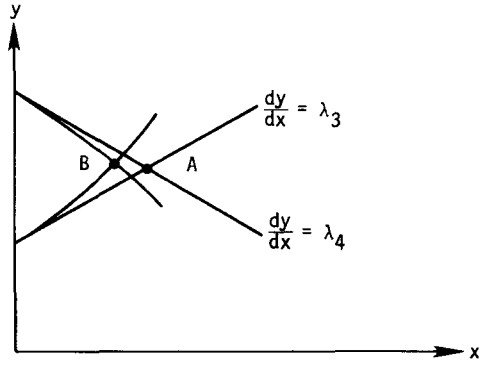

Figure 6.5 Characteristic solution point.

6.3 CLASSICAL SHOCK-CAPTURING METHODS

Shock-capturing schemes are the most widely used techniques for computing inviscid flows with shocks. In this approach the Euler equations are cast in conservation-law form, and any shock waves or other discontinuities are computed as part of the solution. The shock waves predicted by these methods are usually smeared over several mesh intervals, but the simplicity of the approach may outweight the slight compromise in results compared to the more elaborate shock-fitting schemes. Classical shock-capturing methods have the disadvantage that very strong shocks will cause the methods to fail. This failure is usually evidenced by oscillations. Computations in hypersonic flow with very strong shocks typically lead to the appearance of negative pressures and subsequent divergence of the solution during the time-dependent computation process. In addition to this problem, higher-order schemes tend to produce oscillations in the solution. However, these methods are useful and will be modified in later sections to avoid these difficulties. The alternative approach is to fit each shock wave as a discontinuity and solve for the discontinuity as part of the solution. This shock-fitting approach is very elegant and produces shocks that are truly discontinuous. Unfortunately, the procedure for general shock fitting in three dimensions with multiple shocks is extremely complex, and as a result, the use of shock fitting is usually limited to fitting shocks at boundaries.

In supersonic flow, when one boundary of the physical domain is a shock wave, shock fitting is frequently employed, and the shock shape is computed as part of the solution. Since boundary shocks can be fit with either the standard schemes discussed in this section or Section 6.7, the real advantage accrues when a complicated internal shock structure is captured and the special treatment of each shock wave is eliminated. This is a standard approach, where the outer boundary is fit when it is a shock wave and the internal shocks are captured. In this section, we will examine several simple shock-capturing schemes and apply them to example problems to gain experience in understanding the behavior of these numerical methods and interpreting the results that are produced when they are used.

Lax (1954) has shown that shock wave speed and strength are correctly predicted when the conservative form of the Euler equations is used. This means that the physically correct weak solution corresponding to the Rankine-Hugoniot equations for shocks is obtained if the conservation-law form is used and the equations are discretized in a conservative manner. In our study of Burgers' equation in Chapter 4, we saw that incorrect results were produced when the nonconservative form was used. While the nonconservative form of the Euler equations will have a weak solution, the solution depends upon the form of the equations used. In order that the solution satisfy the Rankine-Hugoniot equations, the conservative form must be used when we apply shock-capturing techniques.

As an example of conservation form, consider the supersonic flow of a perfect gas over a 2-D surface. If we assume the x axis forms the body surface

and is also the marching direction, the equations are given by the steady 2-D version of Eq. (5.192) and may be written

$$\frac{\partial \rho u}{\partial x} + \frac{\partial \rho v}{\partial y} = 0 \tag{6.22}$$

$$\frac{\partial (p + \rho u^2)}{\partial x} + \frac{\partial (\rho uv)}{\partial y} = 0 \tag{6.23}$$

$$\frac{\partial (\rho uv)}{\partial x} + \frac{\partial (p + \rho v^2)}{\partial y} = 0 \tag{6.24}$$

For a steady isoenergetic flow, the total enthalpy is constant. In this case, the differential energy equation can be integrated to give

$$H = \frac{\gamma}{\gamma - 1}\frac{p}{\rho} + \frac{u^2 + v^2}{2} = \text{const} \tag{6.25}$$

The system formed by Eqs. (6.22)–(6.24) in conjunction with the constant total enthalpy equation is hyperbolic for supersonic flow, and a solution can be obtained by marching or integrating the equations in the x direction starting from an initial data surface. The geometry for such a marching problem is shown in Fig. 6.6. Initial data are prescribed along the line $x = 0$, and the solution is advanced in the x direction subject to wall boundary conditions and an appropriate condition at $y_{\max}$.

Equations (6.22)–(6.24) are of the form

$$\frac{\partial \mathbf{E}}{\partial x} + \frac{\partial \mathbf{F}}{\partial y} = 0 \tag{6.26}$$

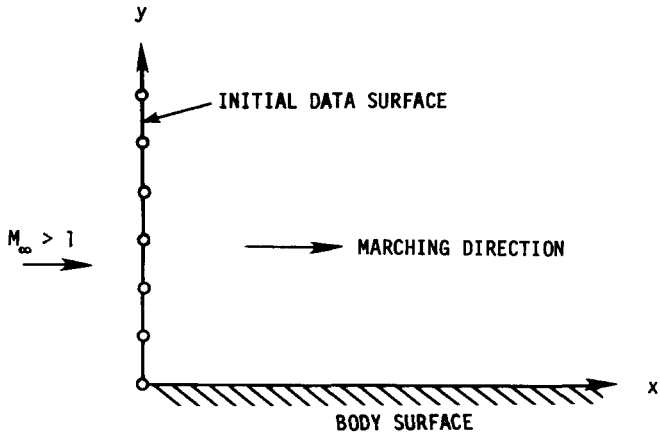

Figure 6.6 Coordinate system for marching problem.

where

$$\mathbf{E} = \begin{bmatrix} \rho u \\ p + \rho u^2 \\ \rho uv \end{bmatrix} \qquad \mathbf{F} = \begin{bmatrix} \rho v \\ \rho uv \\ p + \rho v^2 \end{bmatrix}$$

Equation (6.26) may be integrated with any of the methods presented in Chapter 4 for hyperbolic PDEs. If the forward predictor–backward corrector version of MacCormack's method is applied, Eq. (6.26) may be written

$$\mathbf{E}_j^{\overline{n+1}} = \mathbf{E}_j^n - \frac{\Delta x}{\Delta y}(\mathbf{F}_{j+1}^n - \mathbf{F}_j^n)$$

$$\mathbf{E}_j^{n+1} = \frac{1}{2}\left[\mathbf{E}_j^n + \mathbf{E}_j^{\overline{n+1}} - \frac{\Delta x}{\Delta y}\left(\mathbf{F}_j^{\overline{n+1}} - \mathbf{F}_{j-1}^{\overline{n+1}}\right)\right] \tag{6.27}$$

At the end of the predictor and corrector steps, $\mathbf{E}$ must be decoded to obtain the primitive variables. In this way, the new flux vector can be formed for the next integration step. After advancing the solution, the y component of velocity is immediately known as

$$v = \frac{E_3}{E_1}$$

where the subscripts denote elements of $\mathbf{E}$. A quadratic equation must be solved for the x component of the velocity. If we combine E_2 with the energy equation to eliminate p, we have

$$\rho = \frac{E_2}{u^2 + [(\gamma - 1)/2\gamma](2H - u^2 - v^2)}$$

We now eliminate ρ in favor of u by using

$$\rho = \frac{E_1}{u} \tag{6.28}$$

This yields a quadratic equation for u, which has roots

$$u = \frac{\gamma}{\gamma + 1}\frac{E_2}{E_1} \pm \sqrt{\left(\frac{\gamma}{\gamma + 1}\frac{E_2}{E_1}\right)^2 - \frac{\gamma - 1}{\gamma + 1}(2H - v^2)} \tag{6.29}$$

The correct sign on the radical is typically positive. The density can now be computed from E_1, and the pressure from E_2, as

$$p = E_2 - \rho u^2 \tag{6.30}$$

Having completed this process, $\mathbf{F}$ can be recalculated, and the next step in the integration can be implemented.

Example 6.2 Compute the flow field produced by a 2-D wedge moving at a Mach number of 2.0 if the wedge half angle is 15°. Assume inviscid flow of a perfect gas.

Solution The problem requires that we determine the shock wave location and strength as well as internal flow detail. The wedge and associated flow are shown in Fig. 6.7. In a 2-D wedge flow with an attached shock wave, the flow is conical. This means that flow properties along rays from the vertex of the wedge are constant (Anderson, 1982). This results in a simplification of the problem.

For this problem, the governing PDEs are given by Eqs. (6.22)–(6.24) and the energy equation [Eq. (6.25)]. The boundary conditions are the surface tangency requirement at the wedge surface and free stream conditions outside the shock wave. We recognize that we can select the x axis along the wedge surface and march the equations in this direction so long as the shock layer Mach number is greater than 1. Unfortunately, the shock layer expands as we move downstream, and this eventually causes our outer boundary point (at $y = y_{\max}$) to interfere with the shock wave.

The problem can easily be solved utilizing the fact that the shock wave is straight and that the thickness of the shock layer grows linearly with x. We introduce the independent variable transformation given by

$$\xi = x \qquad \eta = \frac{y}{x} \tag{6.31}$$

This provides the grid shown in Fig. 6.8. We can solve the wedge-flow problem with no difficulty now because the constant η lines grow linearly with x. Since the governing equations are hyperbolic in the ξ direction, initial data must be prescribed along some noncharacteristic surface. The line $\xi = 1$ is an easy choice. The PDEs are integrated in the ξ direction using arbitrarily assigned initial data. Since the solution to 2-D wedge flow is conical, the conical solution will be obtained for large ξ (asymptotically).

If the governing PDEs are transformed from (x, y) into (ξ, η) coordinates, they become

$$\frac{\partial \bar{\mathbf{E}}}{\partial \xi} + \frac{\partial \bar{\mathbf{F}}}{\partial \eta} = 0 \tag{6.32}$$

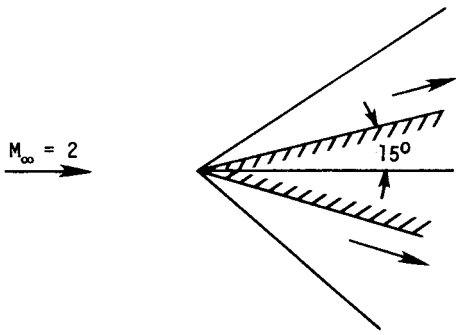

Figure 6.7 Wedge flow with attached shock.

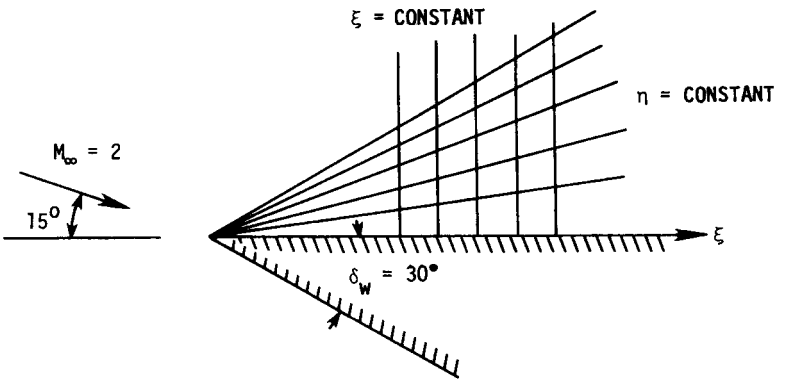

Figure 6.8 Wedge with transformed shock layer.

where

$$\bar{\mathbf{E}} = \xi \mathbf{E}$$

$$\bar{\mathbf{F}} = \mathbf{F} - \eta \mathbf{E}$$

An additional problem can be avoided by utilizing the conical flow property in this problem. The stability of the integration scheme used in solving Eq. (6.32) depends upon the eigenvalue structure of the $[A]$ matrix of the expanded system written in (ξ, η) coordinates.

$$\frac{\partial \mathbf{w}}{\partial \xi} + [A]\frac{\partial \mathbf{w}}{\partial \eta} + \mathbf{H} = 0 \tag{6.33}$$

In this expression, $\mathbf{w}$ is the vector of primitive variables and $\mathbf{H}$ is a source term that occurs in this expanded form. If the eigenvalues of $[A]$ are evaluated, they are found to depend explicitly on the ξ coordinate. That is, ξ appears in the expressions for the eigenvalues. As the solution is marched downstream in ξ, the allowable step size must change as ξ increases if an explicit method such as MacCormack's is used. If the step size did not change as ξ increased, a stability problem would occur. This problem can be avoided if we elect to integrate the equations from $\xi = 1$ to $\xi = 1 + \Delta\xi$ in an iterative manner until a converged solution is obtained.

The application of boundary conditions requires careful consideration. We must include enough points in the η direction so that the shock wave can form naturally and not be interfered with by the fixed free stream conditions, which are maintained at $\eta = \eta_{\max}$. For example, if our shock wave angle (measured from the wedge surface) is 20°, and we elect to use 10 points in the shock layer, then

$$\eta_{\text{shock}} = \tan(20°) = 0.3640$$

$$\Delta\eta = \frac{0.3640}{10 - 1} = 0.0404$$

Suppose we add an additional 5 points using this computed $\Delta\eta$; then

$$\eta_{max} = 0.0404(15 - 1) = 0.5662$$

and the last mesh point is at an angle of 29.52°. This should provide sufficient freedom for the shock wave to form without interference from the fixed boundary condition at η_{max}.

When predictor-corrector methods are used, one or both integration steps may require modification when applied at a solid boundary. For example, a MacCormack forward predictor can be directly applied at the wall but the backward corrector requires modification. One way to assure satisfaction of surface tangency is to also use a forward corrector and overwrite the decoded value of v at the wall with the boundary condition $v = 0$. While the use of forward differences in both the predictor and corrector is generally unstable, the wall boundary condition alters the stability in such a way as to provide a stable solution.

Typical shock-capturing pressure results for wedge flow are presented in Fig. 6.9. These results show an excellent solution, at a Courant number (ν) of one with a sharp shock wave, and very few oscillations. However, the same

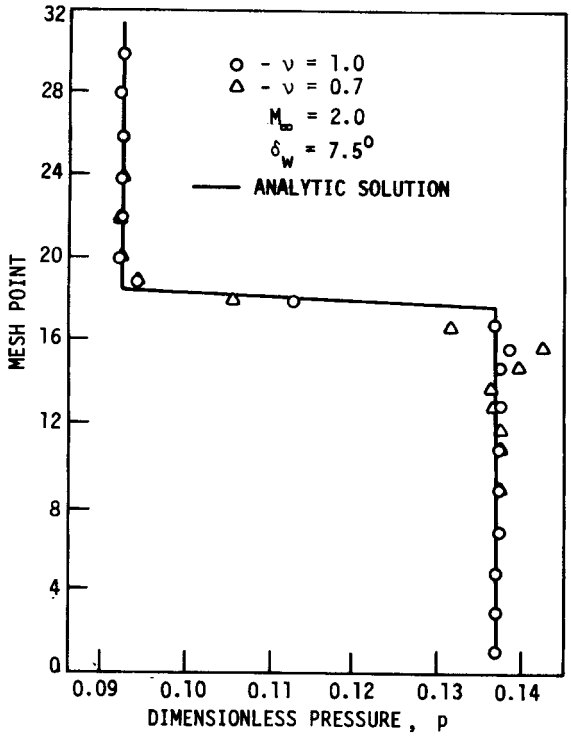

Figure 6.9 Shock-capturing pressure results for wedge flow.

calculation at a Courant number of 0.7 demonstrates the dispersive behavior of second-order methods previously discussed in Chapter 4.

Before we leave the wedge-flow problem, it is worthwhile to note that a solution could also have been obtained using a time-dependent formulation. If the governing PDEs are written in polar coordinates including the time terms, they are of the form

$$\frac{\partial \mathbf{E}}{\partial t} + \frac{\partial \mathbf{F}}{\partial \theta} + \frac{\partial \mathbf{G}}{\partial R} + \mathbf{H} = 0 \tag{6.34}$$

where the origin is at the vertex of the wedge and the vectors are the appropriate polar forms. If we assume a priori that the flow is conical, a solution can be computed in an $R = \text{const}$ plane if the radial derivatives are discarded. This requires a solution of the system

$$\frac{\partial \mathbf{E}}{\partial t} + \frac{\partial \mathbf{F}}{\partial \theta} + \mathbf{H} = 0 \tag{6.35}$$

This system is hyperbolic in time and can be integrated to attain a steady wedge-flow solution. In some ways, the time-dependent set is easier to use. For example, the decoding procedure is much simpler.

As in Example 6.2, the equations of motion are usually transformed into a computational domain. One of the more frequently used transformations is that of Viviand (1974) and Vinokur (1974). This transformation (see Section 5.6.2) assures us that a system of equations in a strong conservation-law form can be written in the same form after changing the independent variables. There may be disadvantages to Viviand's transformed equation form because the Jacobian of the mapping always appears in the denominator of the conservative variable terms. In order to avoid the introduction of errors through the geometry, special care must be taken in forming the metrics.

The difficulty encountered in using a simple rectangular mesh in Example 6.2 could have been eliminated if the shock wave was treated as a discontinuity. In fact, most shock-capturing codes fit boundary shock waves as discontinuities and capture interior shock waves as they develop. While the same philosophy of shock fitting holds for the steady flow marching problem as for time-dependent flows, a slightly different scheme is sometimes used to predict the interior or post-shock pressure when the conservative form of the original equations is used. Consider a system of PDEs of the form given in Eq. (6.26). Suppose we make use of a normalizing transformation,

$$(x, y) \rightarrow (\xi, \eta)$$

$$\xi = x \qquad \eta = \frac{y}{y_s(x)} \tag{6.36}$$

where $y - y_s(x) = 0$ is the equation for the position of the shock wave. As shown in Fig. 6.10, the physical domain is now transformed into a computational domain with the shock wave at $\eta = 1.0$. The conservation form for the governing

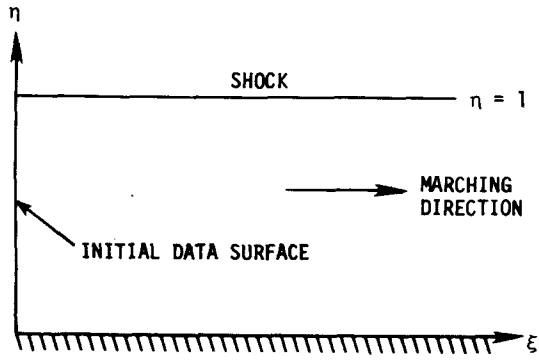

Figure 6.10 Normalizing transformation.

equations using such a transformation may be similar to Viviand's or any other form that conserves the appropriate flux terms. We again assume that the solution for the interior of the shock layer is advanced. At the shock wave, one-sided integration must be used to obtain an estimate for one of the variables. We assume initially that we know everything along an initial data surface, including the shock slope. We advance the solution on the interior, including the shock point. In addition, the shock slope equation (dy_s/dx) is integrated, providing an updated estimate of the new shock position. We now calculate the shock slope at the new location, and the dependent variables other than pressure can then be obtained.

If the pressure on the downstream side of the shock is known, we clearly can determine the density and both velocity components from the Rankine-Hugoniot equations. Our requirement is to develop the expression for shock slope. We write the surface equation of the shock wave as

$$y - y_s(x) = 0 \tag{6.37}$$

The shock normal is then written

$$\mathbf{n}_s = \frac{1}{\left[1 + (dy_s/dx)^2\right]^{1/2}}\left(-\mathbf{i}\frac{dy_s}{dx} + \mathbf{j}\right) \tag{6.38}$$

The normal component of velocity on the free stream side of the shock wave is given by

$$u_{\infty n} = \mathbf{n}_s \cdot \mathbf{V}_\infty = \frac{1}{\left[1 + (dy_s/dx)^2\right]^{1/2}}\left(-u_\infty \frac{dy_s}{dx} + v_\infty\right) \tag{6.39}$$

If this equation is solved for the shock slope, we obtain

$$(u_{\infty n}^2 - u_\infty^2)\frac{dy_s}{dx} = -u_\infty v_\infty \pm \sqrt{u_\infty^2 v_\infty^2 - (u_{\infty n}^2 - u_\infty^2)(u_{\infty n}^2 - v_\infty^2)} \tag{6.40}$$

The term $u_{\infty n}^2$ required in Eq. (6.40) is known from the pressure ratio across the shock as given in Eq. (5.209) and is

$$u_{\infty n}^2 = \frac{\gamma - 1}{2} \frac{p_\infty}{\rho_\infty} \left(1 + \frac{\gamma + 1}{\gamma - 1} \frac{p_2}{p_\infty} \right) \tag{6.41}$$

After the shock slope is computed, all quantities are known at the new location. The same procedure is repeated for both the predictor and corrector steps. We have again performed the shock fitting assuming the post-shock pressure (or other quantity) was known. This follows the approach suggested by Thomas et al. (1972).

Since we are examining methods for either time-dependent or steady supersonic inviscid flows, the governing equations are hyperbolic. Hyperbolic systems are often solved using explicit methods. However, the step size for most explicit schemes is limited by the CFL condition. This can lead to unreasonably long computation times for some problems. To overcome the step size limitation, implicit methods can be used. Examples of implicit algorithms that have been developed for the Euler equations include those of Lindemuth and Killeen (1973), Briley and McDonald (1973), and Beam and Warming (1976). The advantage of implicit methods lies in the unrestricted stability limit. Although more computational effort is required per time step compared to an explicit method, the overall time required to obtain a solution may be less. We will review the development of the basic scheme presented by Beam and Warming (1976) for the conservation form of the governing equations.

The basic system under consideration is of the form given in Eq. (5.192) and is repeated here for convenience:

$$\frac{\partial \mathbf{U}}{\partial t} + \frac{\partial \mathbf{E}}{\partial x} + \frac{\partial \mathbf{F}}{\partial y} = 0 \tag{6.42}$$

where $\mathbf{U}$ is the vector of conservative variables and $\mathbf{E}$ and $\mathbf{F}$ are vector functions of $\mathbf{U}$. If the trapezoidal rule given by Eq. (4.58) is used as the basic integration scheme, the value of $\mathbf{U}$ at the advanced time level is given by

$$\mathbf{U}^{n+1} = \mathbf{U}^n + \frac{\Delta t}{2} \left[\left(\frac{\partial \mathbf{U}}{\partial t} \right)^n + \left(\frac{\partial \mathbf{U}}{\partial t} \right)^{n+1} \right]$$

or

$$\mathbf{U}^{n+1} = \mathbf{U}^n - \frac{\Delta t}{2} \left[\left(\frac{\partial \mathbf{E}}{\partial x} + \frac{\partial \mathbf{F}}{\partial y} \right)^n + \left(\frac{\partial \mathbf{E}}{\partial x} + \frac{\partial \mathbf{F}}{\partial y} \right)^{n+1} \right] \tag{6.43}$$

This expression provides a second-order integration algorithm for the unknown vector $\mathbf{U}^{n+1}$ at the next time level. It is implicit because the derivatives of $\mathbf{U}$ as well as $\mathbf{U}$ appear at the advanced level, thus coupling the unknowns at neighboring grid points. A local Taylor-series expansion of the derivatives of $\mathbf{E}$

and $\mathbf{F}$ is used to obtain a linear equation that can be solved for $\mathbf{U}^{n+1}$. Let

$$\begin{aligned} \mathbf{E}^{n+1} &= \mathbf{E}^n + [A](\mathbf{U}^{n+1} - \mathbf{U}^n) \\ \mathbf{F}^{n+1} &= \mathbf{F}^n + [B](\mathbf{U}^{n+1} - \mathbf{U}^n) \end{aligned} \tag{6.44}$$

where $[A]$ and $[B]$ are defined:

$$[A] = \frac{\partial \mathbf{E}}{\partial \mathbf{U}} \qquad [B] = \frac{\partial \mathbf{F}}{\partial \mathbf{U}}$$

When the linearization given by Eq. (6.44) is substituted into Eq. (6.43), a linear system for $\mathbf{U}^{n+1}$ results and may be written as

$$\begin{aligned} &\left\{[I] + \frac{\Delta t}{2}\left(\frac{\partial}{\partial x}[A]^n + \frac{\partial}{\partial y}[B]^n\right)\right\}\mathbf{U}^{n+1} \\ &\quad = \left\{[I] + \frac{\Delta t}{2}\left(\frac{\partial}{\partial x}[A]^n + \frac{\partial}{\partial y}[B]^n\right)\right\}\mathbf{U}^n - \Delta t\left(\frac{\partial \mathbf{E}}{\partial x} + \frac{\partial \mathbf{F}}{\partial y}\right)^n \end{aligned} \tag{6.45}$$

This is a linear system for the unknown $\mathbf{U}^{n+1}$. Direct solution of Eq. (6.45) is usually avoided owing to the large operation count in treating multidimensional systems. The path usually chosen is to reduce the multidimensional problem into a sequence of one-dimensional inversions. This is done using the method of fractional steps (Yanenko, 1971) or the method of approximate factorization (Peaceman and Rachford, 1955; Douglas, 1955).

Equation (6.45) may be approximately factored into the equation

$$\begin{aligned} &\left([I] + \frac{\Delta t}{2}\frac{\partial}{\partial x}[A]^n\right)\left([I] + \frac{\Delta t}{2}\frac{\partial}{\partial y}[B]^n\right)\mathbf{U}^{n+1} \\ &\quad = \left([I] + \frac{\Delta t}{2}\frac{\partial}{\partial x}[A]^n\right)\left([I] + \frac{\Delta t}{2}\frac{\partial}{\partial y}[B]^n\right)\mathbf{U}^n - \Delta t\left(\frac{\partial \mathbf{E}}{\partial x} + \frac{\partial \mathbf{F}}{\partial y}\right)^n \end{aligned} \tag{6.46}$$

This expression differs from the original Eq. (6.45) by a term that is of $O[(\Delta t)^2]$, and the formal accuracy of our implicit algorithm is maintained as second order. This factored scheme may be written as the alternating direction sequence:

$$\begin{aligned} \left([I] + \frac{\Delta t}{2}\frac{\partial}{\partial x}[A]^n\right)\mathbf{U}' &= \text{RHS of Eq. (6.46)} \\ \left([I] + \frac{\Delta t}{2}\frac{\partial}{\partial y}[B]^n\right)\mathbf{U}^{n+1} &= \mathbf{U}' \end{aligned} \tag{6.47}$$

A simpler algorithm results if the delta form introduced in Chapter 4 is used. Since the operators on both sides of Eq. (6.46) are the same, define

$$\Delta \mathbf{U}^n = \mathbf{U}^{n+1} - \mathbf{U}^n$$

so that

$$\left([I] + \frac{\Delta t}{2}\frac{\partial}{\partial x}[A]^n\right)\left([I] + \frac{\Delta t}{2}\frac{\partial}{\partial y}[B]^n\right)\Delta \mathbf{U}^n = -\Delta t\left(\frac{\partial \mathbf{E}}{\partial x} + \frac{\partial \mathbf{F}}{\partial y}\right)^n \tag{6.48}$$

Again this may be replaced by the alternating direction sequence:

$$\begin{aligned}\left([I] + \frac{\Delta t}{2}\frac{\partial}{\partial x}[A]^n\right)\Delta \mathbf{U}' &= -\Delta t\left(\frac{\partial \mathbf{E}}{\partial x} + \frac{\partial \mathbf{F}}{\partial y}\right)^n \\ \left([I] + \frac{\Delta t}{2}\frac{\partial}{\partial y}[B]^n\right)\Delta \mathbf{U}^n &= \Delta \mathbf{U}'\end{aligned} \tag{6.49}$$

The solution of this system is not trivial. The x and y sweeps each require the solution of a block tridiagonal system of equations assuming the spatial derivatives are approximated by central differences. Each block is $m \times m$ if there are m elements in the unknown $\mathbf{U}$ vector (see Appendix B).

The implicit algorithm developed here used the trapezoidal rule. Generalized time differencing presented by Warming and Beam (1977) can be used to generate a number of implicit algorithms with varying accuracy. This point is discussed in Section 8.3.3. Additional consideration is presented on the required addition of artificial damping in conjunction with nondissipative schemes.

6.4 FLUX SPLITTING SCHEMES

In the previous section, classical shock-capturing methods using central differences were discussed. In this section the concept of *flux-vector splitting* is introduced. The underlying idea behind flux-vector splitting is to split the flux contributions into positive and negative components, where splitting is based on the eigenvalue structure of the system or some other appropriately assumed behavior. In presenting these methods, the view is taken that the fundamental problem that must be solved is to determine the correct flux at the boundaries of the control-volume faces. Interpretation of the numerical methods in terms of the control-volume surface fluxes for the various methods may also be considered in the sense of finite-difference schemes. Wherever this dual interpretation is appropriate, a comparison will be made.

To set the stage for the study of solutions of the Euler equation, consider a control volume as shown in Fig. 6.11. As previously discussed, the conservative form of the governing equations is integrated over the control volume. The 2-D Euler equations are given in Section 5.5.5 in the conservative form:

$$\frac{\partial \mathbf{U}}{\partial t} + \frac{\partial \mathbf{E}}{\partial x} + \frac{\partial \mathbf{F}}{\partial y} = 0 \tag{6.50}$$

where the conservative variables are defined in the usual way. Integrating this

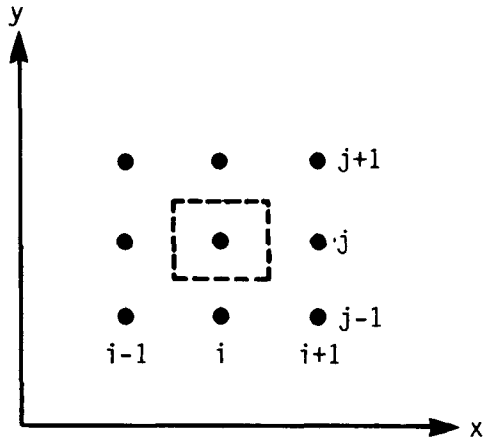

Figure 6.11 Control volume for Euler equations.

equation over the control volume yields the form

$$\int_{\delta v} \frac{\partial \mathbf{U}}{\partial t}\, dv + \int_{\delta v} \left(\frac{\partial \mathbf{E}}{\partial x} + \frac{\partial \mathbf{F}}{\partial y} \right) dv = 0 \tag{6.51}$$

Applying Green's Theorem (Taylor, 1955) to the second term converts this to a surface integral of the form

$$\int_{\delta v} \frac{\partial \mathbf{U}}{\partial t}\, dv + \oint_s (\mathbf{E}\, dy - \mathbf{F}\, dx) = 0 \tag{6.52}$$

where the subscript on the integral around the boundary is denoted by the small s. In discrete form the integration results in

$$\frac{\partial \mathbf{U}}{\partial t} \delta v + \sum_{\text{cell faces}} (\mathbf{E}\, \Delta y - \mathbf{F} \Delta x) = 0 \tag{6.53}$$

where the δv represents the volume of the cell and the Δx and Δy are the arc lengths of the cell sides for the 2-D case. The evaluation of the sum of the fluxes on the boundary requires that the flux values, i.e., the values of **E** and **F**, be known on the surface of the control volume. The evaluation of the flux terms on the control volume surfaces is the fundamental problem in the development of methods for solving the Euler equations.

6.4.1 Steger-Warming Splitting

Steger and Warming (1979) developed an implicit algorithm using a splitting of **E** and **F** in the governing equations. This is similar to the Beam scheme studied earlier in the work of Sanders and Prendergast (1974). In splitting the flux terms, the flux is assumed to be composed of a positive and a negative component. For illustration, consider a 1-D problem where the Euler system

under investigation has the form

$$\frac{\partial \mathbf{U}}{\partial t} + \frac{\partial \mathbf{E}}{\partial x} = 0 \tag{6.54}$$

This system can also be written in the form

$$\frac{\partial \mathbf{U}}{\partial t} + [A]\frac{\partial \mathbf{U}}{\partial x} = 0 \tag{6.55}$$

where $[A]$ is the Jacobian $\partial \mathbf{E}/\partial \mathbf{U}$. This system is hyperbolic if a similarity transformation exists so that

$$[T]^{-1}[A][T] = [\lambda] \tag{6.56}$$

where $[\lambda]$ is a diagonal matrix of real eigenvalues of $[A]$ and $[T]^{-1}$ is the matrix whose rows are the left eigenvectors of $[A]$ taken in order.

According to Steger and Warming, if the equation of state is of the form

$$p = \rho f(e) \tag{6.57}$$

where e is the internal energy, then the flux vector $\mathbf{E}(\mathbf{U})$ is a homogeneous function of degree one in $\mathbf{U}$, which means that

$$\mathbf{E}(\alpha \mathbf{U}) = \alpha \mathbf{E}(\mathbf{U}) \tag{6.58}$$

for any α. This permits the flux vectors $\mathbf{E}$ and $\mathbf{F}$ of the Euler equations to be written in the form

$$\mathbf{E} = [A]\mathbf{U} \tag{6.59}$$

We can use this property and the fact that the system is hyperbolic to achieve the desired split flux form.

Combining Eqs. (6.56) and (6.59), $\mathbf{E}$ may be written

$$\mathbf{E} = [A]\mathbf{U} = [T][\lambda][T]^{-1}\mathbf{U} \tag{6.60}$$

The matrix of eigenvalues is divided into two matrices, one with only positive elements and the other with negative elements. We write the $[A]$ matrix as

$$[A] = [A^+] + [A^-] = [T][\lambda^+][T]^{-1} + [T][\lambda^-][T]^{-1} \tag{6.61}$$

and define

$$\mathbf{E} = \mathbf{E}^+ + \mathbf{E}^- \tag{6.62}$$

so that

$$\mathbf{E}^+ = [A^+]\mathbf{U} \qquad \mathbf{E}^- = [A^-]\mathbf{U} \tag{6.63}$$

The original conservation-law form written using the split-flux notation becomes

$$\frac{\partial \mathbf{U}}{\partial t} + \frac{\partial \mathbf{E}^+}{\partial x} + \frac{\partial \mathbf{E}^-}{\partial x} = 0 \tag{6.64}$$

where the plus and minus signs indicate that the flux components are associated with wave propagation in the positive and negative directions, respectively. The key point is that the flux vector $\mathbf{E}$ can be split into a positive part and a negative part, each associated with the signal propagation directions. The eigenvalues of

$\partial \mathbf{E}^{\pm}/\partial \mathbf{U}$ are not the same as $\lambda^{\pm}$, but the correct sign is preserved. For the 1-D case, the eigenvalues of $[A]$ are the familiar streamline and signal propagation terms written as

$$\lambda_1 = u$$
$$\lambda_2 = u + a$$
$$\lambda_3 = u - a$$

For the supersonic case, with u positive, $\lambda^+ = \lambda$ and $\lambda^- = 0$. For the subsonic case, both λ^+ and λ^- are nonzero. For subsonic flow,

$$[\lambda^+] = \begin{bmatrix} u & & \\ & u + a & \\ & & 0 \end{bmatrix} \tag{6.65a}$$

and

$$[\lambda^-] = \begin{bmatrix} 0 & & \\ & 0 & \\ & & u - a \end{bmatrix} \tag{6.65b}$$

The associated split-flux terms are

$$\mathbf{E}^- = \frac{1}{2}\frac{\rho}{\gamma}(u - a)\begin{bmatrix} 1 \\ u - a \\ \frac{1}{2}(u - a)^2 + \frac{1}{2}a^2\left(\frac{3 - \gamma}{\gamma - 1}\right) \end{bmatrix} \tag{6.66a}$$

and

$$\mathbf{E}^+ = \mathbf{E} - \mathbf{E}^- = \frac{1}{2}\frac{\rho}{\gamma}\begin{bmatrix} (2\gamma - 1)u + a \\ 2(\gamma - 1)u^2 + (u + a)^2 \\ (\gamma - 1)u^3 + \frac{1}{2}(u + a)^3 + \frac{1}{2}a^2\frac{3 - \gamma}{\gamma - 1}(u + a) \end{bmatrix} \tag{6.66b}$$

A first-order upwind scheme is easily constructed with this split-flux idea. A simple integration of the equations for a 1-D problem may be written

$$\mathbf{U}_i^{n+1} = \mathbf{U}_i^n - \frac{\Delta t}{\Delta x}(\mathbf{E}_{i+\frac{1}{2}} - \mathbf{E}_{i-\frac{1}{2}}) \tag{6.67}$$

In this setting, the cell-face values of the flux are composed of both + and − components according to the splitting, i.e.,

$$\mathbf{E}_{i+\frac{1}{2}} = (\mathbf{E}^+ + \mathbf{E}^-)_{i+\frac{1}{2}} \tag{6.68}$$

For a first-order calculation the flux components may be evaluated with an extrapolation consistent with the expressions given in Section 4.4.11 for the MUSCL scheme, where the primitive variables were extrapolated to the cell faces. In the Steger-Warming splitting, the fluxes are extrapolated to the cell faces. However, the MUSCL approach with primitive variables may also be used in this splitting. In the simplest case, the values of $\mathbf{E}^+_{i+\frac{1}{2}}$ are set equal to $\mathbf{E}^+_i$, and

the values of $\mathbf{E}^-_{i+\frac{1}{2}}$ are set equal to $\mathbf{E}^-_{i+1}$. This produces a numerical algorithm of the form

$$\mathbf{U}_i^{n+1} = \mathbf{U}_i^n - \frac{\Delta t}{\Delta x}[(\mathbf{E}^+ + \mathbf{E}^-)_{i+\frac{1}{2}} - (\mathbf{E}^+ + \mathbf{E}^-)_{i-\frac{1}{2}}]$$

or

$$\mathbf{U}_i^{n+1} = \mathbf{U}_i^n - \frac{\Delta t}{\Delta x}(\nabla \mathbf{E}_i^+ + \Delta \mathbf{E}_i^-) \tag{6.69}$$

This is the finite-difference form of Eq. (6.64) when the $\mathbf{E}^+$ derivative is backward differenced and the $\mathbf{E}^-$ term is forward differenced. Based on earlier discussions, the equivalence of the finite-difference and the finite-volume formulations is clear.

A second-order algorithm may be developed by using the trapezoidal scheme given in Section 4.1.10. The integration in time is written

$$\mathbf{U}_i^{n+1} = \mathbf{U}_i^n + \frac{\Delta t}{2}\left[\left(\frac{\partial \mathbf{U}}{\partial t}\right)_i^n + \left(\frac{\partial \mathbf{U}}{\partial t}\right)_i^{n+1}\right] \tag{6.70}$$

where the term $\partial \mathbf{U}^{n+1}/\partial t$ is interpreted as a predicted value for an explicit scheme and is included as part of the computed solution for an implicit technique. In the application of this scheme the derivative at n is written in terms of the fluxes on the surface of the control volume just as in the first-order method. However, the flux terms evaluated at the control-volume surfaces must be second order in space if the result is to be used in the first term of the trapezoidal integration scheme. This can easily be accomplished by noting that the second-order flux is obtained by using the upwind extrapolation formula given in Section 4.4.11. A second-order spatial calculation requires that a linear extrapolation be used for the primitive variables. Here $\mathbf{u}$ represents the vector of primitive variables, and the extrapolation for the positive terms is written

$$\mathbf{u}^+_{i-\frac{1}{2}} = \mathbf{u}_{i-1} + \psi^+(r^+)\tfrac{1}{2}(\mathbf{u}_{i-1} - \mathbf{u}_{i-2}) \tag{6.71}$$

while for the negative terms,

$$\mathbf{u}^-_{i+\frac{1}{2}} = \mathbf{u}_{i+1} + \psi^-(r^-)\tfrac{1}{2}(\mathbf{u}_{i+2} - \mathbf{u}_{i+1}) \tag{6.72}$$

From these extrapolations, the split fluxes may be reformed for the terms in the integration. The $\psi^\pm$ terms are the same limiters presented in Section 4.4.12, and any of the limiters discussed may be used. Split flux schemes will also produce oscillations when higher-order algorithms are constructed, so limiting is necessary. The final algorithm for the second-order upwind scheme may be

written in the following two-step sequence:

$$\mathbf{U}_i^{\overline{n+1}} = \mathbf{U}_i^n - \frac{\Delta t}{\Delta x}(\nabla \mathbf{E}_i^+ + \Delta \mathbf{E}_i^-) \tag{6.73}$$

$$\mathbf{U}_i^{n+1} = \frac{1}{2}\left[\mathbf{U}_i^n + \mathbf{U}_i^{\overline{n+1}} - \frac{\Delta t}{\Delta x}\left(\nabla^2 \mathbf{E}_i^{+n} + \nabla \mathbf{E}_i^{+\overline{n+1}}\right) + \frac{\Delta t}{\Delta x}\left(\Delta^2 \mathbf{E}_i^{-n} - \Delta \mathbf{E}_i^{-\overline{n+1}}\right)\right] \tag{6.74}$$

The 2-D version of this scheme follows with the addition of the appropriate terms.

An implicit algorithm using the trapezoidal rule is easily derived using the split-flux idea, and a first-order spatial scheme takes the form

$$\left([I] + \frac{\Delta t}{2\,\Delta x}(\nabla[A_i^+] + \Delta[A_i^-])\right)\Delta \mathbf{U}_i^n = -\frac{\Delta t}{\Delta x}(\nabla \mathbf{E}^+ + \Delta \mathbf{E}^-) \tag{6.75}$$

where

$$\Delta \mathbf{U}_i^n = \mathbf{U}_i^{n+1} - \mathbf{U}_i^n$$

This is written in the delta form introduced in Section 4.4.7. This algorithm is first-order accurate in space even though it is second-order accurate in time. The spatial accuracy can be improved by simply increasing the order of the spatial operators. Frequently, interest is in the steady-state solution. If this is the case, the right-hand side can be modified to obtain second-order accuracy in space for the steady-state result without altering the block tridiagonal structure of the left-hand side. It is interesting to note that an approximate factorization of the left-hand side of Eq. (6.75) is possible, resulting in the product of two operators

$$\left([I] + \frac{1}{2}\frac{\Delta t}{\Delta x}\nabla[A_i^+]\right)\left([I] + \frac{1}{2}\frac{\Delta t}{\Delta x}\Delta[A_i^-]\right)\Delta \mathbf{U}_i^n = \text{RHS of Eq. (6.75)} \tag{6.76}$$

This permits the algorithm to be implemented in the sequence

$$\left([I] + \frac{1}{2}\frac{\Delta t}{\Delta x}\nabla[A_i^+]\right)\Delta \mathbf{U}_i^* = \text{RHS of Eq. (6.75)} \tag{6.77a}$$

$$\left([I] + \frac{1}{2}\frac{\Delta t}{\Delta x}\Delta[A_i^-]\right)\Delta \mathbf{U}_i^n = \Delta \mathbf{U}_i^* \tag{6.77b}$$

If Eqs. (6.77*a*) and (6.77*b*) are used, each 1-D sweep requires the solution of two block bidiagonal systems. The original system [Eq. (6.75)] requires the solution of a single block tridiagonal system for each time step. It is important to note that savings expected in using Eqs. (6.77*a*) and (6.77*b*) may not be realized for all problems. Usually, the major advantage of using the split form with bidiagonal systems occurs in multidimensional cases.

The use of split-flux techniques for shock-capturing applications produces better results than central-difference methods, but some problems remain even

for this formulation. Using the Steger-Warming splitting, the shock waves are well represented, but some oscillations are produced when a sonic condition is encountered. The problem is that the components of the split flux are not continuously differentiable at sonic and stagnation points. Figure 6.12 shows the split mass flux behavior as the sonic region is traversed. Steger and Warming (1981) attempted to eliminate this problem by modifying the eigenvalues when they change signs to be of the form

$$\lambda^{\pm} = \frac{\lambda \pm \sqrt{\lambda^2 + \epsilon^2}}{2} \tag{6.78}$$

where ϵ is viewed as a blending function to ensure a smooth transition when the λ's change sign. This modification was only moderately successful, and more appropriate schemes employing flux-vector splitting evolved later.

6.4.2 Van Leer Flux Splitting

The problems encountered at sonic transitions and at stagnation points with the Steger-Warming splitting were addressed by van Leer (1982). He proposed a different splitting, defined so that the flux terms were continuously differentiable through sonic and stagnation zones. The conditions van Leer imposed to accomplish a flux splitting were

1. $\mathbf{E} = \mathbf{E}^+ + \mathbf{E}^-$,
2. $\partial \mathbf{E}^+ / \partial \mathbf{U}$ must have all eigenvalues $\geqslant 0$, and
3. $\partial \mathbf{E}^- / \partial \mathbf{U}$ must have all eigenvalues $\leqslant 0$,

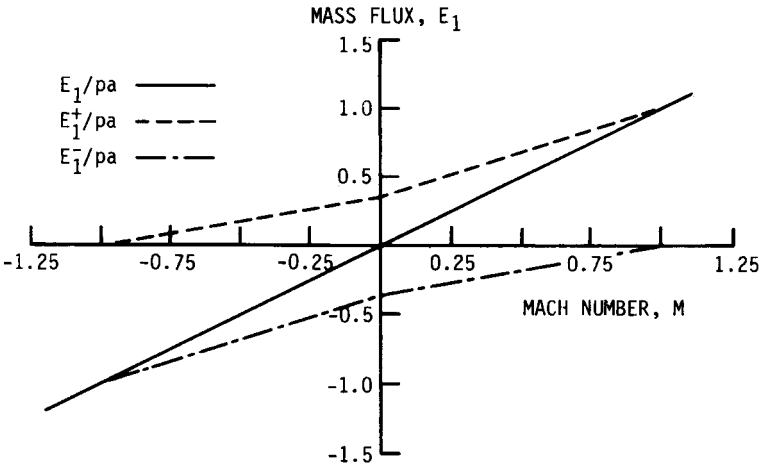

Figure 6.12 Split mass flux using Steger-Warming splitting.

with the following restrictions:

1. $\mathbf{E}^{\pm}$ must be continuous with

$$\mathbf{E}^{+} = \mathbf{E}(\mathbf{U}) \qquad M \geqslant 1$$
$$\mathbf{E}^{-} = \mathbf{E}(\mathbf{U}) \qquad M \leqslant -1$$

2. The components of $\mathbf{E}^{+}, \mathbf{E}^{-}$ must exhibit the same symmetry as $\mathbf{E}$ in terms of Mach number. For each component,

$$\mathbf{E}^{+} = \pm\mathbf{E}^{-}(-M)$$

if

$$\mathbf{E}(M) = \pm\mathbf{E}(-M)$$

3. The Jacobians $\partial\mathbf{E}^{\pm}/\partial\mathbf{U}$ must be continuous.
4. The Jacobians $\partial\mathbf{E}^{\pm}/\partial\mathbf{U}$ must have one eigenvalue vanish for $|M| < 1$.
5. $\mathbf{E}^{\pm}$ must be a polynomial in Mach number of lowest possible order.

Conditions 1 and 2 ensure that this splitting procedure produces the standard upwind differences in supersonic flow. Restrictions 1–3 provide symmetry and eliminate the problem at sonic and stagnation points associated with the Steger-Warming scheme. The fourth restriction ensures that a stationary shock with two interior zones can be constructed, while the last restriction is included to provide uniqueness of the splitting.

For a 1-D problem in (x, t) the van Leer fluxes may be written

$$\mathbf{E}^{+} = \frac{1}{4}\rho a(M+1)^2 \begin{bmatrix} 1 \\ \dfrac{2a}{\gamma}\left(1 + \dfrac{\gamma - 1}{2}M\right) \\ \dfrac{2a^2}{\gamma^2 - 1}\left(1 + \dfrac{\gamma - 1}{2}M\right)^2 \end{bmatrix} \tag{6.79a}$$

$$\mathbf{E}^{-} = \mathbf{E} - \mathbf{E}^{+} \tag{6.79b}$$

The flux terms as presented in Eqs. (6.79) satisfy the constraints of the van Leer splitting and are continuously differentiable at sonic and stagnation points. Splitting for the multidimensional case is accomplished in the same manner as in one dimension with the addition of the necessary flux components.

Both flux splitting schemes have proved to be dissipative (van Leer, 1990, 1992), and some questions have been raised about the various splitting ideas. Van Leer et al. (1987) pointed out that the splitting he proposed does not identify contact surfaces and, in some cases, leads to large dissipation. This is especially apparent in viscous regions, where large errors may occur (see Anderson et al., 1985). Hanel et al. (1987) and Hanel and Schwane (1989) observed that the original flux splitting of van Leer does not preserve total enthalpy in solutions of the steady Euler equations. They proposed a modification

of the energy flux component by writing

$$\mathbf{E}^{\pm}_{\text{energy}} = \pm\tfrac{1}{4}\rho a(M \pm 1)^2 H(u^{\pm}) \tag{6.80}$$

where the total enthalpy H is now included in the split-flux terms.

An additional modification due to Hanel and Schwane (1989) employs upwinding of the transverse momentum flux. While these changes have been shown to improve the dissipation at contact surfaces, and prevent artificial thickening of boundary layers, some problems still appear in computing wall temperatures for viscous flows. Van Leer (1990) applied the Hanel and Schwane (1989) upwind idea to the energy flux in an attempt to resolve this issue.

6.4.3 Other Flux Splitting Schemes

Other ideas for splitting the Euler equations have been suggested. A recent example is provided by the work of Liou and Steffen (1991). They have presented a new scheme, where the pressure and convection terms are treated separately. The flux-vector splitting technique of Liou and Steffan has been dubbed by them the *advection upstream splitting method* (AUSM). The inviscid flux terms are viewed as a combination of scalar quantities convected by an appropriately defined cell interface velocity, and the pressure terms are treated as being governed only by the acoustic wave speeds. The inviscid 1-D flux term is written as

$$\mathbf{E} = \begin{bmatrix} \rho u \\ \rho u^2 \\ u(E_t + p) \end{bmatrix} + \begin{bmatrix} 0 \\ p \\ 0 \end{bmatrix} \tag{6.81}$$

or

$$\mathbf{E} = \mathbf{E}_c + \mathbf{E}_p \tag{6.82}$$

where the subscripts denote convection terms and pressure terms. These terms are discretized differently. The interface fluxes for supersonic flow are selected by taking either the left (L) and right (R) state, depending on the sign of the Mach number. The subsonic case needs a more careful evaluation. For this case, Liou and Steffan have suggested that

$$(\mathbf{E}_c)_{i+1/2} = u_{\frac{1}{2}} \begin{bmatrix} \rho \\ \rho u \\ E_t + p \end{bmatrix}_{L/R} \tag{6.83}$$

where

$$\frac{L}{R} = \begin{cases} L & u_{\frac{1}{2}} > 0 \\ R & \text{otherwise} \end{cases} \tag{6.84}$$

The quantity $u_{\frac{1}{2}}$ is referred to as the advective velocity, and numerous choices exist for defining this value to be used at the cell interface. Liou and Steffan

have suggested that

$$u_{\frac{1}{2}} = a_{L/R} M_{\frac{1}{2}} \tag{6.85}$$

where

$$M_{\frac{1}{2}} = M_L^+ + M_R^- \tag{6.86}$$

and the split Mach numbers for the left and right states use the van Leer definitions

$$M^{\pm} = \pm \tfrac{1}{4}(M \pm 1)^2 \tag{6.87}$$

The interface convective flux terms become

$$(\mathbf{E}_c)_{i+1/2} = M_{\frac{1}{2}} \begin{bmatrix} \rho a \\ \rho u a \\ a(E_t + p) \end{bmatrix}_{L/R} \tag{6.88}$$

The pressure is written as the sum of left and right contributions:

$$p_{\frac{1}{2}} = p_L^+ + p_R^- \tag{6.89}$$

A number of representations can be used for the terms composing $p_{\frac{1}{2}}$. The simplest presented was given as

$$p^{\pm} = \tfrac{1}{2} p(1 \pm M) \tag{6.90}$$

In fact, the splittings used for both the pressure and convection terms can be accomplished in many ways. Unfortunately, the approach that proves to work best is not always clear, and numerous numerical experiments are necessary to explore the effectiveness of a numerical scheme. The fact that there is no unique way to accomplish the flux splitting provides ample opportunity to develop new ideas for solving the Euler equations. The flux splittings presented in this section each have some issues that are unresolved. The Steger-Warming scheme has been modified to eliminate the problems at the stagnation and sonic conditions, with limited success. The van Leer scheme seem to be too dissipative except for use in the solution of the Euler equations, and the AUSM scheme appears to be sensitive to the pressure evaluation. Van Leer (1992) has suggested that split-flux schemes only be applied to the Euler equations because of the dissipative nature of the methods currently available. Work on construction of new schemes that are improvements on existing methods is expected to continue. The work of Zha and Bilgen (1993) is an example.

In the construction of the second-order schemes, the MUSCL approach has been used to extrapolate the primitive variables to the cell interface rather than the fluxes. Anderson et al. (1985) has performed a series of numerical experiments with results that indicate that extrapolation of the primitive variables and reconstruction of the flux give better flow solutions. Based on these results, it is advisable to use primitive-variable extrapolation and flux reconstruction at the cell boundaries wherever practical.

6.4.4 Application for Arbitrarily Shaped Cells

In the previous sections, no information was given regarding the shapes of the control volumes. However, it is usually implicitly assumed that the mesh is structured and the cells in a physical domain are quadrilateral. A significant amount of interest has recently surfaced in applying solvers to cells with arbitrary shapes and in using unstructured grids.

The integration of the conservation law presented in Eq. (6.53) is general and applies to any cell. The conserved variable resulting from the application of the divergence theorem to a control volume is a cell-averaged value, as previously noted in Chapter 4. Calculating the flux values at the cell boundaries may require careful consideration when the cells are of arbitrary shape.

Recently, the use of triangular cells has gained popularity. In this case, the flow variables may be computed for a cell-centered scheme or a vertex (node)-centered scheme. When using finite-volume schemes, it is natural to consider a cell-centered approach. Consider the mesh shown in Fig. 6.13. Each cell is triangular, and the cell-centered conservative variables depend upon careful estimates of the boundary fluxes for accuracy.

If a first-order method is used to solve the Euler equations, the primitive variables at the cell face may be quickly obtained by simple extrapolation of the cell values to the faces using the appropriate upwind directions. Of course, the estimation of the cell-face values and techniques to determine these from the cell-averaged values must be applied not only for split-flux methods but for any numerical method applied on this type of grid. The determination of the required values is more complicated when a higher-order approximation is desired.

Consider a cell-centered scheme and assume that we seek a linear extrapolation of the primitive variables to the control-volume faces in order to obtain second-order accuracy. The centroidal values are known, but gradient information is needed to complete the extrapolation. Let u represent any scalar primitive variable, and consider the cell face value given by

$$u_{cf} = u_i + \nabla u_i \cdot (\mathbf{r}_{cf} - \mathbf{r}_i) \tag{6.91}$$

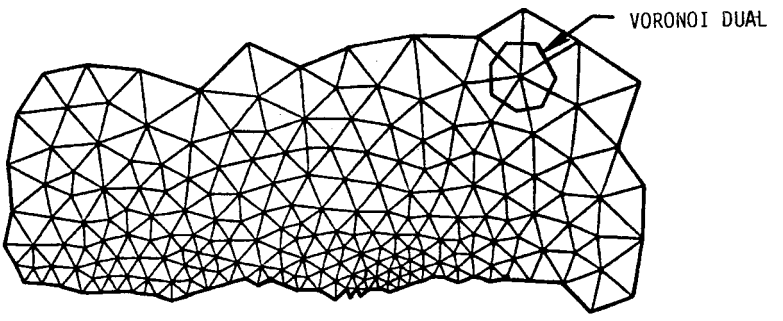

Figure 6.13 Unstructured mesh with triangular cells.

This is a first-order Taylor series expression representing the cell-face values in terms of the cell averages. The term $\mathbf{r}_{cf} - \mathbf{r}_i$ represents the distance from the cell centroid to the midpoint of the cell face, and ∇u_i is the gradient of u_i. The product of these two terms represents the directional derivative toward the cell face midpoint times the distance to the midpoint. In order to evaluate this expression, a way of computing the gradient is needed.

A common technique to establish the gradient (Barth, 1991) is to compute the gradients at the vertices of the cell and use these values to establish a value to use in the extrapolation. For triangular cells a simple average of the vertex gradients is one way of establishing the required value. The vertex values of the gradients are most easily established by using a mesh dual. A Delaunay mesh (Delaunay, 1934) is shown in Fig. 6.13, and the Voronoi dual (Voronoi, 1908) is an appropriate choice for this case. A description of the mesh construction and terminology is given in Chapter 10. It is sufficient for our purposes to use the mesh as given in Fig. 6.13. At any node, an evaluation of the gradient may be made by applying the identity

$$\int_{\delta v} \nabla u \, \delta v = \oint_s u\mathbf{n} \, dl \tag{6.92}$$

to the cell formed by the dual, where $\mathbf{n}$ represents the unit normal to the cell surface. When applied in a discrete sense, this takes the form

$$\nabla u = \frac{1}{\delta v} \sum_s u\mathbf{n} \, \Delta \mathbf{s} \tag{6.93}$$

With this expression, any component of the gradient may be evaluated at the nodal locations in the mesh. Once these values are known, the gradients at the cell centroids may be computed.

This procedure may be used for cell-centered schemes for arbitrary mesh configurations. In calculating higher-order solutions, the gradient terms are limited in the same way as previously indicated. Figure 6.14 shows an NACA 0012 airfoil with the associated unstructured mesh. The corresponding transonic solution for the pressure field is shown in Fig. 6.15. In these calculations a van Leer split-flux scheme was used, and the solver was second order. The pressure data are compared with the calculations of Anderson et al. (1985). In solving the Euler equations on an unstructured mesh, significantly more computational effort and a larger number of cells are probably required to produce the same solution quality when compared to a solution computed on a structured mesh. This is a problem of some concern, but increasing availability of low-cost memory and improved processor speed suggest that storage and speed may not continue to be major problems.

6.5 FLUX-DIFFERENCE SPLITTING SCHEMES

The main challenge in constructing methods for solving the Euler equations is to find ways of estimating the flux terms at the control-volume faces. Several flux-splitting schemes were reviewed in the previous section and were interpreted

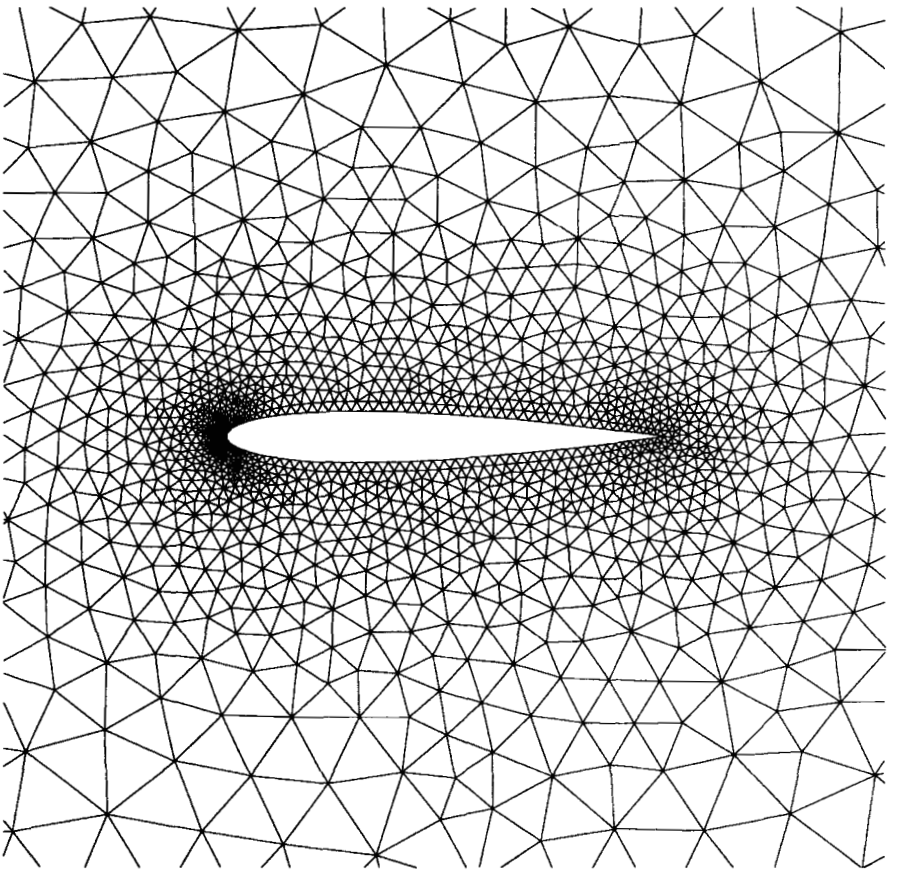

Figure 6.14 Unstructured grid for NACA 0012 airfoil.

as schemes that transport particles according to the characteristic information (van Leer, 1990). In contrast, the changes in the flux quantities at the cell interface using *flux-difference splitting* have been interpreted as being caused by a series of waves. The wave interpretation is derived from the characteristic field of the Euler equations. The problem of computing the cell-face fluxes for a control volume is viewed as a series of 1-D Riemann problems along the direction normal to the control-volume faces. One way of determining these fluxes is to solve the Riemann problem using Godunov's method as outlined in Section 4.4.8 for the 1-D Burgers equation. Of course, the solution in the present case would be for a generalized problem with arbitrary initial states. The original Godunov method has been substantially improved by employing a variety of techniques to accelerate the solution of the nonlinear wave problem (Gottleib and Growth, 1988). Because some of the details of the exact solution, obtained at considerable cost, are lost in the cell-averaged representation of the

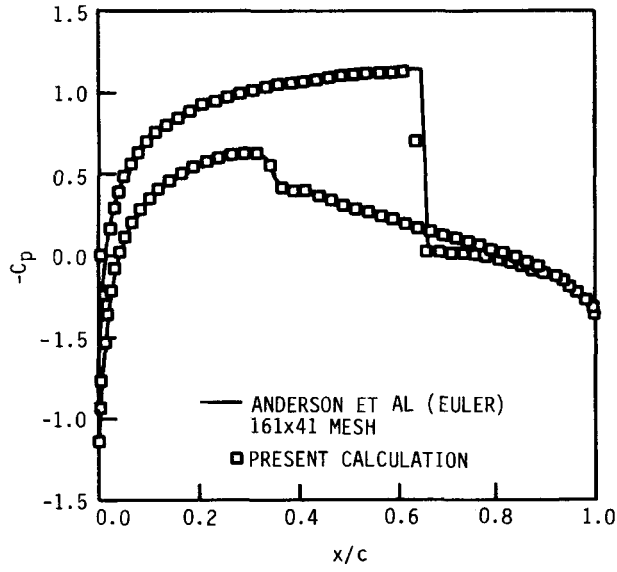

Figure 6.15 Pressure contours for NACA 0012 airfoil in transonic flow. $M = 0.80$, $\alpha = 1.25°$.

data, the solution of the full Riemann problem is usually replaced by methods referred to as approximate Riemann solvers. The Roe method (Roe, 1980) and the Osher scheme (Osher, 1984) are the most well known of these schemes. Owing to its simplicity, the Roe scheme and its many variations have evolved as the method of choice among flux-difference splitting schemes. In the next section, Roe's scheme will be discussed as applied to the Euler equations. This technique is another way of calculating the flux values at the control-volume boundaries in the finite-volume approach.

6.5.1 Roe Scheme

In view of the fact that the Riemann problem requires a solution of a nonlinear system, a significant gain in efficiency can be realized if a solution to a linear problem approximating the original Riemann problem can be obtained. This is the basis for Roe's scheme. Consider the original Riemann problem in the form

$$\frac{\partial \mathbf{U}}{\partial t} + \frac{\partial \mathbf{E}}{\partial x} = 0 \tag{6.94a}$$

$$\mathbf{U}(x,0) = \begin{cases} \mathbf{U}_L & x < 0 \\ \mathbf{U}_R & x > 0 \end{cases} \tag{6.94b}$$

The notation for the left and right states has been used previously in Chapter 4. Roe's linear approximation to the Riemann problem is written

$$\frac{\partial \mathbf{U}}{\partial t} + [\hat{A}]\frac{\partial \mathbf{U}}{\partial x} = 0 \tag{6.95}$$

where the initial conditions are the same as those in the nonlinear problem and $[\hat{A}]$ is Roe's averaged matrix and is assumed to be a constant in this formulation. Recall that the original Jacobian was defined by

$$[A] = \frac{\partial \mathbf{E}}{\partial \mathbf{U}} \tag{6.96}$$

The Jacobian matrix is replaced by $[\hat{A}]$ in this system. The components of the $[\hat{A}]$ matrix are evaluated using averaged values of $\mathbf{U}$ at the interface separating the two states. This is indicated by writing

$$[\hat{A}] = \left[\hat{A}(\mathbf{U}_L, \mathbf{U}_R)\right] \tag{6.97}$$

The Roe-averaged matrix $[\hat{A}]$ is chosen to satisfy certain conditions, so that a solution of the linear problem becomes an approximate solution of the nonlinear Riemann problem. These conditions include the following.

1. A linear mapping relates the vector space $\mathbf{U}$ to the vector space $\mathbf{E}$.
2. As $\mathbf{U}_L$ approaches $\mathbf{U}_R$, i.e., as an undisturbed state is reached,

   $$\left[\hat{A}(\mathbf{U}_L, \mathbf{U}_R)\right] \Rightarrow [A]$$

   when

   $$\mathbf{U}_L \rightarrow \mathbf{U}_R \rightarrow \mathbf{U}$$

   where $[A]$ is the Jacobian of the original system.
3. For any two values $\mathbf{U}_L, \mathbf{U}_R$, the jump condition across the interface must be correct, i.e.,

   $$\mathbf{E}_R - \mathbf{E}_L = [\hat{A}](\mathbf{U}_R - \mathbf{U}_L)$$

4. The eigenvalues of $[\hat{A}]$ are real and linearly independent.

Consider the system of equations given by Eq. (6.95). This is a hyperbolic system that may be diagonalized by writing the constant matrix $[\hat{A}]$ as

$$[\hat{A}] = [\hat{T}][\hat{\Lambda}][\hat{T}]^{-1} \tag{6.98}$$

The original equations can then be cast in the form

$$\frac{\partial \mathbf{U}}{\partial t} + [\hat{T}][\hat{\Lambda}][\hat{T}]^{-1}\frac{\partial \mathbf{U}}{\partial x} = 0 \tag{6.99}$$

Premultiplying by $[\hat{T}]^{-1}$ and defining the vector $\mathbf{W}$ as

$$\mathbf{W} = [\hat{T}]^{-1}\mathbf{U} \tag{6.100}$$

leads to the linear problem

$$\frac{\partial \mathbf{W}}{\partial t} + [\hat{\Lambda}]\frac{\partial \mathbf{W}}{\partial x} = 0 \tag{6.101}$$

where the matrix of eigenvalues $[\hat{\Lambda}]$ is a diagonal matrix. This produces an uncoupled hyperbolic system. The numerical method may be applied to each of the uncoupled equations of this system, and the result transformed back to the original variables. For a single linear equation, the value of W is constant along the characteristic defined by $dx/dt = \lambda_k$. As each of the waves associated with the eigenvalues of the system is crossed, the values of the dependent variables experience a jump. Consequently, the values of W_k are constant between each pair of waves in the domain. Mathematically, this can be stated as

$$W_k = \text{const}$$

when

$$\lambda_{k-1} \leqslant \frac{x}{t} \leqslant \lambda_k$$

Consequently, the value of $\mathbf{W}$ at any point may be written

$$W_k = W_1 + \sum_{j=2}^{k} (W_j - W_{j-1}) \tag{6.102}$$

Again, since $[\hat{A}]$ is a constant matrix, we may write

$$U_k = U_1 + \sum_{j=2}^{k} (U_j - U_{j-1}) \tag{6.103}$$

and the final result is that the flux changes may be written

$$E_k = E_1 + \sum_{j=2}^{k} \delta E_j \tag{6.104}$$

where the flux increments are associated with the crossing of each wave in the system.

If the entire wave system is traversed and the left and right states are identified with appropriate subscripts, then

$$\mathbf{E}_R = \mathbf{E}_L + [\hat{A}](\mathbf{U}_R - \mathbf{U}_L) \tag{6.105}$$

As shown in the previous section, the $[\hat{A}]$ matrix may be split, corresponding to changes that occur across negative and positive waves. Consequently, we may split the calculation of the fluxes into contributions across negative and positive waves to determine appropriate formulas for the cell-face fluxes in the linear Riemann problem. Referring to Fig. 6.16, one notes that the interface flux can be computed by starting at either the left or the right state.

Starting at the left state, we can write

$$\begin{aligned} \tilde{E}_{i+\frac{1}{2}} &= \mathbf{E}_L + [\hat{A}^-](\mathbf{U}_R - \mathbf{U}_L) \\ \mathbf{E}_R &= \tilde{E}_{i-\frac{1}{2}} + [\hat{A}^+](\mathbf{U}_R - \mathbf{U}_L) \end{aligned} \tag{6.106a}$$

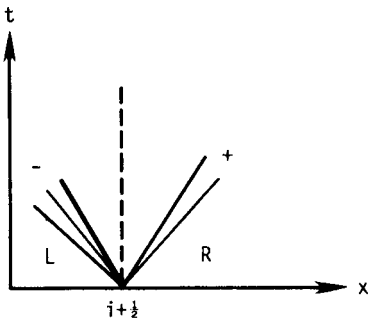

Figure 6.16 Decomposed flux for the linear Riemann problem.

or, as is usually written, the two expressions for the interface flux become

$$\begin{aligned} \tilde{E}_{i+\frac{1}{2}} &= \mathbf{E}_L + [\hat{A}^-](\mathbf{U}_R - \mathbf{U}_L) \\ \tilde{E}_{i+\frac{1}{2}} &= \mathbf{E}_R - [\hat{A}^+](\mathbf{U}_R - \mathbf{U}_L) \end{aligned} \tag{6.106b}$$

A symmetric result is used in applications of computational fluid dynamics, and this may be obtained by averaging the cell-face flux formulas to obtain the following appropriate expression:

$$\tilde{E}_{i+\frac{1}{2}} + \tfrac{1}{2}\{(\mathbf{E}_R + \mathbf{E}_L) - [|\hat{A}|](\mathbf{U}_R - \mathbf{U}_L)\} \tag{6.107}$$

In this equation, $[|\hat{A}|] = [\hat{T}][|\hat{\Lambda}|][\hat{T}]^{-1}$ and $[|\hat{\Lambda}|]$ is the diagonal matrix whose entries are the absolute values of the eigenvalues. The numerical flux expression incorporates upwind influence through the addition of contributions across positive and negative waves. Condition 3 and the subsequent expressions for the interface flux given by Eqs. (6.106) show that the change across any wave depends upon the change in state variables across all waves. This point can be noted by recalling that a diagonalization of the system leads to uncoupled equations providing the changes across each wave in a modified set of variables derived by multiplication by $[\hat{T}]^{-1}$. When the flux values are recovered by multiplying by $[\hat{T}]$, the change in flux across each wave is seen to depend upon the change in $\mathbf{U}$ across the entire system of waves.

The Roe-averaged matrix may be constructed by noting that $\mathbf{U}$ and $\mathbf{E}$ are quadratic functions of the variable $\mathbf{z}$, defined as

$$\mathbf{z} = \sqrt{\rho}\begin{bmatrix} 1 \\ u \\ H \end{bmatrix} \tag{6.108}$$

The conservative variables may be written in terms of the $\mathbf{z}$ variable as

$$\mathbf{U} = \begin{bmatrix} z_1^2 \\ z_1 z_2 \\ \dfrac{z_1 z_3}{\gamma} + \dfrac{1}{2}\dfrac{\gamma - 1}{\gamma} z_2^2 \end{bmatrix} \tag{6.109}$$

where the vector of conservative variables $\mathbf{U}$ is defined by Eq. (5.44) for the 1-D case where $v = w = 0$. The flux term may also be written as

$$\mathbf{E} = \begin{bmatrix} z_1 z_2 \\ \dfrac{\gamma - 1}{\gamma} z_1 z_3 + \dfrac{1}{2} \dfrac{\gamma + 1}{\gamma} z_2^2 \\ z_2 z_3 \end{bmatrix} \tag{6.110}$$

We define the arithmetic average of any quantity with an overbar symbol in the following manner

$$\bar{x}_{i+\frac{1}{2}} = \tfrac{1}{2}(x_i + x_{i+1})$$

and note the exact expansion formula:

$$\Delta(xy)_{i+\frac{1}{2}} = \bar{x}_{i+\frac{1}{2}} \Delta y_{i+\frac{1}{2}} + \bar{y}_{i+\frac{1}{2}} \Delta x_{i+\frac{1}{2}} \tag{6.111}$$

Applying this expansion formula results in conservative variable and flux formulas of the form

$$\mathbf{U}_{i+1} - \mathbf{U}_i = [B](\mathbf{z}_{i+1} - \mathbf{z}_i) \tag{6.112}$$

and

$$\mathbf{E}_{i+1} - \mathbf{E}_i = [C](\mathbf{z}_{i+1} - \mathbf{z}_i) \tag{6.113}$$

where

$$[B] = \begin{bmatrix} 2\bar{z}_1 & 0 & 0 \\ \bar{z}_2 & \bar{z}_1 & 0 \\ \dfrac{\bar{z}_3}{\gamma} & \dfrac{\gamma - 1}{\gamma} \bar{z}_2 & \dfrac{\bar{z}_1}{\gamma} \end{bmatrix} \tag{6.114}$$

and

$$[C] = \begin{bmatrix} \bar{z}_2 & \bar{z}_1 & 0 \\ \dfrac{\gamma - 1}{\gamma} \bar{z}_3 & \dfrac{\gamma + 1}{\gamma} \bar{z}_2 & \dfrac{\gamma - 1}{\gamma} \bar{z}_1 \\ 0 & \bar{z}_3 & \bar{z}_2 \end{bmatrix} \tag{6.115}$$

with the result that

$$\mathbf{E}_{i+1} - \mathbf{E}_i = [C][B]^{-1}(\mathbf{U}_{i+1} - \mathbf{U}_i) \tag{6.116}$$

The matrix $[C][B]^{-1}$ is identical to the Jacobian matrix $[A]$ if the original variables are replaced by an average weighted by the square root of the density. If

$$R_{i+\frac{1}{2}} = \sqrt{\frac{\rho_{i+1}}{\rho_i}} \tag{6.117}$$

then

$$\hat{\rho}_{i+\frac{1}{2}} = R_{i+\frac{1}{2}}\rho_i \tag{6.118}$$

$$\hat{u}_{i+\frac{1}{2}} = \frac{R_{i+\frac{1}{2}}u_{i+1} + u_i}{1 + R_{i+\frac{1}{2}}} \tag{6.119}$$

$$\hat{H}_{i+\frac{1}{2}} = \frac{R_{i+\frac{1}{2}}H_{i+1} + H_i}{1 + R_{i+\frac{1}{2}}} \tag{6.120}$$

where the quantity $\hat{H}$ is the averaged total enthalpy and H is defined by

$$H = \frac{E_t + p}{\rho} \tag{6.121}$$

The development of the averaged matrix has used the so-called parameter vector approach. This "Roe-averaged state" may be directly obtained by solving Eq. (6.105) for the state variables. This follows because the correct averaged matrix is the only one that will provide the correct relationship satisfying these equations. For further details, the reader should consult Roe and Pike (1985).

The numerical flux for the first-order Roe scheme is then written in the form

$$\tilde{\mathbf{E}}_{i+\frac{1}{2}} = \tfrac{1}{2}\left\{\mathbf{E}_i + \mathbf{E}_{i+1} - \left[\hat{T}_{i+\frac{1}{2}}\right]\left[|\hat{\Lambda}_{i+\frac{1}{2}}|\right]\left[\hat{T}_{i+\frac{1}{2}}\right]^{-1}(\mathbf{U}_{i+1} - \mathbf{U}_i)\right\} \tag{6.122}$$

This may be used to calculate a first-order solution using the standard explicit or implicit techniques for advancing the solution in time. In this formula, the problem of expansion shocks must be considered. By way of review, recall that the formulation of the Roe scheme admits an expansion shock as a perfectly appropriate solution of the approximate problem. As a consequence, stationary expansion shocks are not dissipated by this method. An appropriate entropy fix, but one that does not distinguish between shocks and expansions, is easily implemented by replacing the components of $[|\hat{\Lambda}|]$ by $\beta(\hat{\lambda}^l_{i+\frac{1}{2}})$, where

$$\left[|\hat{\Lambda}_{i+\frac{1}{2}}|\right] = \begin{bmatrix} |\hat{\lambda}^1_{i+\frac{1}{2}}| & 0 & 0 \\ 0 & |\hat{\lambda}^2_{i+\frac{1}{2}}| & 0 \\ 0 & 0 & |\hat{\lambda}^3_{i+\frac{1}{2}}| \end{bmatrix} \tag{6.123}$$

and

$$\beta(\hat{\lambda}) = \begin{cases} |\hat{\lambda}| & |\hat{\lambda}| \geqslant \epsilon \\ (\hat{\lambda}^2 + \epsilon^2)/2\epsilon & |\hat{\lambda}| < \epsilon \end{cases} \tag{6.124}$$

In this set of expressions, the Roe average is implied by the circumflex symbol with subscript $i + \frac{1}{2}$.

While the explicit methods described in previous sections may be used with the Roe scheme, more details on the implementation of implicit schemes using flux-difference splitting (FDS) are in order. Consider a simple Euler implicit

scheme resulting in the expression

$$\mathbf{U}_i^{n+1} = \mathbf{U}_i^n - \frac{\Delta t}{\Delta x}\left(\tilde{\mathbf{E}}_{i+\frac{1}{2}}^{n+1} - \tilde{\mathbf{E}}_{i-\frac{1}{2}}^{n+1}\right) \tag{6.125}$$

Define the residual $\mathbf{R}$ as

$$\mathbf{R} = \frac{1}{\Delta x}\left(\tilde{\mathbf{E}}_{i+\frac{1}{2}} - \tilde{\mathbf{E}}_{i-\frac{1}{2}}\right) \tag{6.126}$$

In terms of the residual, the scheme may be written

$$\left(\frac{[I]}{\Delta t} + \frac{\partial \mathbf{R}}{\partial \mathbf{U}}\right)(\mathbf{U}_i^{n+1} - \mathbf{U}_i^n) = -\mathbf{R}_i^n \tag{6.127}$$

where the linearization of the equations is performed as in the previous section with flux-vector splitting (FVS) implicit schemes and $[I]$ represents the identity matrix. Implicit schemes result in coupled systems that must be solved simultaneously, and the structure of the coefficient matrices of the system is important. The elements of $\partial \mathbf{R}/\partial \mathbf{U}$ result in filling the ith row of the coefficient matrix with a bandwidth corresponding to the functional dependence of $\mathbf{R}_j$ on $\mathbf{U}_i$, i.e.,

$$\frac{\partial \mathbf{R}_j}{\partial \mathbf{U}_{i-1}}, \frac{\partial \mathbf{R}_j}{\partial \mathbf{U}_i}, \frac{\partial \mathbf{R}_j}{\partial \mathbf{U}_{i+1}}, \text{ etc.} \tag{6.128}$$

Barth (1987) has considered exact linearizations as indicated here and an additional linearization, leading to what he has called the "frozen" matrix scheme, given by

$$\left(\frac{[I]}{\Delta t} + [M]^n\right)(\mathbf{U}_i^{n+1} - \mathbf{U}_i^n) = -\mathbf{R}_i^n = -[M]^n \mathbf{U}_i^n \tag{6.129}$$

The idea of the frozen matrix scheme is that various alterations of the $[M]$ matrix may be used. If one is only interested in a steady-state result, any approach that causes the residual to vanish (as rapidly as possible) is appropriate.

For illustration, consider an FDS scheme with a first-order Roe flux:

$$\tilde{\mathbf{E}}_{i+\frac{1}{2}} = \tfrac{1}{2}\left\{\mathbf{E}_i + \mathbf{E}_{i+1} - [T][|\Lambda|][T]^{-1}\delta \mathbf{U}_{i+\frac{1}{2}}\right\} \tag{6.130}$$

As a simplification in the notation, let the dissipation term be given as

$$\Delta|\tilde{\mathbf{E}}_{i+\frac{1}{2}}| = [T][|\Lambda|][T]^{-1}\delta \mathbf{U}_{i+\frac{1}{2}} \tag{6.131}$$

With this notation, the residual vector for the Roe FDS may be written

$$\mathbf{R}_i = \frac{1}{2\,\Delta x}\left[\mathbf{E}_{i+1} - \mathbf{E}_{i-1} - \left(\Delta|\tilde{\mathbf{E}}_{i+\frac{1}{2}}| - \Delta|\tilde{\mathbf{E}}_{i-\frac{1}{2}}|\right)\right] \tag{6.132}$$

and the exact local linearization of the Jacobian produces elements of the form

$$\frac{\partial \mathbf{R}_i}{\partial \mathbf{U}_{i+1}} = \frac{1}{2\,\Delta x}\left([A_{i+1}] - \frac{\partial \Delta|\tilde{\mathbf{E}}_{i+\frac{1}{2}}|}{\partial \mathbf{U}_{i+1}}\right) \tag{6.133a}$$

$$\frac{\partial \mathbf{R}_i}{\partial \mathbf{U}_i} = \frac{1}{2\,\Delta x}\left(-\frac{\partial \Delta|\tilde{\mathbf{E}}_{i+\frac{1}{2}}|}{\partial \mathbf{U}_i} + \frac{\partial \Delta|\tilde{\mathbf{E}}_{i-\frac{1}{2}}|}{\partial \mathbf{U}_i}\right) \tag{6.133b}$$

$$\frac{\partial \mathbf{R}_i}{\partial \mathbf{U}_{i-1}} = \frac{1}{2\,\Delta x}\left(-[A_{i-1}] + \frac{\partial \Delta|\tilde{\mathbf{E}}_{i-\frac{1}{2}}|}{\partial \mathbf{U}_{i-1}}\right) \tag{6.133c}$$

FVS and FDS produce different evaluations for terms like $\partial \Delta|\mathbf{E}|/\partial \mathbf{U}$. In order to understand this difference, the FVS idea can be employed in a setting where the numerical flux is represented in a form similar to the FDS approach. The linearizations then require treatment of similar terms for both techniques. For the FDS scheme,

$$\frac{\partial \Delta|\tilde{\mathbf{E}}_{i+\frac{1}{2}}|}{\partial \mathbf{U}_{i+1}} = |A_{i+\frac{1}{2}}| + \frac{\partial |A_{i+\frac{1}{2}}|}{\partial \mathbf{U}_{i+1}}(\mathbf{U}_{i+1} - \mathbf{U}_i) \tag{6.134}$$

while the equivalent calculation for the FVS schemes is

$$\frac{\partial \Delta|\tilde{\mathbf{E}}_{i+\frac{1}{2}}|}{\partial \mathbf{U}_{i+1}} = |A_{i+1}| + \frac{\partial |A_{i+1}|}{\partial \mathbf{U}_{i+1}}\mathbf{U}_{i+1} \tag{6.135}$$

In both of these approaches, the second terms involve differentiation of matrix elements and then matrix multiplication. Note the second term of the FDS linearization is multiplied by the difference in $\mathbf{U}$. This would suggest that for reasonable changes in $\mathbf{U}$, the second term of the FDS linearization is smaller than that produced using FVS. Consequently, linearization errors produced will also be smaller. The effect of the use of these approximate linearizations on convergence rate has been examined by Barth (1987) and by Jesperson and Pulliam (1983). Their results show better convergence properties in time asymptotic calculations for a variety of steady-state problems using FDS schemes. Other linearizations have been considered by Harten (1984), Chakravarthy and Osher (1985), and numerous others. However, the linearizations presented here for either exact or approximate cases, where the second terms are neglected, are conservative and will provide satisfactory results.

6.5.2 Second-Order Schemes

Several different techniques are used to extend FDS methods to higher order. The MUSCL idea has been explored and used with success in Chapter 4 and in the section on flux-vector splitting. Yee (1989) has constructed a framework where both MUSCL and non-MUSCL approaches to higher-order schemes can be described through similar numerical flux functions. The numerical flux for

the non-MUSCL approach may be written

$$\tilde{\mathbf{E}}_{i+\frac{1}{2}} = \frac{1}{2}\left\{\mathbf{E}_i + \mathbf{E}_{i+1} + \left[\hat{T}_{i+\frac{1}{2}}\right]\hat{\mathbf{\Phi}}_{i+\frac{1}{2}}\right\} \tag{6.136}$$

and the corresponding form for the MUSCL approach is

$$\tilde{\mathbf{E}}_{i+\frac{1}{2}} = \frac{1}{2}\left\{\mathbf{E}\left(\mathbf{U}^r_{i+\frac{1}{2}}\right) + \mathbf{E}\left(\mathbf{U}^l_{i+\frac{1}{2}}\right) + \left[\hat{T}_{i+\frac{1}{2}}\right]\hat{\mathbf{\Phi}}_{i+\frac{1}{2}}\right\} \tag{6.137}$$

The $[\hat{T}]$ matrix is evaluated at some average such as the Roe average, and the elements of $\hat{\mathbf{\Phi}}$ are the same as the scalar case, but each element is evaluated with the same symmetric average. In the MUSCL approach, the average state between i and $i + 1$ is replaced by the right and left states, as indicated in the MUSCL extrapolation. Limiting is accomplished by reducing (limiting) the slopes in the extrapolation to cell faces. The dissipation term is written in terms of the limited variables and, in general, includes an entropy fix. The construction of the numerical flux in this form permits one to limit the wave strengths in the non-MUSCL approach (Roe, 1984) rather than restrict the slopes using the MUSCL idea. It is argued that this is a better interpretation of the physics. When this idea is implemented, the limiters are slightly different, but the general form of the flux function can be written the same way.

The form of $\hat{\mathbf{\Phi}}$ may be written

$$\hat{\mathbf{\Phi}}_{i+\frac{1}{2}} = \left[|\hat{\Lambda}_{i+\frac{1}{2}}|\right]\left[\hat{T}_{i+\frac{1}{2}}\right]^{-1}(\mathbf{U}_{i+1} - \mathbf{U}_i) \tag{6.138}$$

where the wave strengths are given by

$$\boldsymbol{\alpha}_{i+\frac{1}{2}} = \left[\hat{T}_{i+\frac{1}{2}}\right]^{-1}(\mathbf{U}_{i+1} - \mathbf{U}_i) \tag{6.139}$$

With this notation, the form of the last term in the numerical flux, using the idea of local characteristics, may be written

$$\left[\hat{T}_{i+\frac{1}{2}}\right]\hat{\mathbf{\Phi}}_{i+\frac{1}{2}} = \left[\hat{T}_{i+\frac{1}{2}}\right]\left[|\hat{\Lambda}_{i+\frac{1}{2}}|\right]\boldsymbol{\alpha}_{i+\frac{1}{2}} \tag{6.140}$$

The form of $\hat{\mathbf{\Phi}}$ now is in terms of the wave strengths, and the general description of this term for the various methods will appear in terms of the wave strengths and the appropriate limiters.

A second-order Roe scheme using the MUSCL idea was used to solve Burgers' equation in Section 4.4.11. In that case, the limiting was applied to the variables extrapolated to the cell faces. For the non-MUSCL approach the limiting is applied through the dissipation term. A non-MUSCL second-order Roe-Sweby scheme may be developed where the elements of $\hat{\mathbf{\Phi}}$ take the form

$$\left(\hat{\mathbf{\Phi}}^l_{i+\frac{1}{2}}\right)^R = -\left\{|\lambda^l_{i+\frac{1}{2}}| - \frac{\psi(r^l)}{2}\left[|\lambda^l_{i+\frac{1}{2}}| - \frac{\Delta t}{\Delta x}\left(\lambda^l_{i+\frac{1}{2}}\right)^2\right]\right\}\alpha^l_{i+\frac{1}{2}} \tag{6.141}$$

In this expression the definition of r^l is

$$r^l = \frac{w^l_{i+1+\zeta} - w^l_{i+\zeta}}{w^l_{i+1} - w^l_i} \tag{6.142}$$

where w^l are components of the characteristic variable vector $\mathbf{W}$ and ζ is defined as the sgn(λ). The limiter $\psi(r^l)$ may be any of the limiters previously discussed in Section 4.4.12. The limiter is expressed in terms of the characteristic variables with this formulation.

Another method arrived at by the characteristic variable extension was originally developed by Harten (1984) and later modified by Yee (1986). The elements of $\hat{\mathbf{\Phi}}$ for this second-order upwind scheme are written

$$\left(\phi^l_{i+\frac{1}{2}}\right)^{\mathrm{HY}} = \sigma\left(\lambda^l_{i+\frac{1}{2}}\right)\left(g^l_{i+1} - g^l_i\right) - \psi\left(\lambda^l_{i+\frac{1}{2}} + \gamma^l_{i+\frac{1}{2}}\right)\alpha^l_{i+\frac{1}{2}} \tag{6.143}$$

The definition of σ is

$$\sigma(s) = \frac{1}{2}\left[\beta(s) - \frac{\Delta t}{\Delta x}s^2\right] \tag{6.144}$$

and

$$\gamma^l_{i+\frac{1}{2}} = \sigma\left(\lambda^l_{i+\frac{1}{2}}\right)\begin{cases}\left(g^l_{i+\frac{1}{2}} - g^l_i\right)/\alpha^l_{i+\frac{1}{2}} & \alpha^l_{i+\frac{1}{2}} \neq 0\\ 0 & \alpha^l_{i+\frac{1}{2}} = 0\end{cases} \tag{6.145}$$

The limiter function in this case is denoted by g^l_i and may be written as

$$g^l_i = \mathrm{minmod}\left(\alpha^l_{i-\frac{1}{2}}, \alpha^l_{i+\frac{1}{2}}\right) \tag{6.146}$$

or

$$g^l_i = \left(\alpha^l_{i+\frac{1}{2}}\alpha^l_{i-\frac{1}{2}} + |\alpha^l_{i+\frac{1}{2}}\alpha^l_{i-\frac{1}{2}}|\right)/\left(\alpha^l_{i+\frac{1}{2}} + \alpha^l_{i-\frac{1}{2}}\right) \tag{6.147}$$

For other limiters that may be used, the reader is referred to the review by Yee (1989).

In Chapter 4 a general formulation was given to provide time integration of the equations for flux formulas similar to those given above. A similar general formulation for the integration can be written for systems of equations and appears in the following form:

$$\mathbf{U}^{n+1}_i + \theta\frac{\Delta t}{\Delta x}\left(\mathbf{E}^{n+1}_{i+\frac{1}{2}} - \mathbf{E}^{n+1}_{i-\frac{1}{2}}\right) = \mathbf{U}^n_i - (1-\theta)\frac{\Delta t}{\Delta x}\left(\mathbf{E}^n_{i+\frac{1}{2}} - \mathbf{E}^n_{i-\frac{1}{2}}\right) \tag{6.148}$$

In this expression, θ has the same meaning as used previously in Chapter 4. For $\theta = 0$ the scheme is explicit; the $\theta = 1$ case represents backward Euler differencing, and when $\theta = \frac{1}{2}$, this reduces to the trapezoidal scheme. The backward Euler method is first order in time, while the trapezoidal scheme is second order in time. If the explicit scheme is used, stability limitations will generally be encountered with first-order time differencing and second-order spatially accurate fluxes. With the use of limiters, the stability problem may be suppressed. However, this is not recommended. For time asymptotic calculations

of steady-state flows, the backward Euler scheme with second-order spatial fluxes or the trapezoidal scheme are recommended. Depending upon the time accuracy desired, these implicit schemes may also be used for time-accurate calculations. If a time-accurate solution is desired, the flux Jacobians must also be correctly treated.

6.6 MULTIDIMENSIONAL CASE IN A GENERAL COORDINATE SYSTEM

In previous sections the basic concepts used to compute solutions of 1-D time-dependent flow were discussed. In practical applications, calculations are almost always multidimensional and are usually performed using a boundary conforming grid. This grid may be structured or unstructured, and the numerical method should be applicable to either case in a finite-volume formulation.

In Chapter 5 the general form of the Euler equations in conservative form was written as

$$\frac{\partial \mathbf{U}}{\partial t} + \frac{\partial \mathbf{E}}{\partial x} + \frac{\partial \mathbf{F}}{\partial y} = 0 \tag{6.149}$$

For simplicity, only the 2-D case will be studied, since the extension to three dimensions follows the same path. For a transformation to a general coordinate system, the conservative equation becomes

$$\frac{\partial \mathbf{U}_1}{\partial t} + \frac{\partial \mathbf{E}_1}{\partial \xi} + \frac{\partial \mathbf{F}_1}{\partial \eta} = 0 \tag{6.150}$$

where the subscript 1 is used to denote the altered conservative variables defined by

$$\mathbf{U}_1 = \mathbf{U}/J \tag{6.151a}$$

$$\mathbf{E}_1 = [\xi_x \mathbf{E} + \xi_y \mathbf{F}]/J \tag{6.151b}$$

$$\mathbf{F}_1 = [\eta_x \mathbf{E} + \eta_y \mathbf{F}]/J \tag{6.151c}$$

and the Jacobian J is

$$J = \xi_x \eta_y - \xi_y \eta_x$$

The flux terms and the corresponding limiters need to be more generally interpreted for application to complex geometries.

In order to proceed with the extension, let the Jacobian matrices of the fluxes be identified in the same manner as before, with the subscript 1 indicating the transformed coordinate system:

$$[A_1] = \xi_x [A] + \xi_y [B] \tag{6.152a}$$

$$[B_1] = \eta_x [A] + \eta_y [B] \tag{6.152b}$$

where

$$[A] = \partial \mathbf{E}/\partial \mathbf{U} \tag{6.153a}$$

$$[B] = \partial \mathbf{F}/\partial \mathbf{U} \tag{6.153b}$$

The eigenvalues of the $[A_1]$ and $[B_1]$ matrices will be denoted by λ_{a1} and λ_{b1}. The new matrices $[A_1]$ and $[B_1]$ may be written

$$[A_1] = [T_1][\Lambda_{a1}][T_1]^{-1} \tag{6.154a}$$

$$[B_1] = [S_1][\Lambda_{b1}][S_1]^{-1} \tag{6.154b}$$

The application of the ideas of the previous sections to multidimensional problems is based upon computing the cell-face flux terms as a series of 1-D calculations. The Riemann problem is solved as if the flow was normal to the cell face in each case. Considering this, severely skewed grids should be avoided wherever possible, as is true in any numerical calculation. The application of the idea of a 1-D Riemann problem at the cell interface in multidimensional problems has been carried out with good success. Much work continues to be done in creating a truly multidimensional Riemann solver, but success has been limited at best (Parpia and Michelak, 1993). A good review of this approach and the difficulties encountered is given in the paper by van Leer (1992). Another technique that has been explored to improve the applicability of the Riemann solver in the multidimensional case is to use the idea of a rotated difference stencil. The idea is to orient the local coordinates so the Riemann problem is solved along coordinate lines. This is similar to the work earlier reported by Davis (1984) using more classical methods. While some authors report good success with this approach (Kontinos and McRae (1991, 1994), it is not clear that the improvement in accuracy justifies the additional complexity. For a review of other work using the rotated difference idea, the papers of Deconick et al. (1992), Leck and Tannehill (1993), and Levy et al. (1993) are suggested.

At the beginning of Section 6.4, the equations for inviscid flow were integrated around a general control volume in physical space. The cell-face areas and volumes appeared explicitly. The metrics of the transformations contained in the conservation form of the general equations appear when the transformed equations are used. In either case, the Riemann problem is solved normal to the cell faces with the relationships between the geometry of the cells as given in Section 8.3.3.

The numerical flux function that must be treated in the generalized case may be written in a general form:

$$\hat{\mathbf{E}}_{i+\frac{1}{2},j} = \frac{1}{2}\left[\left(\frac{\xi_x}{J}\right)_{i+\frac{1}{2},j}(\mathbf{E}_{i,j} + \mathbf{E}_{i+1,j}) + \left(\frac{\xi_y}{J}\right)_{i+\frac{1}{2},j}(\mathbf{F}_{i,j} + \mathbf{F}_{i+1,j}) + [T_{i+\frac{1}{2},j}][\mathbf{\Phi}_{i+\frac{1}{2},j}]/J_{i+\frac{1}{2},j}\right] \tag{6.155}$$

In this formulation the matrix $[T_{i+\frac{1}{2},j}]$ is the eigenvector matrix associated with $[A_1]$. The computational coordinates are denoted by ξ and η, and the metric coefficients correspond to the projections of the cell-face areas as shown in Section 8.3.3. If $\mathbf{U}_{i+\frac{1}{2},j}$ denotes the symmetric average,

$$\mathbf{U}_{i+\frac{1}{2},j} = \tfrac{1}{2}(\mathbf{U}_{i,j} + \mathbf{U}_{i+1,j}) \tag{6.156}$$

or a Roe average, then the quantity $\lambda^l_{a,i+\frac{1}{2},j}$ represents the eigenvalues of $[A_1]$ evaluated at $\mathbf{U}_{i+\frac{1}{2},j}$, and a similar notation may be used for the eigenvalues of $[B_1]$. We may also define the wave strengths for the multidimensional case as

$$\alpha_{a,i+\frac{1}{2},j} = [T]^{-1}(\mathbf{U}_{i+1,j} - \mathbf{U}_{i,j}) \tag{6.157}$$

for the ξ direction, and a corresponding form for the η direction. The notation for the other terms in Eq. (6.155) is

$$\left(\frac{\xi_x}{J}\right)_{i+\frac{1}{2},j} = \frac{1}{2}\left[\left(\frac{\xi_x}{J}\right)_{i,j} + \left(\frac{\xi_x}{J}\right)_{i+1,j}\right] \tag{6.158}$$

The averaged values of the metrics and Jacobians are used in order to preserve the free stream. This is similar to the geometric conservation requirements that appear in finite-difference formulations (Hindman, 1981).

The Φ term that contains the limiters for symmetric or upwind total variation diminishing methods may be written in the same form as previously given. The structure of the limiter must be interpreted in terms of the altered eigenvalues associated with the generalized directions.

The MUSCL approach leads to a slightly different formulation of the flux terms, but the general form is the same as previously defined:

$$\hat{\mathbf{E}}_{i+\frac{1}{2},j} = \frac{1}{2}\left\{\left(\frac{\xi_x}{J}\right)_{i+\frac{1}{2},j}\left[\mathbf{E}\left(\mathbf{U}^R_{i+\frac{1}{2},j}\right) + \mathbf{E}\left(\mathbf{U}^L_{i+\frac{1}{2},j}\right)\right] + \left(\frac{\xi_y}{J}\right)_{i+\frac{1}{2},j}\left[\mathbf{F}\left(\mathbf{U}^R_{i+\frac{1}{2},j}\right) + \mathbf{F}\left(\mathbf{U}^L_{i+\frac{1}{2},j}\right)\right] + [T_{i+\frac{1}{2},j}]\Phi_{i+\frac{1}{2},j}/J_{i+\frac{1}{2},j}\right\} \tag{6.159}$$

In the MUSCL formulation, some liberty exists in selecting the quantity that is limited. There are a number of choices that can be made that will provide acceptable results. These include limiting the primitive variables, the characteristic variables, or any other quantity that is used in the extrapolation. The appropriate form of the limiter depends upon the choice of the extrapolation variable. The primitive variables are normally the best choice.

An explicit scheme is easily constructed with the same predictor-corrector algorithm as used in Chapter 4. In this case, one may predict at time $t + (\Delta t/2)$ and use the results to form the fluxes needed to advance the solution to the next time level. Perhaps the most well-known explicit scheme that has been employed to solve hyperbolic problems in fluid mechanics is the MacCormack (1969) method. An approximate finite-volume form of this method may be constructed

by using the standard MacCormack method for the first two steps with an added third step to provide the selective dissipation to control the oscillations present in conventional shock-capturing methods. This may be written in the form

$$\bar{\mathbf{U}}^{n+1}_{1,i,j} = \mathbf{U}^{n}_{1,i,j} - \frac{\Delta t}{\Delta \xi}(\mathbf{E}^{n}_{1,i+1,j} - \mathbf{E}^{n}_{1,i,j}) - \frac{\Delta t}{\Delta \eta}(\mathbf{F}^{n}_{1,i,j+1} - \mathbf{F}^{n}_{1,i,j})$$

$$\bar{\bar{\mathbf{U}}}^{n+1}_{1,i,j} = \frac{1}{2}\left[\bar{\mathbf{U}}^{n+1}_{1,i,j} + \mathbf{U}^{n}_{1,i,j} - \frac{\Delta t}{\Delta \xi}\left(\bar{\mathbf{E}}^{n+1}_{1,i,j} - \bar{\mathbf{E}}^{n+1}_{1,i-1,j}\right) - \frac{\Delta t}{\Delta \eta}\left(\bar{\mathbf{F}}^{n+1}_{1,i,j} - \bar{\mathbf{F}}^{n+1}_{1,i,j-1}\right)\right]$$

$$\mathbf{U}^{n+1}_{1,i,j} = \bar{\bar{\mathbf{U}}}^{n+1}_{1,i,j} + \frac{1}{2}\left(\frac{\bar{T}_{i+\frac{1}{2},j}\bar{\mathbf{\Phi}}_{i+\frac{1}{2},j}}{J_{i+\frac{1}{2},j}} - \frac{\bar{T}_{i-\frac{1}{2},j}\bar{\mathbf{\Phi}}_{i-\frac{1}{2},j}}{J_{i-\frac{1}{2},j}}\right)$$

$$+ \frac{1}{2}\left(\frac{\bar{T}_{i,j+\frac{1}{2}}\bar{\mathbf{\Phi}}_{i,j+\frac{1}{2}}}{J_{i,j+\frac{1}{2}}} - \frac{\bar{T}_{i,j-\frac{1}{2}}\bar{\mathbf{\Phi}}_{i,j-\frac{1}{2}}}{J_{i,j-\frac{1}{2}}}\right) \tag{6.160}$$

The third step is a postprocessing step appended to the classical MacCormack method in order to eliminate the deficiencies associated with calculations through strong shocks that are present in the classical methods. In this step the overbar quantities may be evaluated either at time level n or at the end of the second step.

Other techniques for generating explicit methods may be used. Many of the standard integration schemes for ordinary differential equations have been used to advance the solution in time. The most popular of these schemes is the Runge-Kutta (R-K) method described in detail for use on time-continuous systems in the work of Lomax et al. (1970) and applied extensively by Jameson et al. (1981) and Jameson (1987). The formulation of the R-K procedure is described in Section 4.1.13, where application is made to the linear wave equation.

Implicit schemes may be constructed using a number of techniques. Most common among these is the simple Euler implicit method or the trapezoidal scheme described in Chapter 4 as well as the Euler implicit scheme considered in the last section. As in the 1-D case, implicit methods create the necessity of calculating the flux Jacobians. The discussion presented in the previous section applies not only to the 1-D problem, but equally well to any number of dimensions. The linear system produced must be solved as efficiently as possible, and this becomes the major effort in computing a solution with an implicit method.

In Section 4.3, several techniques were presented for solving scalar systems. In solving systems of equations that result from the conservation laws, the same methods apply, and to some extent, the same philosophy may be followed. For example, one of the goals that is used in solving the 1-D equations is to try to create tridiagonal systems of equations. The Thomas algorithm is then applied to obtain a direct solution. The same methodology may be applied in the multi-equation case, where the goal is to have block tridiagonal systems. This naturally suggests the use of approximate factorization, as discussed earlier in

this chapter. In 3-D problems the errors introduced by this method have historically proved difficult to control. However, through suitable preconditioning, the use of approximate factorization has been shown to be effective for any number of dimensions (Choi and Merkle, 1993). Many applications of the approximate factorization approach may be found in the literature (Beam and Warming, 1976); Steger, 1977; Pulliam, 1985). Other techniques used to solve these equations include LU factorizations as described in Section 4.3.4. The technique employed to solve the linear system of equations for an implicit scheme will also depend upon the application. If only the steady-state solution is of interest, the implicit operator may be modified in any way that accelerates convergence of the solution to the steady-state value. On the other hand, if the transient is of importance, the implicit as well as the explicit operator must be retained or approximated as closely as possible (in non-iterative schemes) to provide time-accurate results.

Approximations to the implicit side of the equations have been the most popular modification to the basic implicit algorithms. These modifications have the largest influence on reducing resources needed to compute solutions to the equations of fluid flow. The approximate factorization scheme employed by Beam and Warming (1976) was modified by a diagonalization procedure by Pulliam and Chaussee (1981), reducing the operation count for the solution of the system. Another idea is to use a lower-order implicit operator and a higher-order explicit operator when computing time-asymptotic solutions. Such procedures have been advocated in the work by Steger and Warming (1982) and Rai (1987). Other approaches to the problem of solving systems of equations, with the banded structure common to the problems of computational fluid dynamics, include the LU factorization schemes noted in Section 4.3.4 and the modifications to LU factorization with Gauss-Seidel iteration recently presented by Yoon and Kwak (1993). In recent applications of implicit methods, the concept of using local iteration schemes to compute solutions of arbitrary accuracy have been developed and used with success. In general, the problem of computing a solution could be viewed as having two separate issues. The first is that a banded matrix structure will probably result from the implicit scheme and some ingenuity will be required to solve the system in an efficient manner. The other issue is that the modification of the implicit operator in many cases can be accomplished by viewing changes as alterations of the dissipation term in the numerical flux terms. These two issues are obviously coupled but should be recognized as significant in accelerating computations for implicit schemes.

6.7 BOUNDARY CONDITIONS FOR THE EULER EQUATIONS

In computing solutions to PDEs, the application of boundary conditions is a key ingredient. The technique used in implementing the boundary conditions can have a major effect on the stability and convergence of the numerical solution. The way that boundary conditions are applied in solving analytical problems is usually well defined. This is not necessarily the case when applying boundary

conditions for the discrete problem. In this case, reasonable approximations have been found to work, although the exact form may be different from that expected in comparison to the analytical case.

In the solution of flow field problems, appropriate conditions must be applied on the domain boundaries. Since only finite domains may be considered because of limitations in computer memory and speed, we are forced to specify conditions on boundaries at a finite distance from the airfoil, body, aircraft, or other geometry that is of interest in the simulation. These conditions depend upon the type of boundary and the type of flow regime. For hyperbolic problems the number of boundary conditions needed can be determined by a careful evaluation of the direction that information is carried by the characteristics. The number of boundary conditions that must be supplied is equal to the number of characteristics that are directed from the exterior of the region toward the boundary. This will become apparent below, when specific conditions and boundaries are considered. For elliptic and parabolic problems, the application of boundary conditions usually results in the specification of a set of dependent variables on the boundary or the specification of the normal derivatives. These problems require a different approach because of the different physics involved.

As an example, consider a supersonic flow over a body and the different types of domain boundaries that are present. At the inflow boundary the flow is entirely supersonic. If one examines the direction of signal propagation for these conditions, the characteristics carry information from the exterior of the domain toward the interior in all cases. For this steady case the solution for the flow over the representative body may be obtained using a marching procedure. Reference to the characteristics (see Fig. 6.17) shows that the signals are carried into the domain from the upstream region by both the streamline characteristics as well as the characteristics involving the acoustic speeds. This indicates that all information at the inflow boundary for a supersonic flow must be specified using the free stream conditions. There are no characteristics that carry information from the interior of the domain to the boundary. For a time-dependent flow, it should also be clear that a supersonic inflow will always carry information toward the boundary from the exterior [see Fig. 6.18(a)]. In this case the inflow conditions are always prescribed, as is the case for the steady marching problem. For subsonic flow the characteristics carry information toward the domain boundary both from the interior and the exterior [Fig. 6.18(b)]. The boundary conditions are used to replace the information carried to the boundary by the characteristics from the exterior.

In order to understand the development of boundary condition procedures in more than one dimension, consider the 2-D Euler equation written in (x, y) coordinates:

$$\frac{\partial \mathbf{U}}{\partial t} + \frac{\partial \mathbf{E}}{\partial x} + \frac{\partial \mathbf{F}}{\partial y} = 0$$

This equation can be expanded and written in the form

$$\frac{\partial \mathbf{U}}{\partial t} + [A]\frac{\partial \mathbf{U}}{\partial x} + [B]\frac{\partial \mathbf{U}}{\partial y} = 0 \tag{6.161}$$

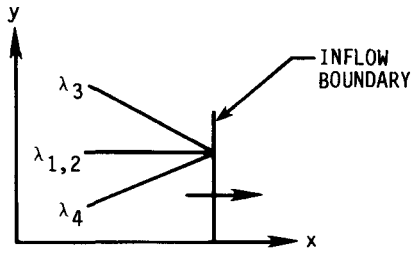

Figure 6.17 Inflow boundary conditions for steady supersonic flow.

It should be understood that this equation could have been written in generalized (ξ, η) coordinates and the ideas for applying boundary conditions would be developed in the same way. The differences would be that the contravariant velocities as well as the computational coordinates appear in the flux terms.

The Jacobian matrices $[A],[B]$ and the dependent variables are those associated with the equations written in the (x, y) system, while the Jacobians written in generalized coordinates would be in terms of the contravariant velocities. At an inflow boundary, assume that the positive x direction points from the free stream toward the interior of the domain. The y direction is assumed to lie along the boundary, with the boundary defined as a constant x surface. In the case where general (ξ, η) coordinates are used, the inflow boundary would be defined as a constant ξ surface with the η coordinate changing as one moves along the surface. Returning to the formulation in the (x, y) system, we write the governing differential equation in the form

$$\frac{\partial \mathbf{U}}{\partial t} + [T][\Lambda_a][T]^{-1} \frac{\partial \mathbf{U}}{\partial x} + [S][\Lambda_b][S]^{-1} \frac{\partial \mathbf{U}}{\partial y} = 0 \qquad (6.162)$$

In this form the dependent variables may be either the primitive variables or the conservative variables denoted by **U**. Usually, primitive variables are used to develop the compatibility relations. The compatibility equations written in the (t, x) direction are desired for the development of boundary conditions on a constant x surface. If the governing system written in primitive variables is premultiplied by the $[T]^{-1}$ matrix, the compatibility equations are obtained.

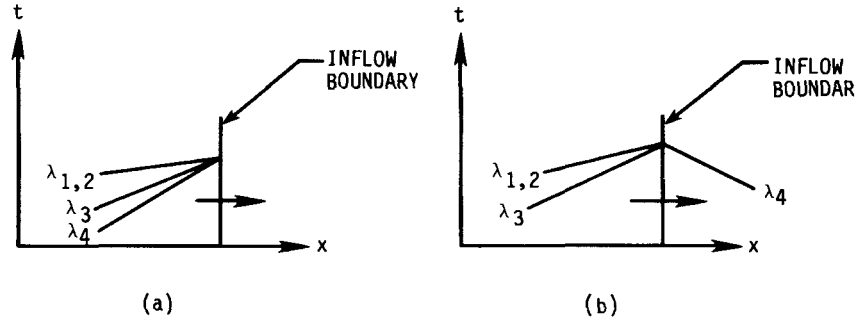

Figure 6.18 Inflow boundaries for time-dependent flow. (a) Supersonic flow. (b) Subsonic flow.

These equations may be integrated along with the boundary conditions to provide a solution at either inflow or outflow boundaries. The spatial terms must be differenced according to the direction of propagation of signals. If the elements of the $[T]^{-1}$ matrix are assumed to be constant and a new set of variables $\mathbf{W}$ is defined as $[T]^{-1}\mathbf{U}$, the compatibility equations may be written as

$$\frac{\partial \mathbf{W}}{\partial t} + [\Lambda_a]\frac{\partial \mathbf{W}}{\partial x} + [T]^{-1}[S][\Lambda_b][S]^{-1}[T]\frac{\partial \mathbf{W}}{\partial y} = 0 \tag{6.163}$$

The terms in the vector $\mathbf{W}$ are called characteristic variables, Riemann variables, or sometimes Riemann invariants in the literature. The use of characteristic variables seems to be the most appropriate choice of notation in the multidimensional case. The matrix $[\Lambda]$ denotes the matrix of eigenvalues and, for the case under consideration, consists of four elements corresponding to the repeated streamline characteristics and the wave fronts defining the subsonic or supersonic flow:

$$\begin{aligned} \lambda_{1,2} &= u, u \\ \lambda_{3,4} &= u \pm a \end{aligned} \tag{6.164}$$

For subsonic inflow the streamline characteristics are both positive. The remaining characteristics representing the acoustic wave fronts are composed of one characteristic that is positive and one that is negative. The one with the negative slope carries information from the interior to the boundary of the domain and therefore may be viewed as a valid equation to be retained in the evaluation of the inflow conditions. The other characteristics all have positive slopes, which indicates that information is carried from the free stream to the inflow boundary. Therefore these three equations must be discarded, and the boundary conditions must provide the missing three pieces of data required to close the problem at the inflow boundary.

The compatibility equations for the multidimensional case cannot be written in a perfectly diagonalized form as in the 1-D case. As a consequence, the transverse terms in this case, the terms involving derivatives in the y direction, must be retained when the integration of the compatibility equations is performed to establish the conditions at a boundary. In establishing the boundary conditions for an inflow, the assumption is often made that the transverse terms do not contribute measurably and may be neglected. The resulting equation is the 1-D compatibility equation, and it can be explicitly integrated along the characteristics. This integration yields the Riemann invariants in the 1-D case. These invariants at the inflow boundary are set by the free stream and are used as the inflow boundary conditions. The form of these conditions is given as

$$\begin{aligned} w_1 &= \left[\frac{p}{\rho^\gamma}\right] \\ w_2 &= v \\ w_3 &= u + \left[\frac{2a}{\gamma - 1}\right] \end{aligned} \tag{6.165}$$

These values of w at the inflow plane are evaluated using free stream conditions. The second value of w_2 has been set equal to the tangential velocity and is somewhat arbitrary, since this is a 1-D approximation. For supersonic flows the characteristics all carry the same sign, and free stream conditions are set at the inflow boundary, since no upstream influence is present.

At outflow boundaries the characteristics all carry the same sign for the supersonic case, and the solution must be determined entirely from conditions based on the interior. The compatibility conditions may be integrated using a suitable upwind approximation to appropriately account for the signals. If the outflow is subsonic, the analysis shows that one characteristic has a negative slope, indicating that one condition must be specified and that only three of the compatibility conditions are valid. This condition is not arbitrary but must be selected to ensure that the numerical problem is well posed (Yee, 1981). At an outflow boundary it is permissible to specify the pressure, the density, or the velocity normal to the cell. The choice of outflow boundary conditions usually depends on the way the flow solver is influenced by the boundary conditions. Hirsch (1990) suggests that the density should be among the imposed conditions for a subsonic inflow boundary. The choice of boundary conditions that work best will change owing to the manner of implementation, and the exact form of these conditions will be different for different codes.

Characteristic-based boundary conditions have been extensively used in computational fluid dynamics codes. While these methods give excellent results, they sometimes constitute a case of overkill, in the sense that a simpler boundary condition implementation would have worked equally as well. For example, simple extrapolation methods work well in many cases and are very easy to apply. The idea of extrapolation can be applied to either inflow or outflow boundaries, and any combination of primitive variables, characteristic variables, or conservative variables may be used. The easiest extrapolation to use is to set the adjacent cell values equal. This is equivalent to the enforcement of a zero slope condition on the variable. Higher-order extrapolation procedures may be employed as well.

In applying boundary conditions at inflow or outflow boundaries, the use of FVS and FDS schemes may simplify the accounting for signal propagation directions and the correct application of exterior information. Parpia (1994) has shown that these inflow boundaries may be treated without any special conditions if the exterior cells simply are assigned the correct free stream conditions and the standard split-scheme operator is then used as if the boundary cells were interior cells. Since the characteristic signal propagation directions are correctly accounted for in the scheme, the correct information is applied at the boundaries through the numerical method. This simplifies the boundary condition procedure by a significant amount.

Impermeable surfaces such as solid boundaries present another situation where a valid set of boundary conditions is needed. At a solid boundary, the correct boundary condition for the Euler equations is that the material derivative of the surface must vanish. Let the equation of the surface be given by

$$F(x, y) = y - f(x) = 0 \tag{6.166}$$

where the surface is assumed to be independent of time. The inviscid tangency condition for a steady flow simply states that the velocity component normal to the surface is zero and may be written in the form

$$v = u\frac{\partial f}{\partial x} = u\left(\frac{\partial y}{\partial x}\right)_{\text{surface}} \tag{6.167}$$

When the Euler equations are solved using a cell-centered finite-volume method, the surface tangency condition makes all fluxes on the surface vanish, and the only remaining term that must be evaluated is the surface pressure. An approximate value for the surface pressure may be established by simple extrapolation from the interior. A more common approach is to solve the normal momentum equation to find a suitable value at the surface. If the normal momentum equation is written at the body, the pressure gradient is balanced by the centrifugal force term and may be written in the form

$$\frac{\partial p}{\partial n} = \frac{\rho v_t^2}{R} \tag{6.168}$$

where v_t represents the tangential velocity and R the radius of curvature of the surface. With this information, an approximation to the pressure at the surface may be written. This is accomplished by using the pressure computed at the first cell center and employing a Taylor series to find the pressure at the cell face corresponding to the body surface. This approach is easily applied in an (x, y) system, where the body surface is represented by a constant y surface because the normal direction is the same as the y direction. However, it is a simple matter to write the series expansion to obtain the wall pressure in a general coordinate system. If the body surface is not a cell boundary, the boundary conditions required include the variables necessary to find the full array of primitive variables. For this case the equations of motion need to be solved at the body surface, and a method that permits integration at this location must be found. Sometimes the simplest boundary condition procedure for a solid surface is to use the idea of *reflection*. If the body is located on the cell boundary, the ghost-cell values are established by assigning the reflected values at its cell center (see Fig. 6.19). The tangential velocity in the ghost cell is set equal to the tangential velocity in the first cell, while the velocity in the ghost cell normal to the body is taken to be the negative of the first cell value. In addition, the density and the pressure values are equated to the first cell values. With the

Figure 6.19 Body-surface representation. (a) Cell face; (b) grid point.

ghost-cell conditions known, the correct flux values at the body surface needed to continue the calculations can be obtained in a number of ways. One way is to use characteristic ideas with information carried from the ghost cell and the first cell to the shared body-surface segment. In this case the body-surface segment would be a constant η curve in generalized coordinates, and the cell-centered values of the characteristic variables consistent with the propagation directions are then used to determine the surface conditions. The body-surface boundary condition (flow tangency) is also implemented in the surface-flux evaluation. Of course, the same procedure used in the interior flow field may also be used once the appropriate values of the dependent variables in the ghost cells are available.

Other ways of dealing with the body-surface conditions have been shown to be very useful. The compatibility equations can be written and discretized to obtain a system of equations for the body-surface conditions when the surface tangency requirement is imposed. In this case, the characteristic that carries information from the interior of the body is replaced by the body-surface condition. The discretized compatibility conditions include the equations along the streamline (body surface in this case) as well as the acoustic front equation. Kentzer (1970) proposed a scheme of applying the surface tangency condition in conjunction with the compatibility equations. In his approach, the surface tangency condition is used in differential form. If a time-dependent flow is considered, the time derivative of the tangency condition is employed. Others have implemented various forms of these conditions to compute surface solutions based on the characteristic information available at the body (Chakravarthy et al., 1980; Chakravarthy, 1983; Rai and Chaussee, 1994).

When the compatibility equations are used to determine the body boundary conditions, the equations are integrated along the characteristics. In this case, assuming that the (x, y, t) system previously employed can be a usable model, the body-surface boundary condition replaces the compatibility equation in the (y, t) direction, corresponding to the positive eigenvalue. This assumes that the body surface is at $y = 0$ with the interior of the body defined for $y < 0$. The same approach can be used in steady marching problems.

For codes where the numerical method is a cell-centered scheme the body surface is often a cell face. In this case the only remaining term in the inviscid flux is the body pressure. Consequently, a simple wave corrector may be used to evaluate the body-pressure term. This may be viewed as integration across the waves, as opposed to the ideas presented previously, where the equations were integrated along the characteristics. In this sense, the Roe scheme may be directly employed to obtain a simple wave corrector for hyperbolic problems. For the time-dependent case the characteristic variable form for the equations of motion show that the velocity normal to the cell face is proportional to the change in cell surface pressure. This permits the normal velocity to be corrected to satisfy the surface tangency condition by correcting the pressure with a weak expansion or compression wave. Abbett (1973) proposed that for problems where a steady supersonic flow was being computed, a test to evaluate the velocity misalignment with the body surface be made after the flow field solution

had been advanced. The flow misalignment is then corrected by turning the flow back parallel to the body by introducing a simple wave. When a cell-centered scheme with a cell center located on the body is used, the velocity is computed on the body surface. Otherwise, the body-surface velocity is not computed. Consequently, the misalignment of the velocity vector must be approximated by using the cell-center value from the first cell in the flow field. The velocity vector can be divided into a component normal to the surface and a component tangent to the surface.

The velocity components in the respective directions are (u, v, w). Let the unit vector normal to the surface be

$$\mathbf{n} = \frac{\nabla F}{|\nabla F|}$$

where the body-surface equation is given by

$$F(x_1, x_2, x_3) = x_1 - f(x_2, x_3) = 0 \tag{6.169}$$

Therefore the body surface normal is

$$\mathbf{n} = \frac{\mathbf{i}_1/h_1 - [(\mathbf{i}_2/h_2)(\partial f/\partial x_2)] - [(\mathbf{i}_3/h_3)(\partial f/\partial x_3)]}{\left\{1/h_1^2 + [(1/h_2)(\partial f/\partial x_2)]^2 + [(1/h_3)(\partial f/\partial x_3)]^2\right\}^{1/2}} \tag{6.170}$$

The velocity vector can be divided into a component normal to the surface and a component tangent to the surface. If the normal velocity is computed as

$$\mathbf{u}_{\text{nor}} = (\mathbf{V} \cdot \mathbf{n})\mathbf{n} \tag{6.171}$$

the small misalignment angle $\Delta\theta$, representing the orientation of the velocity vector with respect to a surface tangent, becomes

$$|\sin(\Delta\theta)| = \frac{|\mathbf{u}_{\text{nor}}|}{|\mathbf{V}|} \tag{6.172}$$

We may write this as

$$\sin(\Delta\theta) = \frac{\mathbf{V} \cdot \mathbf{n}}{|\mathbf{V}|} \tag{6.173}$$

The geometry of this problem is shown in Fig. 6.20. The misalignment angle $\Delta\theta$ is clearly shown. The velocity vector $\mathbf{V}$ represents the velocity computed at the

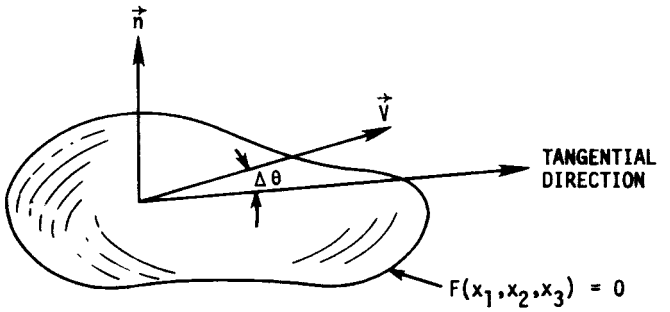

Figure 6.20 Velocity vector orientation on body surface.

body surface using the integration scheme. If MacCormack's method was used to solve the equations of motion, the velocity vector **V**, shown in Fig. 6.20, is the value at the end of the corrector step. Again, remember that a forward corrector must be used at the body.

In order to turn the velocity vector through an angle $\Delta\theta$ so that it is parallel to the body, a weak wave is introduced into the flow. If $\Delta\theta$ is positive, an expansion is required. As the flow turns through an angle $\Delta\theta$, the body-surface pressure must also change. For weak waves the pressure is related to the flow turning angle by the expression [see NACA Report 1135 (Ames Research Staff, 1953)].

$$\frac{p_2}{p_1} = 1 - \frac{\gamma M^2}{\sqrt{M^2 - 1}}\Delta\theta + \gamma M^2\left[\frac{(\gamma + 1)M^4 - 4(M^2 - 1)}{4(M^2 - 1)^2}\right](\Delta\theta)^2 + \cdots \tag{6.174}$$

In this expression, M and p_1 are the Mach number and pressure before turning, while p_2 represents the pressure after the turn takes place. With the pressure known from Eq. (6.174), the density change can now be computed. This is one point where Abbett's scheme requires additional information. It is assumed that the value of the surface entropy is known. At least along the streamline that wets the body, the value of p/ρ^γ is known. The new surface pressure (p_2) is used in conjunction with the surface entropy to calculate a new density ρ_2.

The magnitude of the velocity in the tangential direction is computed by use of the steady energy equation. If H is the total enthalpy, the velocity along the body surface is calculated as

$$|\mathbf{V}_2| = \sqrt{2\left(H - \frac{\gamma}{\gamma - 1}\frac{p_2}{\rho_2}\right)} \tag{6.175}$$

The velocity components must now be determined. The direction of the new velocity vector along the surface is obtained by subtracting the normal velocity from the original velocity computed using the integration routine. This produces the result

$$\mathbf{V}_T = \mathbf{V} - (\mathbf{V} \cdot \mathbf{n})\mathbf{n} \tag{6.176}$$

and represents the tangential component of the original velocity. It is assumed that the new surface velocity vector is in the same direction. The new velocity $\mathbf{V}_2$ is given by

$$\mathbf{V}_2 = |\mathbf{V}_2|\frac{\mathbf{V}_T}{|\mathbf{V}_T|} \tag{6.177}$$

This boundary condition routine is relatively easy to apply and provides excellent results (see Kutler et al., 1973). One of the major problems is that of determining the proper direction for the final velocity vector. Abbett's method assumes this final velocity vector lies in the tangent plane of the body in the direction of the

intersection of the tangent plane and the plane formed by the unit normal and the original velocity vector. No out-of-plane correction is used.

In supersonic flow, it is common procedure to attempt to fit the outer boundary of the physical domain when a shock wave is coincident with the outer boundary. This procedure may be followed in either time-dependent or steady flow. The process of shock fitting saves memory and produces a precise description of the shock front that one obtains from the computational procedure. The process of fitting the shock wave is a matter of satisfying the Rankine-Hugoniot equations while simultaneously requiring that the solution on the downstream side of the shock be compatible with the rest of the flow field.

In the time-dependent problem the solution for the flow variables downstream of a shock is determined by the free stream conditions, the shock velocity, and the shock orientation. If we know the free stream conditions, the initial shock slope, and the shock velocity, the shock pressure can be considered as the primary unknown in the shock-fitting procedure. The normal procedure is to combine the Rankine-Hugoniot equations with one compatibility equation to provide the expression for shock acceleration and post-shock conditions. For example, once the downstream pressure has been determined from the integration on the interior, the other downstream flow variables may be computed using the Rankine-Hugoniot equations:

$$
\begin{aligned}
\mathbf{n}_s &= \frac{\mathbf{i}\eta_x + \mathbf{j}\eta_y}{\sqrt{\eta_x^2 + \eta_y^2}} \\
u_{\infty n} &= |\mathbf{V}_\infty \cdot \mathbf{n}_s| \\
M_s &= \left\{ \frac{1}{2\gamma} \left[\frac{p_2}{p_\infty}(\gamma + 1) + (\gamma - 1) \right] \right\}^{1/2} \\
V_s &= a_\infty M_s - u_{\infty n} \\
u_{2n} - u_{\infty n} &= \frac{2a_\infty(1 - M_\infty^2)}{(\gamma + 1)M_s} \\
\rho_2 &= \rho_\infty \left(\frac{p_2}{p_\infty} + \frac{\gamma - 1}{\gamma + 1} \right) \left[\frac{1}{1 + (\gamma - 1)(p_2/p_\infty)/(\gamma + 1)} \right] \\
\mathbf{V}_2 &= \mathbf{V}_\infty + (u_{2n} - u_{\infty n})\mathbf{n}_s[\text{sign}\,(\mathbf{V}_\infty \cdot \mathbf{n}_s)]
\end{aligned}
\tag{6.178}
$$

The subscript ∞ refers to free stream conditions, subscript 2 denotes conditions immediately downstream of the shock wave, and subscript s indicates the shock surface, and n indicates the normal to this surface. Equations (6.178) can easily be derived from the relative velocity expression for the shock motion and the Rankine-Hugoniot equations. Figure 6.21 illustrates the notation and the orientation of the shock in physical space. Consistent with the discussion of boundary condition procedures, only one characteristic carries information from

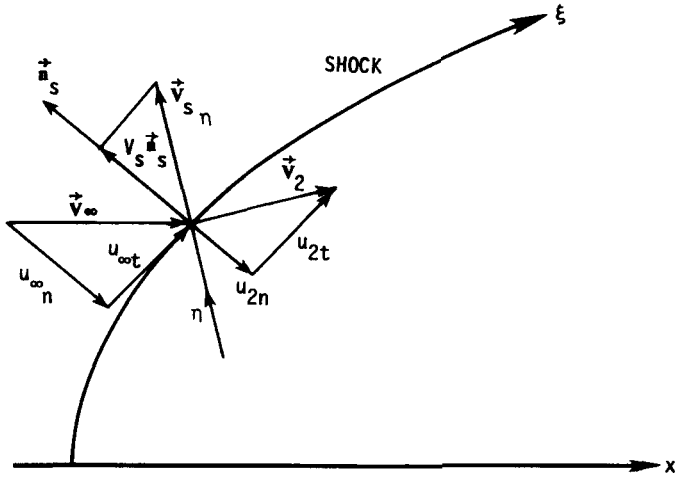

Figure 6.21 Shock geometry.

the interior to the shock wave. If this characteristic is λ_4, the corresponding compatibility equation (where τ is the transformed time) is

$$\sum_{i=1}^{4} s_{4i}(w_{i\tau} + \lambda_4 w_{i\eta} + g_i) = 0 \tag{6.179}$$

Since we have the shock wave as one boundary of our domain, we may write

$$\frac{\partial w_i}{\partial \tau} = \frac{\partial w_i}{\partial p}\frac{\partial p}{\partial \tau} \tag{6.180}$$

That is, we explicitly include the dependence of the w_i variables on the shock pressure. The derivative $\partial w_i/\partial p$ can be explicitly evaluated from Eq. (6.178). If we substitute Eq. (6.180) into Eq. (6.179), an expression for the time rate of change of pressure is obtained:

$$\frac{\partial p}{\partial \tau}\sum_{i=1}^{4} s_{4i}\frac{\partial w_i}{\partial p} = -\sum_{i=1}^{4} s_{4i}(\lambda_4 w_{i\eta} + g_i) \tag{6.181}$$

The $w_{i\eta}$ derivatives in this expression are evaluated using backward differences, which is consistent with the fact that information is being carried along a positive characteristic. The expression given in Eq. (6.181) permits p_τ to be computed, and then time derivatives of the other variables can be obtained using Eq. (6.180). These expressions are then integrated to provide the updated dependent variables. The shock position is updated by integrating the known shock speed. Moretti (1974, 1975) prefers to use the shock speed as the dependent variable. This can be easily accomplished within the above analysis.

The dependence of the w_i variables given in Eq. (6.180) is replaced by

$$\frac{\partial w_i}{\partial \tau} = \frac{\partial w_i}{\partial V_s}\frac{\partial V_s}{\partial \tau} \tag{6.182}$$

where we again compute $\partial w_i/\partial V_s$ from the Rankine-Hugoniot equations. Substituting this expression into our compatibility equation yields an equation that may be solved for the shock acceleration

$$\frac{\partial V_s}{\partial \tau}\sum_{i=1}^{4} s_{4i}\frac{\partial w_i}{\partial V_s} = -\sum_{i=1}^{4} s_{4i}(\lambda_4 w_{i\eta} + g_i) \tag{6.183}$$

Once the shock acceleration is known, the velocity and position are obtained by integration in time. The new dependent variables are computed from the Rankine-Hugoniot equations using the new shock velocity.

Boundary shock fitting is also used when the solution of the Euler equations is obtained using a marching procedure. This was discussed in Section 6.3, and a general procedure was given to compute the shock wave shape as part of the solution.

The boundary condition procedures presented in this section have been successfully applied to solve the Euler equations. While a limited number of ideas have been presented here, the literature abounds with different boundary condition application procedures. However, most of the ideas follow the guidelines given here. As a final comment, it is frequently necessary to specify more on a boundary than is required in the analytic formulation of the problem when using a numerical method. This should not be surprising, since the modification of the continuous problem also has a major effect on the application of the boundary conditions. At least, one should expect the boundary conditions to enter the computational procedure in ways not anticipated.

6.8 METHODS FOR SOLVING THE POTENTIAL EQUATION

While solutions of the Euler equations are computed on a routine basis, finding the flow field for a complete configuration is still a time-consuming procedure. More rapid computational procedures that preserve accuracy are desirable in many applications where repetitive calculations are needed. A case in point is in preliminary design. Many geometric configurations and modifications are studied, and fast reliable methods are needed in order to evaluate each change in the proposed design. Potential methods are well suited for these situations.

As is well known in fluid mechanics, a hierarchy of equations exists based upon the order of the approximation attempted or the assumptions made in the derivation of the governing equation. As we consider reductions from the Euler equations, the next logical step is to consider the solution provided by a full potential formulation.

The *full potential equation* in conservative or nonconservative form is frequently used for solving transonic flow problems. In developing the full

potential equation, the existence of the velocity potential requires that the flow be irrotational. Furthermore, Crocco's equation [Eq. (5.187)] requires that no entropy production occur. Thus no entropy changes are permitted across shocks in supersonic flows when a full potential formulation is used. At first glance, this appears to be a poor assumption. However, experience has shown that the full potential and Euler solutions do not differ significantly if the component of the Mach number normal to the shock is close to 1. The entropy production across a weak shock is dependent on the normal Mach number M_n, and is approximately (Liepmann and Roshko, 1957)

$$\frac{\Delta s}{R} \sim \frac{2\gamma}{\gamma + 1}(M_n^2 - 1)^3 \tag{6.184}$$

This shows that the assumption of no entropy change across a shock is reasonable so long as the normal component of the Mach number is sufficiently close to 1. It is important to note that the restriction is on the normal component of the local Mach number and not the free stream Mach number.

If the irrotational flow assumption is valid, we expect solutions of the potential equation to yield results nearly as accurate as solutions to the Euler equations even in supersonic and transonic flows with shocks. Difficulties in solving the Euler equations are not completely circumvented by the potential formulation, since we retain the nonlinear fluid behavior even with this simplification. We will discuss the application of the potential equation to typical flow problems later in this section.

The full potential approximation to the Euler equations can be developed in either a nonconservative or conservative form. The nonconservative form of the steady potential equation may be written for two dimensions as [Eq. (5.197)]

$$\left(1 - \frac{u^2}{a^2}\right)\phi_{xx} - \frac{2uv}{a^2}\phi_{xy} + \left(1 - \frac{v^2}{a^2}\right)\phi_{yy} = 0 \tag{6.185}$$

where

$$u = \frac{\partial \phi}{\partial x} \qquad v = \frac{\partial \phi}{\partial y} \tag{6.186}$$

and a is the speed of sound, which may be obtained from the energy equation

$$\frac{a^2}{\gamma - 1} + \frac{u^2 + v^2}{2} = H = \text{const} \tag{6.187}$$

The nonconservative form of the potential equation is sometimes referred to as the quasi-linear form of the full potential equation. In our discussion of solutions of the Euler equations, the use of the nonconservative form did not produce acceptable results at the shocks. A similar condition holds here, and the solutions for flows with shocks obtained with the nonconservative form appear to have mass sources at the shock. Most recent techniques use a conservative formulation. The conservative form of the full potential equation is simply the

continuity equation:

$$\frac{\partial \rho u}{\partial x} + \frac{\partial \rho v}{\partial y} = 0 \tag{6.188}$$

This equation is written in nondimensional form, where the asterisks denoting nondimensional variables have been omitted. The velocity components are related to the potential as noted above, and the density is calculated from the energy equation in the form

$$\rho = \left[1 - \frac{\gamma - 1}{2} M_\infty^2 (u^2 + v^2 - 1)\right]^{1/(\gamma-1)} \tag{6.189}$$

In this formulation, the velocity components and the density are nondimensionalized by the free stream values. We wish to solve Eqs. (6.188) and (6.189) subject to the surface tangency condition, written as

$$\frac{\partial \phi}{\partial n} = 0 \tag{6.190}$$

and appropriate boundary conditions at infinity.

When the full potential equation is solved, care must be exercised in correctly treating the spatial derivative terms, as was the case for the spatial derivatives for the Euler equations. Since the potential equation eliminates entropy changes, both expansion shocks and compression shocks are valid solutions, and the expansion shocks must be eliminated. In cases where this possibility exists, the addition of dissipation through upwinding is the most obvious choice. Artificial viscosity may be added either by explicit means or through the more widely used method of upwinding.

The evolution of methods for solving the potential equation is worth reviewing. Murman and Cole (1971), in a landmark paper treating transonic flow, pointed out that derivatives at each mesh point in the domain of interest must be correctly treated using type-dependent differencing. They were particularly interested in solving the transonic small-disturbance equation, but the same idea is applicable to the full potential equation. To illustrate type-dependent differencing used by Murman and Cole, consider the nonconservative equation [Eq. (6.185)]. This equation is hyperbolic at points where

$$\frac{u^2 + v^2}{a^2} - 1 > 0$$

and elliptic at points where

$$\frac{u^2 + v^2}{a^2} - 1 < 0$$

Consider the case when the flow is aligned with the x direction. If the flow is subsonic, the equation is elliptic, and central differences are used for the derivatives. If the flow is supersonic, the equation is hyperbolic at the point of

interest, and the streamwise second derivative is retarded in the upstream direction. The expressions for the finite-difference representation of the second derivatives at point (i, j) become

$$\begin{aligned}
\phi_{xx} &= \frac{\phi_{i,j} - 2\phi_{i-1,j} + \phi_{i-2,j}}{(\Delta x)^2} \\
\phi_{xy} &= \frac{\phi_{i,j+1} - \phi_{i,j-1} - \phi_{i-1,j+1} + \phi_{i-1,j-1}}{2\,\Delta x\,\Delta y} \\
\phi_{yy} &= \frac{\phi_{i,j+1} - 2\phi_{i,j} + \phi_{i,j-1}}{(\Delta y)^2}
\end{aligned} \tag{6.191}$$

The grid points used for both supersonic and subsonic points are shown in Fig. 6.22.

The structure of the point clusters shown in Fig. 6.22 illustrates the correct type dependence for either supersonic or subsonic points. The location of the points used in the finite-difference representation of the steady potential equation shows that it is desirable to use an implicit scheme to compute solutions. If we consider only supersonic flow so that no elliptic points exist in the field, a solution can be obtained using an explicit formulation. This is not advisable if the flow is only slightly supersonic at some field points because the CFL stability criterion prohibits reasonable step sizes. In that case an explicit solution even for purely supersonic flow becomes impractical.

If we examine the truncation error in the finite-difference representation of ϕ_{xx} at hyperbolic points, we find the leading terms to be of the form

$$\Delta x(u^2 - a^2)\phi_{xxx} \tag{6.192}$$

This provides a positive artificial viscosity at all points where $u^2 > a^2$. If the differencing given in Eq. (6.191) is used at an elliptic point, the artificial viscosity becomes negative and a stability problem results. Jameson (1974) pointed out that difficulty arises in those cases where the flow is supersonic and the x component (u) of the velocity is less than the speed of sound. The problem can be understood by considering a case where the flow is not aligned with the x direction, as shown in Fig. 6.23. The proper domain of dependence for all points

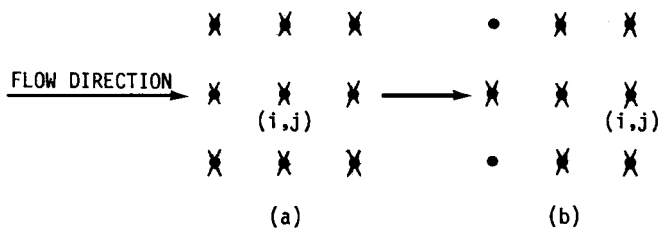

Figure 6.22 Type-dependent differencing. (a) Elliptic point; (b) hyperbolic point.

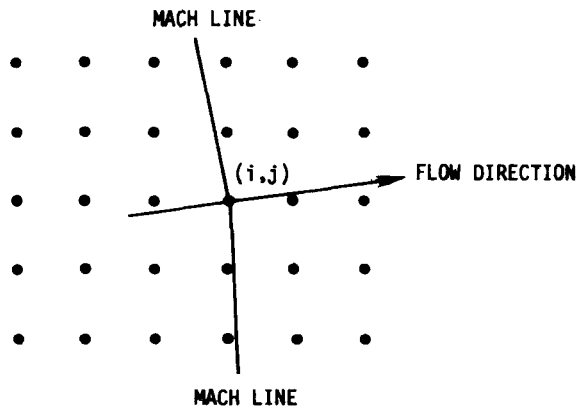

Figure 6.23 Flow with nonaligned mesh system.

is not included. One of the y coordinates of a point in the finite-difference molecule lies behind one of the characteristics passing through the point $(i\,\Delta x, j\Delta y)$. In order to remedy this problem, Jameson introduced his well-known rotated difference scheme. The idea is to write the potential equation in natural coordinates as

$$(a^2 - V^2)\phi_{ss} + a^2\phi_{nn} = 0 \tag{6.193}$$

where s and n are distances along and normal to the streamlines. By applying the chain rule for partial derivatives, the second derivatives may be written in terms of x and y as

$$\begin{aligned} \phi_{ss} &= \frac{1}{V^2}\left(u^2\phi_{xx} + 2uv\phi_{xy} + v^2\phi_{yy}\right) \\ \phi_{nn} &= \frac{1}{V^2}\left(v^2\phi_{xx} - 2uv\phi_{xy} + u^2\phi_{yy}\right) \end{aligned} \tag{6.194}$$

Both x and y derivative contributions to ϕ_{ss} are lagged or retarded, while central differences are used for the ϕ_{nn} term. When the flow is aligned with the grid, the rotated scheme reduces to that given in Eq. (6.191) and produces an artificial viscosity with leading term of the form

$$\left(1 - \frac{a^2}{V^2}\right)(\Delta s\, u^2\phi_{sss} + \cdots) \tag{6.195}$$

This provides us with a positive artificial viscosity for all points where the flow is supersonic, and we expect shock waves to form only as compressions. While the concept of artificial viscosity is used as a means of explaining the behavior of the solutions of the full potential equation, it should be understood that the same conclusions regarding proper treatment of the various terms can be reached by a careful analysis of the finite-difference equations.

Hafez et al. (1979) applied the idea of artificial compressibility in transonic flows in order to provide artificial viscosity in supersonic regions. This concept was originally introduced by Harten (1978) in attempting to devise better methods of shock capturing in supersonic flows. Holst and Ballhaus (1979) and Holst (1979) used an upwind density bias to provide the necessary artificial viscosity. The method presented below incorporates these ideas and is very useful for solving the full potential equation.

To understand the role of density biasing in providing an artificial viscosity, it is instructive to consider the 1-D form of the potential equation:

$$\frac{\partial}{\partial x}\left(\rho \frac{\partial \phi}{\partial x}\right) = 0 \tag{6.196}$$

This expression may be approximated to second order by writing

$$\nabla(\rho_{i+1/2}\,\Delta\phi_i) = 0 \tag{6.197}$$

where the notation is as previously defined. For elliptic points, Eq. (6.197) is satisfactory. For hyperbolic points, an artificial viscosity must be added such as that used by Jameson (1975):

$$-\Delta x(\mu\phi_{xx})_x \tag{6.198}$$

where

$$\mu = \min\left\{\begin{matrix} 0 \\ \rho\left(1 - \dfrac{\phi_x^2}{a^2}\right)\end{matrix}\right. \tag{6.199}$$

As previously noted, this explicit addition of artificial viscosity is equivalent to the type-dependent differencing introduced by Murman and Cole (1971). Jameson (1975) has shown that Eq. (6.198) is equivalent to a term with the form

$$-\Delta x(\nu\rho_x\phi_x)_x \tag{6.200}$$

where

$$\nu = \max\left\{\begin{matrix} 0 \\ 1 - \dfrac{a^2}{\phi_x^2}\end{matrix}\right. \tag{6.201}$$

This form is obtained by differentiation of the 1-D form of the energy equation. If this artificial viscosity form is incorporated into the potential equation, the finite-difference approximation to Eq. (6.196) becomes

$$\frac{\partial}{\partial x}\left(\rho \frac{\partial \phi}{\partial x}\right) \approx \nabla[\rho_{i+1/2}\,\Delta\phi_i] - \nabla\left[\nu_i(\rho_{i+1/2} - \rho_{i-1/2})\,\Delta\phi_i\right] = 0 \tag{6.202}$$

This expression, due to Holst and Ballhaus (1979), is second-order accurate and centrally differenced in subsonic regions. In supersonic regions this is a first-order upwind scheme due to the addition of the artificial viscosity. The differencing

becomes more strongly biased in the upwind direction as the Mach number increases. In subsonic regions the density biasing is switched off.

The difference expression given by Eq. (6.202) can also be written

$$\frac{\partial}{\partial x}\left(\rho\frac{\partial\phi}{\partial x}\right) \approx \nabla(\tilde{\rho}_{i+1/2}\,\Delta\phi_i) = 0 \tag{6.203}$$

if the new density is identified by

$$\tilde{\rho}_{i+\frac{1}{2}} = (1 - \nu_i)\rho_{i+\frac{1}{2}} + \nu_i\,\rho_{i-\frac{1}{2}} \tag{6.204}$$

where the values at the cell midpoint are obtained from the energy equation [Eq. (6.189)]. In this expression for $\rho_{i+\frac{1}{2}}$, only u appears and is evaluated as $(\phi_{i+1} - \phi_i)/\Delta x$. Equations (6.203) and (6.204) show that the effect of adding artificial viscosity is equivalent to using a retarded density. In Jameson's (1975) method, the artificial viscosity is explicitly added, while in the scheme outlined here, the artificial viscosity is included in the treatment of the density. If the artificial viscosity ν is chosen as given in Eq. (6.199), the two techniques give identical results. If $\nu = 0$, the scheme is valid only in elliptic regions and is unstable for supersonic flow. However, if ν is set equal to a positive constant, the scheme can be used for both subsonic and supersonic flows. It should be noted that the resulting method is first order and highly dissipative when ν is set equal to a constant.

Other techniques for including the upwind or density-biasing effect have been developed that are more accurate. Shankar et al. (1985) used a streamwise flux-biasing approach that has proven to be effective. The value of $\tilde{\rho}_{i+\frac{1}{2}}$ is written in terms of mass flux values in the streamwise direction for the 1-D case as

$$\tilde{\rho} = \frac{1}{u}\left[\rho u \pm \Delta x\frac{\partial}{\partial x}(\rho u)^{-}\right] \tag{6.205}$$

where the negative sign is used with a backward difference and the positive with a forward difference. The term $(\rho u)^{-}$ is defined as

$$\begin{aligned} (\rho u)^{-} &= \rho u - \rho^* u^* \qquad u > u^* \\ (\rho u)^{-} &= 0 \qquad\qquad\quad u \leqslant u^* \end{aligned} \tag{6.206}$$

and the starred quantities represent the sonic values of the density and the velocity. For steady flow these values are constant and generally depend only on the free stream Mach number. If the flow is unsteady, the values are computed at all points due to the unsteady behavior of the flow. In order to use flux biasing, four different cases must be evaluated, and these will be detailed below.

In solving the potential equation, methods for computing solutions of the steady equations using relaxation are popular. When relaxation methods are used, the behavior of the equations switches whenever sonic lines are encountered. If the time-dependent form of the governing equations is used for the general case, the solution procedure is valid for either steady or unsteady

flow. However, the special treatment of the density still needs to be carried during the solution process.

The unsteady potential equation may be written

$$\left[\frac{\rho}{J}\right]_\tau + \left[\rho\frac{U}{J}\right]_\xi + \left[\rho\frac{V}{J}\right]_\eta = 0 \tag{6.207}$$

where U, V are the contravariant velocities given by

$$\begin{aligned} U &= \xi_t + a_{11}\phi_\xi + a_{12}\phi_\eta \\ V &= \eta_t + a_{21}\phi_\xi + a_{22}\phi_\eta \end{aligned} \tag{6.208}$$

with the usual definitions for the metric coefficients,

$$\begin{aligned} a_{11} &= \xi_x^2 + \xi_y^2 \qquad a_{12} = \xi_x\eta_y + \xi_y\eta_x \\ a_{21} &= \xi_x\eta_y + \xi_y\eta_x \qquad a_{22} = \eta_x^2 + \eta_y^2 \end{aligned} \tag{6.209}$$

and J is the Jacobian. In the unsteady formulation the density is given by

$$\rho = \left\{1 - \frac{\gamma - 1}{2}M_\infty^2\left[2\phi_\tau + (U + \xi_\tau)\phi_\xi + (v + \eta_\tau)\phi_\eta - 1\right]\right\}^{1/(\gamma-1)} \tag{6.210}$$

We seek a solution of Eq. (6.207), and any scheme that provides the desired accuracy may be used. Shankar et al. (1985) used a Newton method to solve this equation, and we present the basic idea of their approach.

The conservative form of the continuity equation may be written as a function of the velocity potential in the form

$$F[\phi] = 0 \tag{6.211}$$

In this expression the value of ϕ is the unknown at each mesh point at the $n + 1$ time level. The standard Newton iteration scheme for computing this value of ϕ is

$$F[\phi_*] + \left(\frac{\partial F}{\partial \phi}\right)_{\phi_*}(\phi - \phi_*) = 0 \tag{6.212}$$

The asterisk denotes the iteration value for ϕ. That is, the iteration procedes by starting with an assumed value of ϕ at the $n + 1$ level. Initially, this value of ϕ is assigned to ϕ_*. After the first Newton iteration, the new values of ϕ that result are then assigned to the ϕ_* array. In this manner, the iteration continues until ϕ approaches ϕ_* within the desired accuracy.

The solution procedure begins with a specific treatment of the time- and spatial-derivative terms. The details of this treatment are outlined below.

Treatment of the time derivatives. The time derivative may be formed in a number of ways. In order to provide flexibility in selecting the temporal

accuracy, the term

$$\frac{\partial}{\partial \tau}\left[\frac{\rho}{J}\right]$$

may be written in the following form:

$$\frac{(a_1 - \theta b_1)\left[(\rho/J)^{n+1} - (\rho/J)^n\right] - \theta b_1\left[(\rho/J)^n - (\rho/J)^{n-1}\right]}{D_1} \tag{6.213}$$

where the denominator is defined as

$$D_1 = a_1 \Delta\tau_1 - \theta b_1(\Delta\tau_1 + \Delta\tau_2) \tag{6.214}$$

and

$$\begin{aligned} a_1 &= (\Delta\tau_1 + \Delta\tau_2)^2 \\ b_1 &= \Delta\tau_1^2 \\ \Delta\tau_1 &= \tau^{n+1} - \tau^n \\ \Delta\tau_2 &= \tau^n - \tau^{n-1} \end{aligned} \tag{6.215}$$

The time accuracy of the method is controlled by θ, where a value of zero corresponds to first-order accuracy and one provides a second-order accurate scheme.

The unknown shown in the time discretization is the density. However, we write the density in terms of ϕ following the original Newton iteration procedure. Thus we write the density in the following form:

$$\rho(\phi_* + \Delta\phi) = \rho(\phi_*) + \Delta\rho \tag{6.216}$$

where

$$\Delta\rho = \frac{\partial \rho}{\partial \phi}\Delta\phi \tag{6.217}$$

and

$$\Delta\phi = \phi - \phi_* \tag{6.218}$$

The density derivative is evaluated by writing

$$\Delta\rho = \frac{\partial \rho}{\partial \phi_t}\Delta\phi_t + \frac{\partial \rho}{\partial \phi_\xi}\Delta\phi_\xi + \frac{\partial \rho}{\partial \phi_\eta}\Delta\phi_\eta \tag{6.219}$$

With the time derivative approximated by $1/\Delta\tau$, we obtain the density change by differentiation, resulting in the expression for $\Delta\rho$:

$$\Delta\rho = \left[-\frac{\rho}{a^2}\left(\frac{1}{\Delta\tau_1} + U\frac{\partial}{\partial \xi} + V\frac{\partial}{\partial \eta}\right)\right]_{\phi_*}\Delta\phi \tag{6.220}$$

Spatial derivatives. The density appearing in the spatial derivatives is treated in a manner similar to that outlined above. Consistent with the Newton iteration

procedure for ϕ, the spatial derivatives are written as

$$\frac{\partial}{\partial \xi}\left(\rho \frac{U}{J}\right) = \frac{\partial}{\partial \xi}\left(f + \frac{\partial f}{\partial \phi}\Delta\phi\right) \tag{6.221}$$

where

$$f = \left(\rho \frac{U}{J}\right) \tag{6.222}$$

with

$$\frac{\partial f}{\partial \phi} = \frac{1}{J}\left(\rho \frac{\partial U}{\partial \phi} + U \frac{\partial \rho}{\partial \phi}\right) \tag{6.223}$$

The upwinding that must be used when the quantity $(a_{11} - U^2/a^2)$ is negative will create a pentadiagonal matrix. In the interest of computational efficiency, the term $U(\partial\rho/\partial\phi)$ is sometimes neglected because a tridiagonal form is recovered. Since the change in ϕ goes to zero when the solution converges, this should not produce errors. The final form assumed for the spatial derivative becomes

$$\frac{\partial}{\partial \xi}\left(\frac{\tilde{\rho} U}{J}\right) = \left(\tilde{\rho}\frac{U}{J}\right)_{i+\frac{1}{2},j} - \left(\tilde{\rho}\frac{U}{J}\right)_{i-\frac{1}{2},j} \tag{6.224}$$

where the expanded terms may be written

$$\left(\tilde{\rho}\frac{U}{J}\right)_{i+\frac{1}{2},j} = \left\{\frac{\tilde{\rho}}{J}(\xi_t + a_{11}[\phi_* + \Delta\phi]_\xi + a_{12}[\phi_* + \Delta\phi]_\eta)\right\}_{i+\frac{1}{2},j} \tag{6.225}$$

The density $\tilde{\rho}$ is given by $\tilde{\rho}(\phi_*)$, where ϕ_* is the initial guess in the Newton iteration.

In flows with shocks or where $M > 1$, artificial viscosity is added to the scheme by density biasing. This may be accomplished in a number of different ways. The density may be biased strictly in the coordinate direction, so that

$$\tilde{\rho}_{i+\frac{1}{2}} = \rho_{i+\frac{1}{2}} \pm \nu \Delta\xi \left(\frac{\partial \rho}{\partial \xi}\right)_{i+\frac{1}{2}} \tag{6.226}$$

where the coefficient ν takes the usual form,

$$\nu = \max\left(0, 1 - \frac{1}{M^2}\right)_{i+\frac{1}{2}} \tag{6.227}$$

For values of U that are positive, the negative sign and backward differencing are used, while the positive sign and forward differencing are used when U is negative.

Directional flux biasing can also be employed successfully and consists of writing the density in terms of the weighted mass flux. This is written in the form

$$\tilde{\rho} = \frac{1}{q}\left(\rho q \pm \Delta\xi \frac{\partial}{\partial \xi}(\rho q)^{-} \right) \tag{6.228}$$

The streamwise biasing approach weights the density by using the streamwise mass flux and is written

$$\tilde{\rho} = \frac{1}{q}\left(\rho q \pm \Delta s \frac{\partial}{\partial s}(\rho q)^{-} \right) \tag{6.229}$$

where s is the local streamwise coordinate and q represents the speed. This may be written in a form consistent with the previous notation as

$$\tilde{\rho} = \frac{1}{q}\left[\rho q \pm \left(\frac{U}{Q}\Delta\xi \frac{\partial}{\partial \xi} + \frac{V}{Q}\Delta\eta \frac{\partial}{\partial \eta} \right)(\rho q)^{-} \right] \tag{6.230}$$

where

$$Q = (U^2 + V^2)^{\frac{1}{2}} \tag{6.231}$$

with $(\rho q)^{-}$ defined as

$$\begin{aligned} (\rho u)^{-} &= \rho u - \rho^* u^* \qquad u > u^* \\ (\rho u)^{-} &= 0 \qquad\qquad\quad u \leqslant u^* \end{aligned} \tag{6.232}$$

and the starred values represent sonic conditions. These sonic conditions are given by

$$(q^*)^2 = \frac{2}{M_\infty^2(\gamma+1)}\left[1 + \frac{\gamma - 1}{2} M_\infty^2 (1 - 2\phi_\tau - 2\xi_\tau \phi_\xi - 2\eta_\tau \phi_\eta) \right] \tag{6.223}$$

$$\rho^* = (q^* M_\infty)^{2/(\gamma-1)} \tag{6.234}$$

There are four cases that must be considered in the biasing of the density.

1. Subsonic flow. In the case of subsonic flow the velocity is less than the speed of sound at both points under consideration. For $q < q^*$ at $(i + \frac{1}{2}, j)$ and $(i - \frac{1}{2}, j)$, the density term becomes

$$\tilde{\rho}_{i+\frac{1}{2},j} = \frac{1}{q_{i+\frac{1}{2},j}}\left\{ (\rho q)_{i+\frac{1}{2},j} - \left[(\rho q)^{-}_{i+\frac{1}{2},j} - (\rho q)^{-}_{i-\frac{1}{2},j} \right] \right\} \tag{6.235}$$

or

$$\tilde{\rho}_{i+\frac{1}{2},j} = \rho_{i+\frac{1}{2},j} \tag{6.236}$$

2. Supersonic flow. For the case of supersonic flow, the velocity is fully supersonic at both mesh half intervals, $(i + \frac{1}{2}, j), (i - \frac{1}{2}, j)$:

$$q > q^*$$

For $U > 0$, the density becomes

$$\tilde{\rho}_{i+\frac{1}{2},j} = \frac{1}{q_{i+\frac{1}{2},j}}\left\{(\rho q)_{i+\frac{1}{2},j} - \left[(\rho q - \rho^* q^*)_{i+\frac{1}{2},j} - (\rho q - \rho^* q^*)_{i-\frac{1}{2},j}\right]\right\} \tag{6.237}$$

When the flow is steady and supersonic, the value of the density is simplified considerably to

$$\tilde{\rho}_{i+\frac{1}{2},j} = \rho_{i-\frac{1}{2},j}\left(\frac{q_{i-\frac{1}{2},j}}{q_{i+\frac{1}{2},j}}\right) \tag{6.238}$$

3. Transition through a sonic point. Figure 6.24 shows a schematic of transition through a sonic point region along with the shock transition point. For the sonic transition, $q > q^*$ at $(i + \frac{1}{2}, j)$ and $q < q^*$ at $(i - \frac{1}{2}, j)$ for $U > 0$. The density is written

$$\tilde{\rho}_{i+\frac{1}{2},j} = \frac{1}{q_{i+\frac{1}{2},j}}\left\{(\rho q)^{-}_{i+\frac{1}{2},j} - \left[(\rho q - \rho^* q^*)_{i+\frac{1}{2},j} - (\rho q)^{-}_{i-\frac{1}{2},j}\right]\right\} \tag{6.239}$$

This may be more simply written as

$$\tilde{\rho}_{i+\frac{1}{2},j} = \frac{\rho^* q^*}{q_{i+\frac{1}{2},j}} \tag{6.240}$$

4. Transition through a shock. In the case of transition through a shock, $q > q^*$ at $(i - \frac{1}{2}, j)$ and $q < q^*$ at $(i + \frac{1}{2}, j)$. For $U > 0$,

$$\tilde{\rho}_{i+\frac{1}{2},j} = \frac{1}{q_{i+\frac{1}{2},j}}\left\{(\rho q)_{i+\frac{1}{2},j} - \left[(\rho q)^{-}_{i+\frac{1}{2},j} - (\rho q - \rho^* q^*)_{i-\frac{1}{2},j}\right]\right\} \tag{6.241}$$

or in a simpler form,

$$\tilde{\rho}_{i+\frac{1}{2},j} = \rho_{i+\frac{1}{2},j} + \frac{1}{q_{i+\frac{1}{2},j}}(\rho q - \rho^* q^*)_{i-\frac{1}{2},j} \tag{6.242}$$

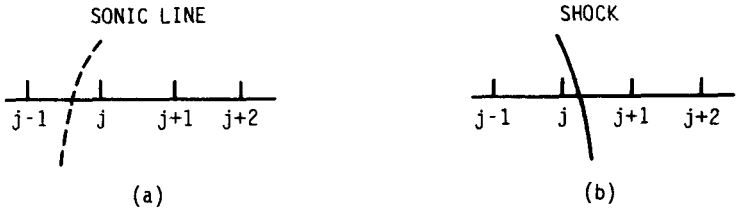

Figure 6.24 Transition. (a) Sonic point. (b) Shock point.

For steady flows it may be shown that flux biasing and the density biasing procedure employed by Holst [1980] give identical results at a purely supersonic point.

The remaining task that must be accomplished to make this full potential formulation applicable to both steady and unsteady problems is to correctly treat the circulation at the boundary of the computational region. In particular, the velocity potential jumps in value across the wake, and an appropriate technique to establish the correct jump is needed. The circulation is defined as

$$\Gamma = \oint \mathbf{V} \cdot d\mathbf{s} \tag{6.243}$$

When circulation is generated in the lifting case, the jump in the velocity potential across the airfoil wake is equal to the circulation, i.e.,

$$\phi_u - \phi_l = \Gamma \tag{6.244}$$

where the u and l subscripts indicate the values taken at the upper and lower sides of the airfoil wake. Kelvin's theorem (Karamcheti, 1966) states that the circulation around a fluid curve remains constant for all time if the curve moves with the fluid. This permits the conservation of circulation to be expressed as

$$\frac{D\Gamma}{Dt} = 0 \tag{6.245}$$

Integrating along the wake cut provides the correct Γ variation relating the values of ϕ across the wake. The circulation is simply convected with the fluid particles, and the most convenient form to use may be written

$$\frac{\partial \Gamma}{\partial t} + U\frac{\partial \Gamma}{\partial \xi} + V\frac{\partial \Gamma}{\partial \eta} = 0 \tag{6.246}$$

This equation may be substantially simplified with the proper choice of coordinates. When this expression is integrated to find the variation in Γ along the wake cut, the recommended practice is to assume that the upper and lower values of ϕ are correct at alternating time steps. This means that the upper and lower values are alternately determined by the solutions of the field equations or the integration of Kelvin's theorem. For the steady flow case, the value of Γ along the wake is set equal to a constant and is simply the jump in ϕ at the trailing edge point.

The unsteady formulation also requires a specification on the normal derivatives of ϕ along the wake cut when the governing equations for ϕ are written. This is usually accomplished by an extrapolation that also includes the calculated value of the circulation. The jump in the second derivative of ϕ across the wake may be written

$$[\phi_{\eta\eta}]_{ul} = -\frac{\rho a_{11}\Gamma_\xi/J}{\rho a_{22}/J} \tag{6.247}$$

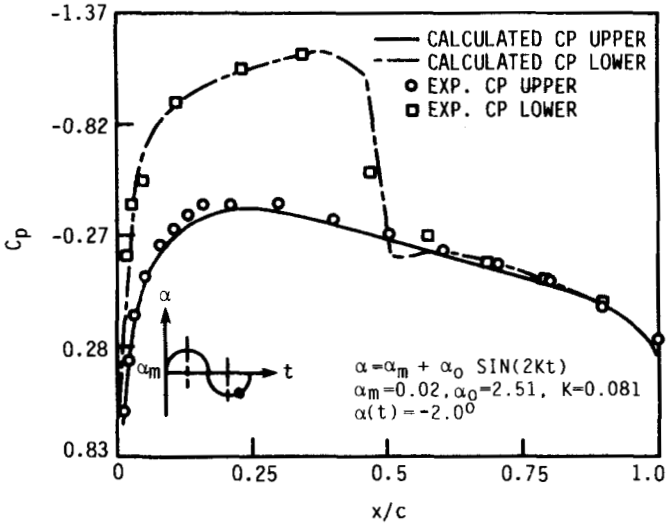

Figure 6.25 Comparison of the unsteady pressure coefficients (Cp) for a NACA 0012 airfoil (Shankar et al., 1985. Copyright © 1985 AIAA. Reprinted with permission).

The pressure is continuous across the wake, and the density is also assumed to be continuous from the lower to the upper side.

In addition to the wake treatment, the body-surface boundary conditions and conditions in the far field require specification. On the body surface the flow must satisfy the surface tangency condition for the steady case, or the more general statement for the unsteady case requires that the normal velocity of the moving surface be equal to the normal component of the fluid velocity. The far field is treated in the same way as the Euler equation boundary conditions, in

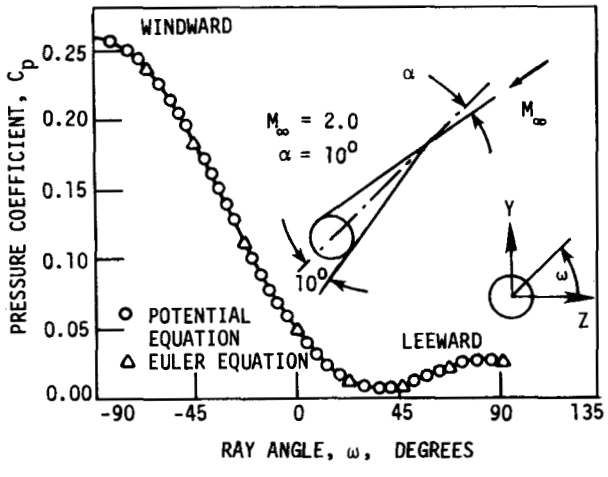

Figure 6.26 Flow over a circular cone.

the sense that the Reimann invariants may be used as outlined in the previous section.

The original unsteady equation (continuity) may be written in the form

$$H(\Delta\phi) - R(\phi^*, \phi^n, \phi^{n-1}, \ldots) = 0 \tag{6.248}$$

In this equation the residual is denoted by R and the operator H may represent the particular scheme selected to compute a solution of the system. Approximate factorization, relaxation, or any other suitable method may be chosen. Figure 6.25 shows the unsteady pressure distribution on an oscillating NACA 0012 airfoil compared to experimental data from AGARD R-702. This is a transonic case and is representative of the unsteady results obtained with full potential formulations. Typical results from steady full potential calculations of supersonic flows from Shankar and Chakravarthy (1981) are shown in Figs. 6.26 and 6.27. In both cases, the agreement with solutions using the Euler equations is excellent. In applications where the assumptions inherent in a potential formulation are valid, the calculated solutions for the flow field will provide a quick, accurate result. In areas such as preliminary design, application of full potential codes

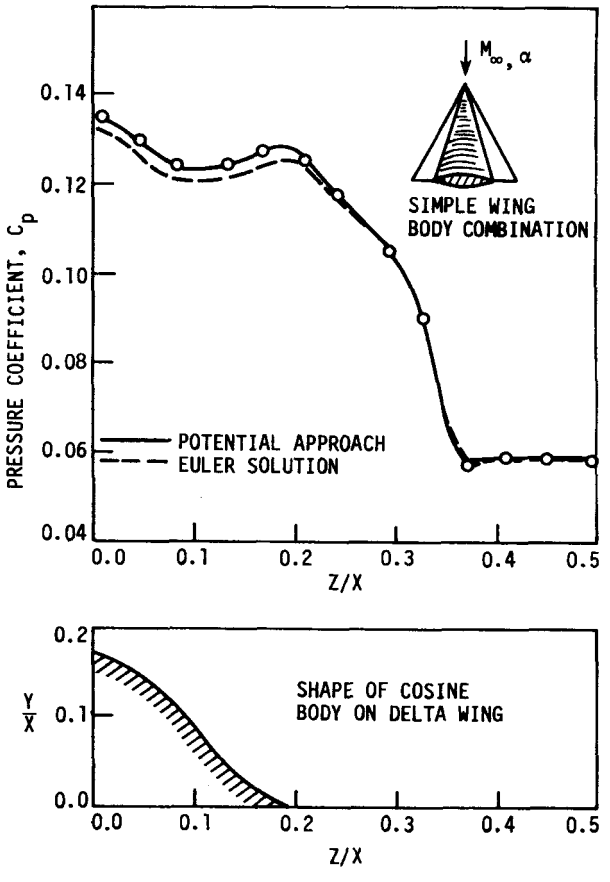

Figure 6.27 Flow over wing-body configuration.

can substantially reduce the computational effort expended in comparison with other approaches.

6.9 TRANSONIC SMALL-DISTURBANCE EQUATIONS

The use of the full potential equation for inviscid transonic flows was discussed in the previous section. Results obtained for airfoils and some 3-D body shapes compare very well with available experimental data. Methods for solving the full potential equation are very efficient and are being used extensively. However, we still find numerous applications where the sophistication provided by the full potential formulation is not required and the accuracy of the solution of the transonic small-disturbance equation is sufficient. In addition, a significant advantage accrues in the application of boundary conditions. Boundary conditions for 2-D problems are applied on the slit in two dimensions or on the plane for 3-D problems. The governing equations are greatly simplified, since complex body-aligned mappings are unnecessary for the application of boundary conditions. This can result in significant reductions in computer time and storage requirements, particularly in 3-D problems.

The transonic small-disturbance equations may be derived by a systematic expansion procedure. The details of this procedure are given by Cole and Messiter (1957) and Hayes (1966) and provide a means of systematically developing higher-order approximations to the Euler equations. In Chapter 5 the transonic small-disturbance equation [Eq. (5.203)] is derived using a perturbation procedure. This may be written in the nondimensional form

$$[K - (\gamma + 1)\phi_x]\phi_{xx} + \phi_{\tilde{y}\tilde{y}} = 0 \tag{6.249}$$

where K is the transonic similarity parameter given by

$$K = \frac{1 - M_\infty^2}{\delta^{2/3}} \tag{6.250}$$

with δ representing the maximum thickness ratio and f the shape function of an airfoil defined by the expression

$$y = \delta f(x) \tag{6.251}$$

The velocity potential used in Eq. (6.249) is the perturbation velocity potential defined in such a way that the x derivative of ϕ is the perturbation velocity in the x direction nondimensionalized with respect to the free stream velocity, and similarly in the y direction. The scaled coordinate $\tilde{y}$ is defined by

$$\tilde{y} = \delta^{1/3} y \tag{6.252}$$

Equation (6.249) is formally equivalent to Eq. (5.203), and both are forms of the Guderley–von Kármán transonic small-disturbance equations. The similarity form given in Eq. (6.249) is the equation originally treated by Murman and Cole (1971) in calculating the inviscid flow over a nonlifting airfoil. The pressure coefficient is the same as Eq. (5.205) and may be written

$$C_p = -2\phi_x$$

For flows that are not considered transonic, we obtain the Prandtl-Glauert equation for subsonic or supersonic flow. This expression has been used in numerous examples in previous chapters and takes the form

$$(1 - M_\infty^2)\phi_{xx} + \phi_{yy} = 0 \tag{6.253}$$

The main point to remember is that the transonic small-disturbance equation is nonlinear and switches from elliptic to hyperbolic in the same manner as the full potential and Euler equations.

In their original paper, Murman and Cole treated the inviscid transonic flow over a nonlifting airfoil and solved the transonic small-disturbance equation as given in Eq. (6.249). In addition to the governing PDE, the necessary body-surface boundary conditions for zero angle of attack are given by

$$\phi_{\bar{y}}(x, 0) = f'(x) \tag{6.254}$$

applied in the plane $\bar{y} = 0$ consistent with the theory. A boundary condition must also be applied at the outer boundary of the computational mesh. For this case, in the far field,

$$\phi \simeq \frac{1}{2\pi\sqrt{K}} \frac{Mx}{x^2 + K\bar{y}^2} \tag{6.255}$$

where

$$M = 2\int_{-1}^{1} f(\xi)\, d\xi + \frac{\gamma + 1}{2} \int\int_{-\infty}^{+\infty} d\xi\, d\eta \tag{6.256}$$

and the airfoil is confined to the interval

$$-1 \leqslant x \leqslant 1$$

In the lifting case, the circulation must be imposed and determined by satisfying the Kutta condition on the airfoil. The far-field boundary condition in this case takes the form of a vortex with the value of circulation determined by the Kutta condition. For development of the far-field boundary condition, the papers by Ludford (1951) and Klunker (1971) are recommended.

Murman and Cole solved Eq. (6.249) for a nonlifting transonic airfoil using line relaxation methods. Type-dependent differencing given in Eq. (6.191) was used for hyperbolic regions, and central differencing was used in the elliptic regions. This switched differencing used by Murman and Cole provides a method that is equivalent to a first-order Roe scheme. The airfoil now appears on the x axis as a line or slit, and boundary conditions are applied there. In this case the airfoil lies between two mesh points at the half-mesh interval, as shown

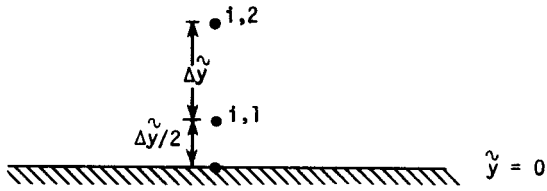

Figure 6.28 Surface boundary point distribution.

in Fig. 6.28. The boundary condition at $\tilde{y} = 0$ enters as a body slope or derivative of ϕ given in Eq. (6.254). At the $(i, 1)$ point, the $\phi_{\tilde{y}\tilde{y}}$ derivative is differenced as

$$\phi_{\tilde{y}\tilde{y}} = \frac{1}{\Delta\tilde{y}}\left(\phi_{\tilde{y}_{i,3/2}} - \phi_{\tilde{y}_{i,1/2}}\right) = \frac{1}{\Delta\tilde{y}}\left[\frac{\phi_{i,2} - \phi_{i,1}}{\Delta\tilde{y}} - \phi_{\tilde{y}}(x,0)\right] \quad (6.257)$$

The surface boundary condition explicitly enters the calculation through the $\phi_{\tilde{y}}$ term.

Figure 6.29 shows the pressure distribution for a circular arc airfoil obtained by solving the transonic small-disturbance equation. As can be seen, the experimental data of Knechtel (1959) and the computed results compare favorably for both the subcritical and supercritical cases. It is interesting that the

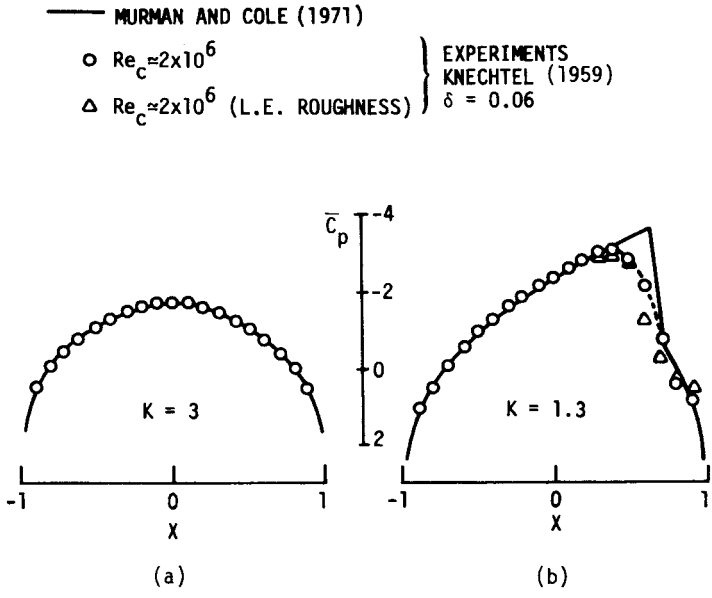

Figure 6.29 Pressure distribution for circular are airfoil. (a) Subcritical case. (b) Supercritical case.

shock location and strength for this example agree well with the experimental measurements. The nonconservative equations of small-disturbance theory for an inviscid flow underestimate shock strength and produce the same effect as a shock–boundary layer interaction on shock strength and location. Thus the nonconservative form has been popular even though the conservative form is mathematically appealing. Numerous applications of the technique, presented by Murman and Cole for solving the transonic small-disturbance equation, have been made since it was originally introduced, and many refinements of the basic method have been developed. However, the main point to remember is that a significant simplification over either the Euler equations or the full potential formulation is realized when this approach is used.

The simplified form of the transonic small-disturbance equation was used in developing solutions for 3-D wings by Bailey and Ballhaus (1972). Their work led to the development of a widely used 3-D code for transonic wing analysis. This code has been used extensively in designing improved wings for flight in the transonic speed regime. For those interested in 3-D transonic flow over wings, the paper by Bailey and Ballhaus is recommended reading.

Most current work in transonic flow is concentrated on developing Euler or Navier-Stokes equation solvers. One area where considerable effort is being expended using the transonic full potential or small-disturbance equations is in the development of design codes. In the inverse design problem the body pressure is prescribed, and the body shape is unknown. For this type of problem a simplified approach offers advantages.

6.10 METHODS FOR SOLVING LAPLACE'S EQUATION

The numerical techniques presented in the previous sections of this chapter were applied to the nonlinear equations governing inviscid fluid flow. Linear PDEs are often used to model both internal and external flows. Examples include Laplace's equation for incompressible inviscid irrotational flow and the Prandtl-Glauert equation, which is valid in compressible flow if the small-perturbation assumptions are satisfied. The methods for solving both of these equations are similar. Finite-difference/finite-volume methods for solving Laplace's equation are presented in Chapter 4 and will not be reviewed here. Instead, the basic idea underlying the use of panel methods will be discussed. These methods have received extensive use in industry.

The advantage of using panel methods is that a solution for the body-pressure distribution can be obtained without solving for the flow field throughout the domain. In this case the problem is reduced to the solution of a system of algebraic equations for source, doublet, or vortex strengths on the boundaries. Using the resulting solution, the body-surface pressures can be computed. Panel schemes require the solution of a large system of algebraic equations. For most practical configurations, the storage and speed capability of modern computers have been sufficient. However, judicious selection of the number of surface

panels and correct placement are essential in obtaining a good solution for the body-surface pressure.

In studying panel methods, we will consider the flow of an incompressible inviscid irrotational fluid that is governed by a solution of Laplace's equation written in terms of the velocity potential. We require

$$\nabla^2\phi = 0 \tag{6.258}$$

in the domain of interest and specify either ϕ or $\partial\phi/\partial n$ on the boundary of the domain. For simplicity, we restrict our attention to the 2-D case, although the fully 3-D problem is conceptually the same. The geometry of the problem under consideration is shown in Fig. 6.30. The basic idea underlying all panel methods is to replace the required solution of Laplace's equation in the domain with a surface integral. This method is developed by the application of Green's second identity to the domain of interest. If u and v are two functions with continuous derivatives through second order (class C^{II}), then Green's second identity may be written

$$\int\int_A (u\nabla^2 v - v\nabla^2 u)\, dA = \oint_s (v\,\nabla u - u\,\nabla v)\cdot \mathbf{n}\, ds$$

where $\mathbf{n}$ is the unit normal to the boundary and s is arc length along the boundary. Suppose we choose u to be the potential ϕ and v to be of the form

$$v = \ln(r)$$

where

$$r = \sqrt{(x-\xi)^2 + (y-\eta)^2}$$

We take (ξ, η) as the coordinates of the point P where ϕ is to be determined and (x, y) as the coordinates of the point Q on the boundary where a source is located. In evaluating the integrals in applying Green's identity, we must

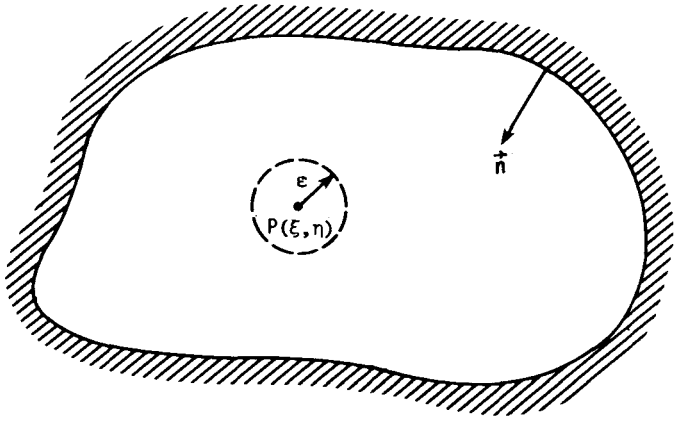

Figure 6.30 Physical domain for Laplace's equation.

exercise caution as (ξ, η) approach (x, y), that is, when $r \to 0$. In order to avoid this difficulty we think of enclosing the point $P(\xi, \eta)$ with a small circle of radius ϵ and apply Green's identity to the region enclosed by the original boundary (B) and that of the small circle enclosing P. Thus

$$0 = \oint_B (v \nabla u - u \nabla v) \cdot \mathbf{n}\, ds - \oint_\epsilon (v \nabla u - u \nabla v) \cdot \mathbf{n}\, ds$$

Consider the second integral with u, v replaced as noted above:

$$\oint_\epsilon [\ln(r) \nabla\phi - \phi \nabla \ln(r)] \cdot \mathbf{n}\, ds$$

On the boundary of the small circle, $r = \epsilon$, and we may write this integral as

$$\ln(\epsilon)\left(\oint \nabla\phi \cdot \mathbf{n}\, ds\right) - \oint \frac{\phi}{r} ds$$

By our original hypothesis, ϕ is a solution of Laplace's equation, and therefore the first term must vanish (see Prob. 2.7). The second term may be written

$$\frac{1}{\epsilon} \oint_\epsilon \phi\, ds$$

which, by the mean-value property of harmonic functions, becomes

$$\frac{1}{\epsilon} \oint \phi\, ds = 2\pi\phi(\xi, \eta)$$

We substitute this result into our original expression to obtain

$$\phi(\xi, \eta) = \frac{1}{2\pi} \oint \left[\ln(r) \frac{\partial\phi}{\partial n} - \phi \frac{\partial \ln(r)}{\partial n} \right] ds \tag{6.259}$$

Thus we have reduced the problem of computing a solution to Laplace's equation in the domain to solving an integral equation over the boundary. The first term represents a Neumann problem, where $\partial\phi/\partial n$ is given on the boundary, while the second is an example of the classical Dirichlet boundary value problem, where ϕ is specified. These integrals correspond to contributions to ϕ from sources and doublets. We could write

$$\phi = \frac{1}{2\pi} \oint \left[\mu \frac{\partial \ln(r)}{\partial n} + \sigma \ln(r) \right] ds \tag{6.260}$$

where we interpret σ as a source distribution and μ as a doublet distribution with axis normal to the bounding surface.

A surface source distribution with density σ per unit length produces a potential at an external point given by

$$\phi = \frac{1}{2\pi} \oint \sigma \ln(r)\, ds \tag{6.261}$$

where the integration is taken over the surface. If we have n surfaces or panels, the total potential at a point P is the sum of the contributions from each panel:

$$\phi_i = \sum_{j=1}^{n} \frac{1}{2\pi} \int_j \phi_j \ln (r_{ij})\, ds_j \tag{6.262}$$

A similar expression can be developed for a doublet distribution.

When a uniform stream is superimposed on the domain that includes the source panels, we include the velocity potential of the free stream and write

$$\phi_i = U_\infty x_i + \sum_{j=1}^{n} \frac{1}{2\pi} \int_j \sigma_j \ln (r_{ij})\, ds_j \tag{6.263}$$

The simplest panel representation to treat numerically is obtained when the source strength of each panel is assumed to be constant. Some advanced methods assume other distributions, and the representation of the velocity potential becomes correspondingly more complex. For a constant source strength per panel,

$$\phi_i = U_\infty x_i + \sum_{j=1}^{n} \frac{\sigma_j}{2\pi} \int_j \ln (r_{ij})\, ds_j \tag{6.264}$$

The geometry appropriate to the above potential distribution is shown in Fig. 6.31. The problem in using the source panel representation for a given body is to determine the source strengths σ_j. This is accomplished by selecting a control point on each panel and requiring that no flow cross the panel. The control point is selected at the midpoint of each panel. We now specify the point P to be at the control point of the ith panel. The boundary condition that no flow passes through the panel at this point is

$$\frac{\partial}{\partial n_i} \phi(x_i, y_i) = 0 \tag{6.265}$$

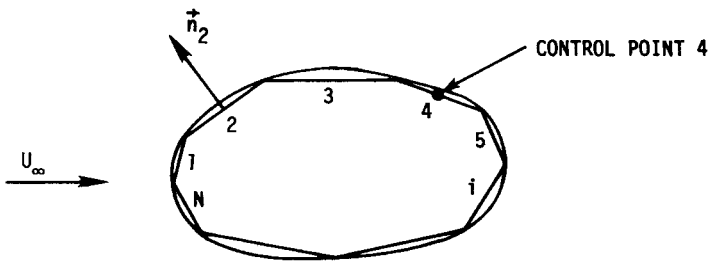

Figure 6.31 Panel representation for general shape.

Since ϕ is the velocity potential, this requires that the normal velocity at the control point of the ith panel vanish. Therefore

$$\sum_{i=1}^{n} \frac{\sigma_j}{2\pi} \int_j \frac{\partial}{\partial n_i} \ln (r_{ij})\, ds_j = -\mathbf{U}_\infty \cdot \mathbf{n}_i \tag{6.266}$$

The dot product is used because the velocity component normal to the surface is required. The velocity induced at the ith control point due to the ith panel is $\sigma_i/2$ and is usually taken out of the above summation. With this convention, we may write

$$\frac{\sigma_i}{2\pi} + \sum_{i \neq j}^{n} \frac{\sigma_j}{2\pi} \int \frac{\partial}{\partial n_i} \ln (r_{ij})\, ds_j = -\mathbf{U}_\infty \cdot \mathbf{n}_i \tag{6.267}$$

Application of this equation to each panel provides n algebraic equations for the n source strengths. Once the σ_j are computed, the pressure coefficients can be determined. When Eq. (6.267) is used to generate the required panel source strengths, the integrand function is most easily developed by using the vector dot product and may be written

$$\frac{\partial \ln (r_{ij})}{\partial n_i} = \nabla_i \ln (r_{ij}) \cdot \mathbf{n}_i \tag{6.268}$$

An example demonstrating the procedure for generating the required algebraic equations is in order.

Example 6.3 Suppose we wish to solve for the pressure distribution on a cylinder of unit radius in an incompressible flow using the method of source panels. The cylinder is to be represented by eight panels, and the configuration is shown in Fig. 6.32.

Solution In order to determine the surface pressures, we must calculate the panel strengths required for all eight panels on the cylinder. This is done by solving the system of algebraic equations generated by the application of Eq.

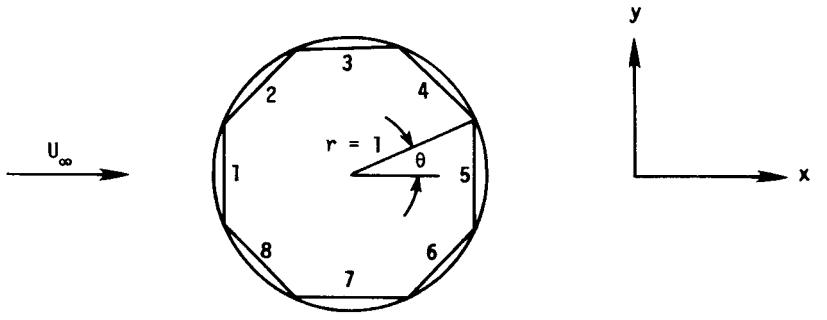

Figure 6.32 Panel representation of cylinder.

(6.267) to each panel. In applying Eq. (6.267) to any panel, the most difficult part is the evaluation of the integral term. In general, it is convenient to view the integral as an influence coefficient and write the system of governing equations in the form

$$[C]\frac{\sigma}{2\pi U_\infty} = -\frac{\mathbf{U}_\infty \cdot \mathbf{n}_i}{U_\infty} \tag{6.269}$$

Using the following notation, we may write the components of $[C]$ as

$$c_{ij} = \begin{cases} \int_j \nabla_i \ln(r_{ij}) \cdot \mathbf{n}_i \, ds_j & i \neq j \\ \pi & i = j \end{cases} \tag{6.270}$$

To demonstrate the application of Eq. (6.270), we elect to compute c_{53}, which represents the normal velocity at the control point of panel 5 due to a constant source strength of magnitude $1/U_\infty$ on panel 3. For this case we write the radius as

$$r_{53} = \left[(x_5 - x_3)^2 + (y_5 - y_3)^2\right]^{1/2}$$

and

$$\nabla_5 \ln(r_{53}) = \frac{(x_5 - x_3)\mathbf{i} + (y_5 - y_3)\mathbf{j}}{(x_5 - x_3)^2 + (y_5 - y_3)^2} \tag{6.271}$$

The unit normal on panel 5 is the unit vector in the positive x direction and

$$\nabla_5 \ln(r_{53}) \cdot \mathbf{n}_5 = \frac{x_5 - x_3}{(x_5 - x_3)^2 + (y_5 - y_3)^2}$$

For this integral, $x_5 = 0.9239$, $y_5 = 0$, and $y_3 = 0.9239$, while x_3 is a variable on panel 3. This reduces the integral required to the form

$$c_{53} = \int_{-0.3827}^{+0.3827} \frac{0.9239 - x}{x^2 - 1.848x + 1.707}\, dx = 0.4018$$

In this expression the arc length along panel 3 is equal to $x - 0.3827$; therefore $ds_3 = dx$, and we use the x coordinates of the panel end points as the integration limits. Notice that the integration proceeds clockwise around the cylinder, which is the positive sense for the domain where a solution of Laplace's equation is required. The $[C]$ matrix is symmetric, i.e., $c_{ij} = c_{ji}$, and the solution for the σ_i must be such that

$$\sum_{i=1}^{n} \sigma_i = 0$$

This requirement is an obvious result of the requirement that we have a closed body.

A comparison of the eight-panel solution with the analytically derived pressure coefficient is shown in Fig. 6.33. Clearly, the panel scheme provides a very accurate numerical solution for this case.

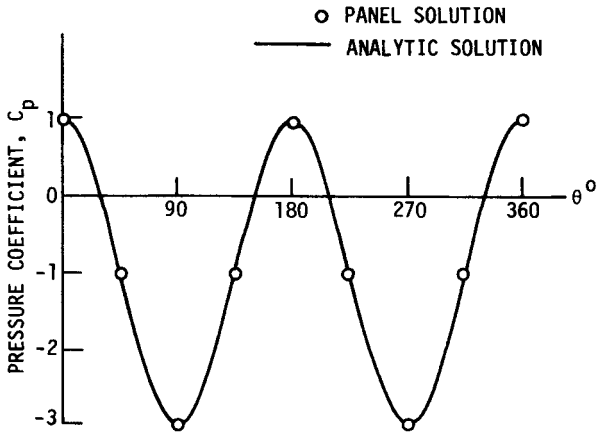

Figure 6.33 Pressure coefficient for a circular cylinder.

We have used the method of source panels in our example to demonstrate the mechanics of applying the technique. We could use doublets or dipoles to construct bodies as well as vortex panels. Clearly, we must include circulation if we are concerned with lifting airfoils. This may be done in a number of ways, but one technique is to use a vortex panel distribution along the mean camber line to provide circulation and satisfy the Kutta condition at a control point just aft of the trailing edge.

Panel methods represent a powerful approach for solving certain classes of flow problems. They have received extensive use and have resulted in a number of standard codes that are used industrywide. For more details on the development of these schemes, the paper by Hess and Smith (1967) provides basic details, while the papers by Rubbert and Saaris (1972) and Johnson and Rubbert (1975) present more advanced ideas.

PROBLEMS

6.1 In Example 6.1, we used a characteristic method to solve for supersonic flow over a wavy wall. Verify the velocity field obtained by solving the Prandtl-Glauert equation [Eq. (6.1)] directly.

6.2 Derive the differential equations of the characteristics of the nonlinear system of equations governing 2-D supersonic flow written in rectangular coordinates [Eq. (6.18)].

6.3 The differential equations of the characteristics obtained in Prob. 6.2 are written in rectangular coordinates. Transform these results using the streamline angle θ, and show that the characteristics are inclined at the local Mach angle, i.e.,

$$\tan(\theta \pm \mu) = \frac{dy}{dx}$$

6.4 Develop the compatibility equations for the nonlinear equations of Prob. 6.2

6.5 Use the results of Probs. 6.2 and 6.4 and solve Example 6.1 using the method of characteristics for the nonlinear equations.

6.6 Complete the derivation in Prob. 6.4 by computing $[T]$. The governing equations are then ready to be numerically integrated using an appropriate upwind scheme.

6.7 The 1-D unsteady Euler equations are given by

$$\mathbf{U}_t + [A]\mathbf{U}_x = 0$$

where

$$\mathbf{U} = [\rho, u, p]^T$$

and

$$[A] = \begin{bmatrix} u & \rho & 0 \\ 0 & u & 1/\rho \\ 0 & \rho a^2 & u \end{bmatrix}$$

Find the following:

(*a*) eigenvalues
(*b*) characteristics
(*c*) left eigenvectors
(*d*) $[T]^{-1}$
(*e*) compatibility equations

6.8 Develop a code to solve for the supersonic flow over the 2-D wedge of Example 6.2. Use a shock-capturing approach and MacCormack's method in solving the steady flow equations. Use 26 grid points with the outer boundary located at an angle of 40° with respect to the wedge surface. Nondimensionalize the governing equations using the procedure given in Section 5.1.7. Let $V_\infty = 1$, $\rho_\infty = 1$, and $p_\infty = 1/(\gamma M_\infty^2)$. Compute this case by integrating from $\xi \cong 0$ to a relatively large value of ξ in order to asymptotically obtain the converged solution. Use the maximum allowable $\Delta\xi$, which can be determined by performing numerical experiments. Compare your numerical solution with the exact solution.

6.9 Solve the wedge-flow problem of Prob. 6.8 by using the unsteady (time-dependent) approach and conical flow. Use the maximum allowable Δt, which can be determined by performing numerical experiments. Compare your numerical solution with the exact solution.

6.10 Develop a code to solve the 2-D supersonic wedge problem of Prob. 6.8, but fit the shock wave as a discontinuity. Use either the conservative or nonconservative form.

6.11 Suppose that a solid boundary lies on a ray (θ = const) in a 2-D flow problem. Use reflection to establish a suitable means of determining the flow variables of the sublayer points. Use rectangular velocity components.

6.12 Develop the appropriate boundary condition procedure using Kentzer's method (see Section 6.7) for the supersonic wedge-flow problem.

6.13 The flux-vector splitting method of Steger and Warming "splits" the system of equations

$$\mathbf{U}_t + \mathbf{E}_x = 0$$

into the following form:

$$\mathbf{U}_t + \mathbf{E}_x^+ + \mathbf{E}_x^- = 0$$

If this method is applied to the system of equations

$$\mathbf{U} = \begin{bmatrix} u \\ v \end{bmatrix} \qquad \mathbf{E} = \begin{bmatrix} cv \\ cu \end{bmatrix}$$

where c is a constant, find the following quantities:

(*a*) $[A]$
(*b*) $[\lambda^+], [\lambda^-]$
(*c*) $[T]^{-1}, [T]$
(*d*) $[A^+], [A^-]$
(*e*) $\mathbf{E}^+, \mathbf{E}^-$

6.14 Repeat Prob. 6.13 for the 1-D unsteady Euler equations given in Prob. 6.7 Assume that $(0 \ll u \ll a)$.

6.15 The split-coefficient matrix method (Chakravarthy, 1979) "splits" the system of equations

$$\mathbf{U}_t + [A]\mathbf{U}_x = 0$$

into the following nonconservative form:

$$\mathbf{U}_t + [A^+]\mathbf{U}_x + [A^-]\mathbf{U}_x = 0$$

where

$$[A^+] = [T][\lambda^+][T]^{-1}$$

$$[A^-] = [T][\lambda^-][T]^{-1}$$

If this method is applied to the system of equations

$$\mathbf{U} = \begin{bmatrix} u \\ v \end{bmatrix} \qquad [A] = \begin{bmatrix} 0 & c \\ c & 0 \end{bmatrix}$$

where c is a constant, find the following quantities:

(*a*) $[\lambda^+], [\lambda^-]$
(*b*) $[T], [T]^{-1}$
(*c*) $[A^+], [A^-]$

6.16 Repeat Prob. 6.15 for the 1-D unsteady Euler equations given in Prob. 6.7. Assume that $0 < u < a$.

6.17 In the CSCM (Conservative Supra-Characteristics Method) flux-difference splitting scheme (Lombard et al., 1983), the system of equations

$$\mathbf{U}_t + \mathbf{E}_x = 0$$

is "split" into the following form:

$$\mathbf{U}_t + [Q^+]\mathbf{E}_x + [Q^-]\mathbf{E}_x = 0$$

where

$$[Q^+] = [T][\lambda^+][\lambda]^{-1}[T]^{-1}$$

$$[Q^-] = [T][\lambda^-][\lambda]^{-1}[T]^{-1}$$

If this method is applied to the system of equations given in Prob. 6.13, find the following quantities:

(*a*) $[\lambda], [\lambda^+], [\lambda^-], [\lambda]^{-1}$
(*b*) $[T], [T]^{-1}$
(*c*) $[Q^+], [Q^-]$

6.18 Repeat Prob. 6.17 for the 1-D unsteady Euler equations given in Prob. 6.7. Assume that $0 < u < a$.

6.19 Apply Roe's scheme to the system of equations given in Prob. 6.13 and find

$$[|A|] = [T][|\Lambda|][T]^{-1}$$

6.20 Apply Roe's scheme to the 1-D unsteady Euler equation given in Prob. 6.7 and find

$$[|A|] = [T][|\Lambda|][T]^{-1}$$

if $0 < u < a$.

6.21 Compute the split-flux mass using Steger-Warming flux-vector splitting and show that the van Leer flux-vector splitting eliminates the discontinuities in derivatives as indicated in Fig. 6.12.

6.22 Verify Eqs. (6.114) and (6.115).

6.23 Develop a code to solve Prob. 6.9 using the Steger-Warming flux-vector splitting scheme.

6.24 Develop a code to solve Prob. 6.9 using van Leer flux-vector splitting.

6.25 Write a computer code to solve the 1-D shock tube problem using van Leer flux-vector splitting. Assume that the low-pressure end of the infinitely long shock tube is at standard atmospheric conditions and the high-pressure end has a pressure of 10 atm and standard atmospheric temperature.

6.26 Develop a code to solve Prob. 6.25 using the advection upstream splitting (AUSM) method.

6.27 Develop a code to solve Prob. 6.25 using a first- and second-order Roe scheme.

6.28 Show that Eq. (6.197) is a second-order representation of the 1-D potential equation.

6.29 Show that the retarded density formulation of Eq. (6.203) is equivalent to Eq. (6.202).

6.30 Derive Eq. (6.210).

6.31 Show that Eq. (6.260) is a valid representation for the potential in an incompressible fluid flow.

6.32 Compute c_{43} of Example 6.3.